Master thesis

Water Management in a High Current Density PEM Electrolysis Cell

in the study programme Renewable Energy Systems
Department Environment Engineering
Faculty of Life Sciences
Hamburg University of Applied Sciences

submitted by:

Name:	Tobias Reum
Matriculation number:	█████
E-Mail:	████████████████

First examiner:	Prof. Dr. Marion Siegers
Second examiner:	Dr. Nils Baumann

This thesis was supervised and prepared in the laboratory of the Fraunhofer ICT, Pfinztal, Germany.

Pfinztal, November 22nd, 2019

Affidavit

I declare that I prepared this Master Thesis on my own without any external help or assistance. Used literature and internet sources are completely listed in the appendix of this work. I assure to have marked everything that has been taken from the work of third parties.

Tobias Reum

██████ November 22nd, 2019

Abstract

Water electrolysis and fuel cell systems are storage technologies with great potential capacities but suffer from high costs. Noble metals are used for electrocatalysts and separate plants are needed to work in both operation modes. The running costs are also subject of optimization. This includes costs for water pumps, gas storage next to the main topic efficiency.

This work deals with the issue of investment costs as well as running costs. Requirements for industrial use is next to long-term stability an increased current density. This allows relatively small plants to produce high amounts of hydrogen gas. For this, high efficiency as well as optimizing the transport issues of water and gas inside the membrane electrode assemblies is needed. The running costs include the costs for pumps and deionized water, needed to prevent degradation of the membrane and the electrocatalyst.

First, thin membranes for 4 cm^2 active area are tested for their suitability for water electrolysis. Nafion$^®$ 211 and Nafion$^®$ XL are examined on their mechanical stability. While the former does regularly break at increased contact pressures - needed to reduce the ohmic contact resistance between electrode and membrane -, the reinforced Nafion$^®$ XL is properly suited for this and does not break even at high contact pressures of 60 bar and elongated operation of several days and repeated start-up and humidification changes before failing.

The Nafion$^®$ XL is then optimized for their electrocatalyst amount which is iridiumdioxide. Loadings from 0.26 mg/cm^2 to 0.94 mg/cm^2 are tested. While the highest amount of electrocatalyst shows the highest efficiency with 1.69 V at 1 A/cm^2, the efficiency increase per loading can be a major factor when trying to reduce the electrocatalyst amount. Even a low loading of 0.44 mg/cm^2 proves to show good results while needing less costly electrocatalyst.

Two analyses are conducted to examine the water effects inside the cell. First, the electro-osmotic drag coefficient - the amount of water dragged by protons through the membrane - is analyzed at current densities up to 5 A/cm^2. Higher current densities do seem to hinder water molecules to be transported and require a lower electro-osmotic

drag coefficient to be accounted for, even though the total transported amount is increasing.

Second, the stability depending on the fed water is examined. Different amounts of water are tested for stable operation of water electrolysis. It is found that for lower current densities of up to 2 A/cm^2, the optimal stoichiometry is around 10 or higher. At stoichiometries below this level, the current density is not stable at constant voltages. Also, higher stoichiometries are necessary for stable operation at higher current densities. The effects of start-up show inertia of the system and require further investigation.

Acknowledgements

At this point, I want to thank all those people who aided me in the preparation of my master thesis - be it professionally or personally.

Prof. Dr. Marion Siegers of the University of Applied Sciences Hamburg supervised this thesis. I greatly appreciated her effort, her interest in the topic and the various productive discussions we had. She really invested a lot of time and I hope she was as happy with the work as I was and still am. She helped me avoiding a lot of obstacles and developing a target-orientated focus. Working for a motivated professor might mean a lot of work, but that is how we learn. I am very grateful for her willingness and help!

Furthermore, I want to thank the Fraunhofer ICT for giving me the opportunity to prepare this thesis in cooperation with them. Especially Dr. Nils Baumann, who not only supervised me at the ICT in aiding with the new electro-chemical focus and the project cooperation. But also for the always open door for discussions and the very good personal relationship. I really liked his way of leadership, and I will miss the games evenings. More colleagues supported me every day in both professional and personal ways, Eduardo Daniel Gomez Villa, Lars Zick, Dr. Carsten Cremers, and many more. Naming all would simply make this list too long. I had a great time and wish you all the best!

Lastly, I want to thank my parents for always helping me in any way possible and supporting me in my not-so-conventional course of life. I will settle down some day, I promise.

Thank you all!

Tobi

Contents

List of Figures

List of Tables

List of Symbols and Abbreviations

character	unit	meaning
A	cm^2	membrane area
A_{cell}	cm^2	cell area
A_{cylinder}	cm^2	cylinder area
A_{MEA}	cm^2	sprayed MEA area
A_{ref}	cm^2	reference area
A_{tot}	cm^2	total sprayed area
a	-	water activity
B_{O_2}	-	ratio of molar mass of water and oxygen
C	mol/m^3	concentration
C_{a}	mol/m^3	concentration of water at anode
C_{c}	mol/m^3	concentration of water at cathode
c_{p}	J/(kg*K)	heat capacity at constant pressure (of water)
DI	-	deionized (water)
D_{w}	m^2/s	water diffusion coefficient
D_λ	m^2/s	diffusion coefficient of the membrane
E^0	V	standard potential/thermoneutral voltage
EW	g/mol	equivalent weight (dry membrane mass per mole of sulfonic acid groups)
F	C/mol	Faraday constant
FC	-	fuel cell
f	-	factor on relative sprayed amount on mask holes
$f_{\text{w}-\%,\text{binder}}$	-	weight percentage of binder in spraying ink
$f_{\text{w}-\%,\text{IrOx}}$	-	weight percentage of iridiumoxide in spraying ink
GDL	-	gas diffusion layer
ΔG	kJ/mol	change in Gibb's energy
ΔH	kJ/mol	change in enthalpy
ΔH^0	kJ/mol	change in enthalpy at standard conditions

character	unit	meaning
I	A	current
I_{max}	A/cm^2	maximum current
i	A/cm^2	current density
i_{max}	A/cm^2	maximum current density
j_{loading}	A/cm^2	current per loading
K_{D}	m^2	(intrinsic) permeability, here: Darcy constant
k	-	number of electrons participating in a reaction
l	m	edge length
MEA	-	membrane electrode assembly
M	kg/mol	molar mass
$M_{\mathrm{H_2O}}$	kg/mol	molar mass of water
$M_{\mathrm{H_2}}$	kg/mol	molar mass of molecular hydrogen
$M_{\mathrm{H+}}$	kg/mol	molar mass of atomar hydrogen
$M_{\mathrm{m,dry}}$	kg/mol	molar mass of the dry membrane
$M_{\mathrm{O_2}}$	kg/mol	molar mass of molecular oxygen
m	g	mass
m_{after}	g	mass of membrane after spraying process
m_{before}	g	mass of membrane before spraying process
m_{c}	g	mass water due to concentration gradient
m_{eo}	g	mass water due to electro-osmotic gradient
$m_{\mathrm{H_2}}$	g	mass of molecular hydrogen
$m_{\mathrm{H_2O,cons}}$	g	consumed mass of water
$m_{\mathrm{H_2O,tot}}$	g	total mass of water fed to the anode
m_{IrOx}	g	mass of iridiumoxide
$m_{\mathrm{IrOx,ref}}$	g	mass of iridiumoxide on reference area
$m_{\mathrm{nocurrent}}$	g/s	reference water mass (at no current)
$m_{\mathrm{O_2}}$	g	mass of molecular oxygen
m_{p}	g	mass water due to pressure gradient
$\dot{m}$	g/s	mass flow
$\dot{m}_{\mathrm{a}}$	g/s	water mass flow into the anode
$\dot{m}_{\mathrm{a,out}}$	g/s	water mass flow out of the anode
$\dot{m}_{\mathrm{a,out,l}}$	g/s	liquid water mass flow out of the anode
$\dot{m}_{\mathrm{a,out,g}}$	g/s	gaseous water mass flow out of the anode

character	unit	meaning
$\dot{m}_{\mathrm{co}}$	g/s	concentration gradient water mass flow
$\dot{m}_{\mathrm{c}}$	g/s	water mass flow into the cathode
$\dot{m}_{\mathrm{c,out}}$	g/s	water mass flow out of the cathode
$\dot{m}_{\mathrm{c,out,l}}$	g/s	liquid water mass flow out of the cathode
$\dot{m}_{\mathrm{c,out,g}}$	g/s	gaseous water mass flow out of the cathode
$\dot{m}_{\mathrm{eo}}$	g/s	electro-osmotic drag water mass flow
$\dot{m}_{\mathrm{H_2,real}}$	g/s	real produced hydrogen mass flow
$\dot{m}_{\mathrm{H_2,theo}}$	g/s	theoretical produced hydrogen mass flow
$\dot{m}_{\mathrm{H_2O,cons}}$	g/s	consumed water flow
$\dot{m}_{\mathrm{H_2O,feed}}$	g/s	feed water flow
$\dot{m}_{\mathrm{H_2O,tot}}$	g/s	total mass flow of water fed to the anode
$\dot{m}_{\mathrm{H^+}}$	g/s	hydrogen mass flow
$\dot{m}_{\mathrm{net}}$	g/s	net water mass flow
$\dot{m}_{\mathrm{nocurrent}}$	g/s	reference water mass flow (at no current)
$\dot{m}_{\mathrm{O_2}}$	g/s	molecular oxygen mass flow
$\dot{m}_{\mathrm{p}}$	g/s	pressure gradient water mass flow
$\Delta m_{\mathrm{a,out,l}}$	g	liquid water mass difference in container due to current density
Δm_{i}	g	water mass difference in container due to current density
n_{eo}	-	electro-osmotic drag coefficient
n_{d}	-	drag coefficient
$\dot{n}_{\mathrm{gas}}$	mol/s	gas molar flow
$\dot{n}_{\mathrm{H_2}}$	mol/s	molar flow of molecular hydrogen
$\dot{n}_{\mathrm{H_2O}}$	mol/s	molar flow of water
$\dot{n}_{\mathrm{H_2O}}$	mol/s	molar flow of water by electro-osmotic drag
$\dot{n}_{\mathrm{H^+}}$	mol/s	molar flow of atomar hydrogen
$\dot{n}_{\mathrm{O_2}}$	mol/s	molar flow of molecular oxygen
$\dot{n}_{\mathrm{tot}}$	mol/s	total molar flow

character	unit	meaning
OER	-	oxygen evolution reaction
PE	-	polymer electrolyte
PEM	-	polymer electrolyte membrane
PFSA	-	perfluorosulfonic-acid
PTL	-	porous transport layer
PTFE	-	polytetrafluoroethylene
p	N/m^2 or bar	pressure
Δp	N/m^2 or bar	1-dimensional pressure gradient
∇p	N/m^2 or bar	3-dimensional pressure gradient
p_a	N/m^2 or bar	anode pressure
p_c	N/m^2 or bar	cathode pressure
p_cylinder	bar	pressure in cylinder (air pressure)
$p_{\mathrm{H_2O}}$	bar	partial pressure of water
p_peri	%	relative power of peristaltic pump (anode)
p_s	bar (or kPa)	saturation pressure of water
p_stamp	bar	compacting pressure on the stamp
$\dot{Q}$	W	heating power
$\dot{Q}_{\mathrm{H_2O,a}}$	W	heating power for the water inflow of the anode
$\dot{Q}_{\mathrm{H_2O,c}}$	W	heating power for the water inflow of the cathode
r_holes	m	radius of holes in spraying mask
ΔS	kJ/mol	change in entropy
T	K or °C (or s)	temperature (or period)
T_cell	K	temperature of the cell
T_dh	K	temperature of the dehumidifier
TPB	-	triple phase boundary
t	s	time
t_m	m	membrane thickness
t_PTL	m	porous transport layer thickness
U	V	voltage
U_a	V	activation overpotential/losses
U_cell	V	voltage across cell
U_i	V	voltage at current density
U_t	V	transport overpotential/losses
U_Ω	V	ohmic overpotential/losses
UI	-	polarization/voltage-current curve
URFC	-	unitized regenerative fuel cell
WE	-	water electrolysis

character	unit	meaning
X	-	mixing ratio
X_{O_2}	- (g_{H_2O}/g_{O_2})	mixing ratio of water in oxygen
x_w	-	molar water content
$x_{w,a}$	-	molar water content at the anode
ϵ	-	porosity
η_F	-	Faraday efficiency
η_i	-	efficiency at current density
λ	-	water content
μ	$N * s/m^2$	dynamic viscosity
ξ	-	water stoichiometry
ρ	g/m^3	density of water
$\rho_{A,IrOx}$	mg/cm^2	loading (mass per area) of iridiumoxide
$\rho_{A,IrOx,MEA}$	mg/cm^2	loading (mass per area) of iridiumoxide on MEA area
$\rho_{A,IrOx,tot}$	mg/cm^2	loading (mass per area) of iridiumoxide on total sprayed area
$\rho_{m,dry}$	g/m^3	density of the dry membrane
σ_i	A/cm^2	standard deviation of current density

1 Introduction

Increasing contribution of renewable power generation in the total power sector - so far mostly in the electrical energy sector - leads to increasing fluctuality of the grid. Non-constant power generation and loads decrease the stability of the grid and make flexible power consumption and generation necessary. While battery systems can act as a short-term storage for electrical energy, the potential capacity for long-term storage is limited. Hydrogen can fill that role not only as a long-term storage but also allowing sector coupling for heating systems and mobility as it can be stored highly efficiently and produced from excess electrical energy in the grid via electrolysis. The backwards reaction from chemically stored energy to electrical energy can be done using traditional gas turbines with generators or fuel cells.

Fuel cells and water electrolysis systems are highly efficient. While electrolysis systems efficiencies range around 80 %, fuel cells have purely electrical efficiencies of 50 %. Waste heat usage on the product side or more sophisticated gas fuel usage on the educt side can increase the efficiency even further [1]. While the cycle efficiency is therefor usually higher for batteries (up to 90 % for Li-ion [2]), the capacity of gas storage possibilities [3, 4] and the low energy losses over time can make fuel cell and electrolysis technology attractive. [5, 6]

There are five major technologies for fuel cell systems working with hydrogen as fuel: alkaline, polymer electrolyte membrane, phosphoric acid, molten carbonate and solid oxide. High temperature technologies like molten carbonate and solid oxide can also operate with natural gas and internal reforming. Polymer electrolyte membrane technology can also work as an electrolysis system, is working at low temperature and utilizes a solid polymer membrane acting as electrolyte. As both fuel cells and electrolysis systems, they therefor do not need sophisticated electrolyte management and can follow loads quickly enough for mobility applications or short-term energy storage applications. Furthermore, due to the thin membrane, ohmic resistances are low and due to the solid membrane, the product gas purity is high. This also enables the technology to operate under differential pressure, enabling easier storage of compressed gaseous hydrogen. However, the catalysts are noble metals and costly. They are also highly sensitive to fuel impurities,

especially carbon monoxide. [7, 8]

The BMWi[1] funded project Re-Flex focuses on polymer electrolyte membrane technology. To this day, electrolysis and fuel cell systems are usually split into two different devices. This is called a discrete regenerative fuel cell. A unitized regenerative fuel cell combines these two operating conditions in one single cell: To generate hydrogen from electrical power during water electrolysis mode and to generate electricity from hydrogen and oxygen during fuel cell mode. The aim is to reduce investment costs especially for power grid applications, because the auxiliaries do not have to be implemented in two separate systems. The heat exchangers, pumps and condensers can then be used in both operation modes. [9]

During the development process, several challenges were encountered: The ohmic resistance is a major loss factor in water electrolysis. The catalyst on the oxygen side needs to be improved not only efficiency-wise but also according to the necessary amount for long-term operation. Additionally, the water management under the changing operating conditions can not precisely be calculated. All three topics are subject of this work: ohmic losses, amount of electro-catalyst and the water management.

1.1 Motivation

Achieving high current density is a main objective for industrial water electrolysis. This allows a high product gas mass flow at lower investment costs. This makes not only low ohmic resistance needed, which can be solved using thinner membranes. Lower thickness means higher proton conductivity, but at the same time higher gas crossover. Optimizing the electrocatalyst does play a role for high currents as well as high efficiency, but it is also a major cost factor. Costly metals are often used for electrocatalysts, so reducing the amount lowers the investment costs. However, less electrocatalyst plays a role for efficiency of the cell and long-term operation, since the electrocatalyst degrades over time.

Polymer electrolyte membranes are not water tight: Pressure and concentration gradients and the so-called electro-osmotic drag effect have an influence on the water amount on both sides. The membrane also needs to be humidified to allow protons to cross,

---

[1]Bundesministerium fř Wirtschaft und Energie, Germany.

otherwise the conductivity and therefor the voltage and then the power breaks down. Especially the water electrolysis mode is not covered by extensive analysis and there are only few scientific papers dealing with this effect. [10–15] The effects of high current density (up to $i_{\mathrm{max}} = 5$ A/cm^2) on water transport effects inside the cell have been neglected and still need to be researched.

Improving the understanding of water crossing effects can lead to a more efficient use of the feeding water: From reducing the amount of fed water over optimization of its cooling effects to prevention of water starvation. The reduction of total water consumption is especially important since for polymer electrolyte membrane water electrolysis, deionized water has to be used. [16] The auxiliary power needed for cooling or heating and the amount of deionized water can be reduced and have significant effects on efficiency and operating costs.

1.2 Objective

The first aim is to enable high current densities at improved efficiencies in polymer electrolyte membrane water electrolysis. For this, thin membranes are used for reduced ohmic resistance. The Nafion® 211 and the Nafion® XL are to be tested for mechanical stability. Electrolysis cells are built and tested for efficiency during operation. The electrocatalyst amount is also examined for optimized efficiency at minimum costs. The objective is to enable a high current density cell with low amounts of electrocatalyst.

The second aim of this thesis is to develop a deeper understanding of the water management during water electrolysis. The electro-osmotic drag plays a major role in high current density operation of a water electrolysis cell, because it increases with the current. However, Medina and Santarelli [10] report a lower electro-osmotic drag coefficient at higher current densities. Because they only tested up to 1 A/cm^2, the effect of decreasing electro-osmotic drag at increased current densities needs to be further examined.

The feed water flow to the anode is also a cost factor for water electrolysis. Water needs to be fed as an educt, but is also required to humidify the membrane and the reaction area, the triple phase boundary. Transport effects of water within the membrane like the aforementioned electro-osmotic drag, but also concentration and pressure gradient during pressurized cathode operation need to be accounted for as well. The amount of

water needed to be fed into the anode to allow stable operation is examined. This can reduce costs by allowing smaller pumps and tube diameters for the water inlets as well as less amount of deionized water.

In this work a test stand is developed to analyze these operating conditions. Experimental analysis includes the different parameters, the measurements of polarization curves, current densities across the membrane and the amount of water fed into the membrane electrode assembly as well as the excess water amount flowing out of each electrode. The three different water crossing effects through the membrane - pressure, concentration, electro-osmotic drag - are also analyzed mathematically.

The ultimate objective is to allow high current density electrolysis with minimum electrocatalyst mass needed as well as a reduction in the feed water flow while still ensuring the completely humidified polymer electrolyte membrane at high current densities.

2 Theoretical Background

To understand the effects involved in the determination of proper water management, several topics concerning polymer electrolyte membrane (PEM) water electrolysis (WE) need to be discussed more in depth. The focus lies upon WE and water transport effects and the analysis of membranes and electrocatalyst masses suitable for WE. Research of bi-functional electrocatalysts - suitable for both WE and fuel cell (FC) modes - is an important factor for unitized regenerative fuel cells (URFC), but it plays a minor role in the water management.

2.1 Water Electrolysis

WE is the process of splitting water into hydrogen and oxygen by the application of an electrical potential. In PEM WE, the following reaction occurs at the anode:

$$H_2O \longrightarrow \frac{1}{2} O_2 + 2\,H^+ + 2\,e^-\,. \tag{2.1}$$
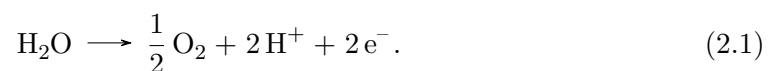
This is the oxygen evolution reaction (OER). The protons move through the electrolytic membrane towards the cathode, where they produce hydrogen according to the following reaction:

$$2\,H^+ + 2\,e^- \longrightarrow H_2\,, \tag{2.2}$$

which leads to the total reaction:

$$H_2O \longrightarrow \frac{1}{2} O_2 + H_2\,. \tag{2.3}$$
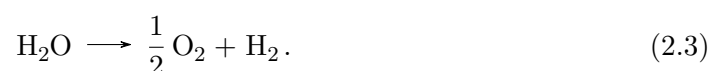
The total reaction including membrane electrode assembly (MEA) and electrodes is shown in figure 2.1. The stoichiometry for H:O is therefor 2:1, meaning: two hydrogen atoms are produced for each oxygen atom. For H:H_2O it is 2:1 as well: two hydrogen atoms are produced per water molecule.

Since WE is not a favorable reaction in thermodynamic terms (endothermic), energy has to be supplied to keep it going. This electrical potential needs to be higher than the
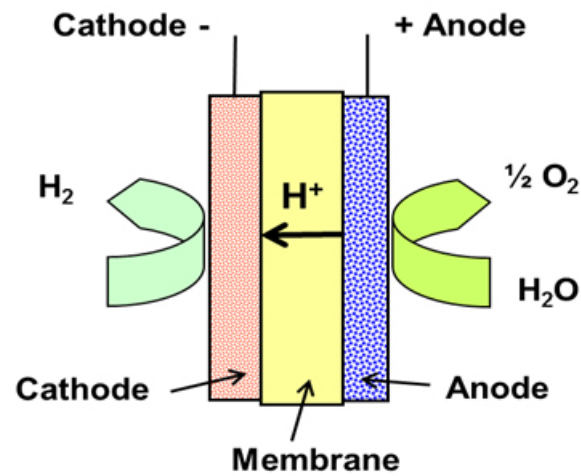
Figure 2.1: Water electrolysis reaction. The H_2O feed is shown as well as the products H_2 and $1/2$ O_2 and the movement of the proton H^+ across the membrane from the positively charged anode to the negatively charged cathode. Based on [17].

theoretical standard potential of an electrolysis cell. The standard potential E^0 can be calculated using:

$$E^0 = \frac{\Delta H}{k * \text{F}} \,, \tag{2.4}$$

with ΔH being the change in enthalpy, k the amount of electrons participating in the reaction and F the Faraday constant. According to equations (2.1) and (2.2), there are two electrons participating in the total reaction ($k = 2$). The Faraday constant is F = 96485.33 C/mol. ΔH is used because splitting a water molecule not only requires reversible energy - which would be the Gibb's energy ΔG, usually used in fuel cells -, but also heat. This is not reversible and therefor lost as an entropy increase ΔS depending on the temperature T. [18]

$$\Delta H = \Delta G + T * \Delta S \,. \tag{2.5}$$

However, the change in enthalpy at standard conditions ($p = 1$ bar, $T = 25\ °\text{C}$) can be taken from tables as $\Delta H^0 = 285.83$ kJ/mol. The electrochemical standard potential E^0 (sometimes also called thermoneutral voltage) can therefor be calculated using equation (2.7):

$$E^0 = \frac{\Delta H^0}{n * F} = \frac{285.83 \text{ kJ/mol}}{2 * 96485.33 \text{ C/mol}} = 1.48 \text{ V} , \qquad (2.6)$$

2.1.1 Polarization Curve

The polarization curve - also called voltage-current (UI) curve - characterizes the efficiency of the cell at different currents. Figure 2.2 shows a characteristic UI curve for water electrolysis. With increasing current density, the cell voltage increases. This is mainly due to three major loss effects: activation, ohmic and mass transport losses. They add to the thermoneutral voltage according to:

$$U_{\text{cell}} = E^0 + U_{\text{a}} + U_{\Omega} + U_{\text{t}} , \qquad (2.7)$$

with U_{cell} being the applied voltage, E^0 the electrochemical standard potential (or thermoneutral voltage), U_{a} the voltage due to activation losses, U_{Ω} due to ohmic losses and U_{t} due to mass transport losses.

Activation losses refer to the rate of the chemical reactions that take place on the surface of the electrodes. It mainly deals with effects while initiating proton transfer being influenced by electrocatalysts. They are high at lower currents, but increase only slightly at higher values. Ohmic losses are linearly dependent on the current according to Ohm's law. They include resistance of the wiring and imperfect electrode connections. Mass transport losses increase significantly at higher currents. Due to the high current, more molecules need to be transferred to and from the triple phase boundary (TPB) - the region where electrolyte (here: PE membrane), catalyst and fuel are in contact with each other. Bubbles and other flow hindrances can lower the efficiency of this process.

2.1.2 Faraday Efficiency

The Faraday efficiency η_{F} describes the losses of ions and electrons participating in unwanted side reactions. For example, hydrogen peroxide can form on the anode, water recombination can occur depending on the catalysts used and electrons can cross the PE membrane without passing through the load. It can be calculated as the ratio of real produced hydrogen $\dot{m}_{\text{H}_2,\text{real}}$ divided by the theoretical amount $\dot{m}_{\text{H}_2,\text{theo}}$:

$$\eta_{\text{F}} = \frac{\dot{m}_{\text{H}_2,\text{real}}}{\dot{m}_{\text{H}_2,\text{theo}}} . \qquad (2.8)$$
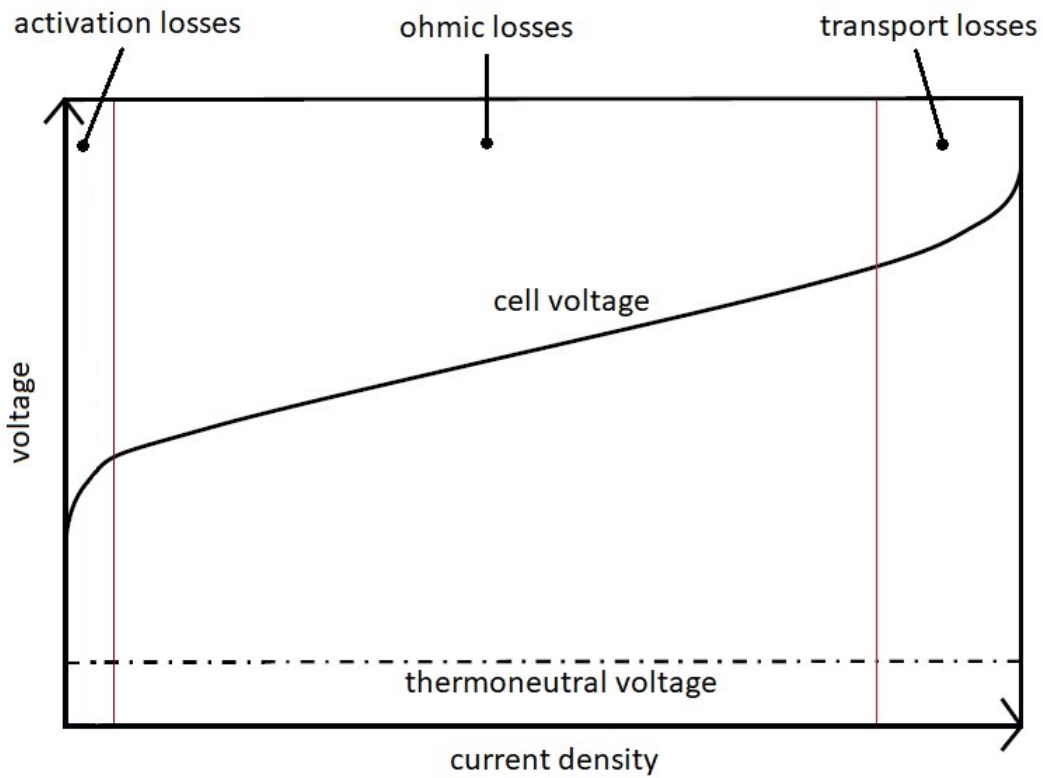
Figure 2.2: An exemplary UI curve including the characteristic losses for the curve's regions. Based on [19].

Tijani and Rahim [20] report efficiencies above 90 % at high current densities and low anode pressure. Elevating either electrode pressures increases the losses, while increasing current density decreases them. While temperature seems to have low impact on the Faraday efficiency, the membrane thickness influences it significantly - thicker membranes allowing less cross-over effects. Two exemplary graphs can be seen in figure 2.3.

High current densities for WE means values up to $i = 5$ A/cm^2 at voltages below 2.2 V [38] or even 2.0 V [39] without much explanation and probably refers to degradation of catalysts and electrode materials.
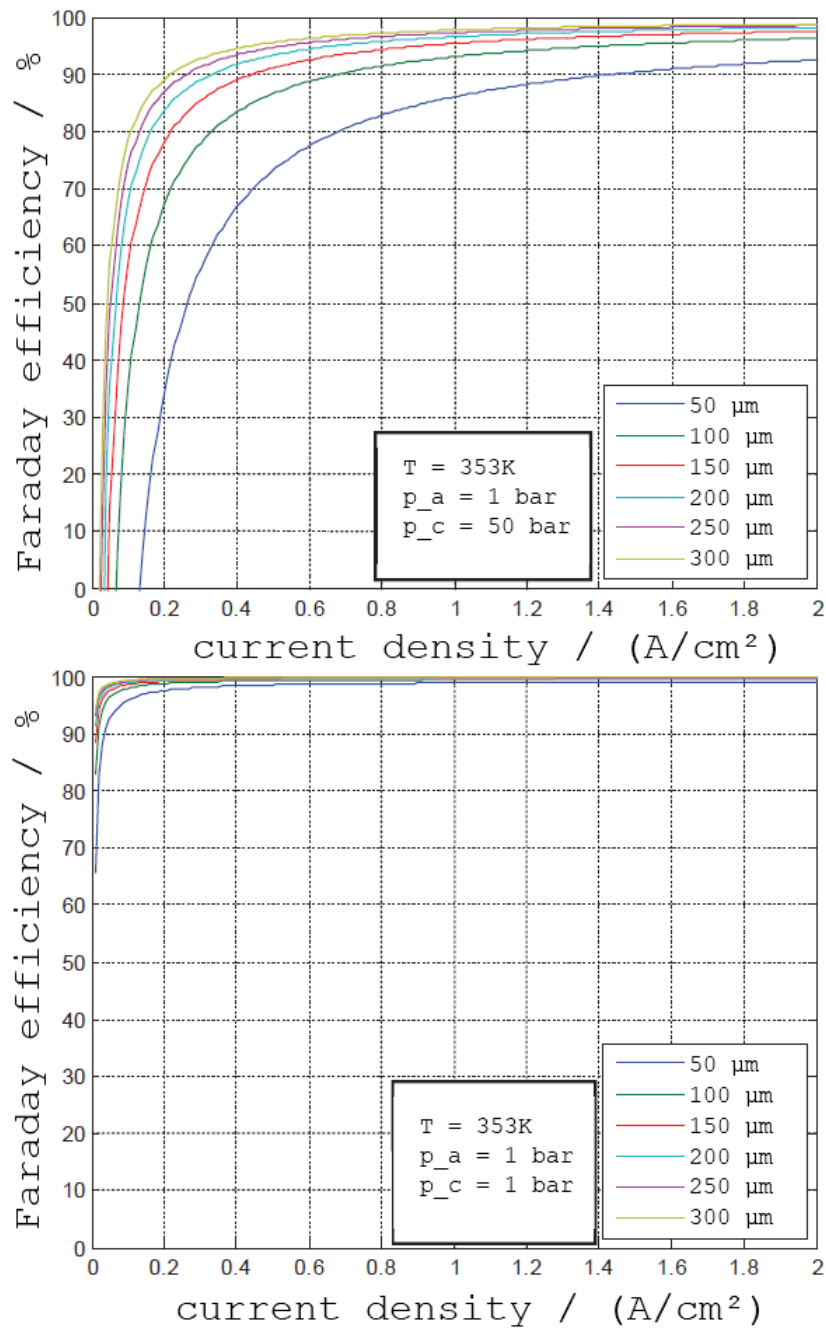
Figure 2.3: Two graphs showing the Faraday efficiency over the current density at two different cathode pressures. The lengths refer to the thickness of the membrane, general temperature and pressure settings are shown as well. Increased cathode pressures increase the gas crossover. [20]

2.2 Polymer Electrolyte Membrane

PE membranes are conducting for protons, but gases like hydrogen and oxygen can not be transported through it. This is why they are also referred to as proton exchange membranes. Nafion[®2] for example uses sulfonic acid groups with a negative polarity connected to a polytetrafluoroethylene (PTFE) backbone. They are therefor perfluorosulfonic-acid (PFSA) ionomer membranes. Those acid groups become surrounded by water molecules when the membrane is humidified. This allows protons to move from one acid group to the next. During WE mode, hydrogen can split its electron at the anode and donate it to the electrode, move through the membrane and reform at the cathode to molecular hydrogen. The basic structure of Nafion[®] is shown in figure 2.4.

The proton conductivity of the membrane depends on the humidification level of the membrane. Higher humidity leads to higher conductivity. This is the reason the water management is important to keep the humidification level high without flooding the electrode. However, this is also the reason why Nafion[®] generally can not be used for higher temperatures, because water begins to evaporate at around 100 °C depending on the pressure of the system.

Commercially available membranes are usually described by the membrane thickness and the equivalent weight (EW). The equivalent weight is the number of grams of dry Nafion[®] per mole of sulfonic acid groups. Generally speaking, lower EW values indicate a higher proton conductivity. [22] The thickness of the membrane influences the mechanical stability and the conductivity - thinner membranes have a lower stability, but also lower resistance.

For WE, thicker membranes are used. This increases the ohmic resistance of the membrane itself, but it gives higher mechanical stability - not only does WE often operate at increased cathode pressures and needs more mechanical strength compared to operation in FC mode, the developed gases can also cross over the membrane (see figure 2.3). If hydrogen is pushed through the PE membrane by the pressure difference, not only dangerous gas mixtures can form but also the product mass is decreasing with less hydrogen being storable.

---

[2]Nafion[®] is a commercially available PE membrane by DuPont de Nemours, Inc.
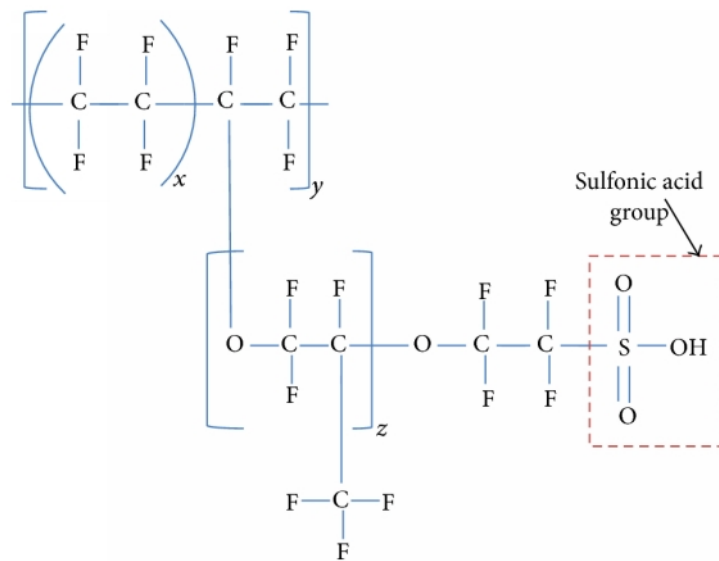
Figure 2.4: Structure of Nafion® with sulfonic acid group ($x = 5 - 13.5$, $y = 1000$, $z \geq 1$). [21]

2.2.1 Electrocatalyst

To increase the reaction rate, catalysts are needed at the electrodes. While for FC mode this can be platinum for both sides, WE mode requires a different catalyst on the anode - the oxygen side - for high efficiencies during OER. Iridiumdioxide and rutheniumdioxide are most commonly used, but also their unoxidized forms and mixtures are being researched. For the cathode - the hydrogen side -, platinum remains the most common electrocatalyst. Variations and mixtures do exist however.

Catalysts can be directly applied to the membrane or to the electrodes pressed onto the membrane. In the first variant, the connection to the membrane for the moving protons is better. Binder material - usually Nafion® mixed into the catalyst material - can improve the connection of the electrocatalyst to the membrane. The second shows a better electrical contact. Figure 2.5 shows an exemplary structure of electrocatalyst mixed with an ionomer binder.

Another important factor for the catalyst is the structure. The catalyst material needs to have a large surface in contact with the fuel and the membrane or electrode respectively. The TPB is the only area where the actual reaction takes place. This means that at some
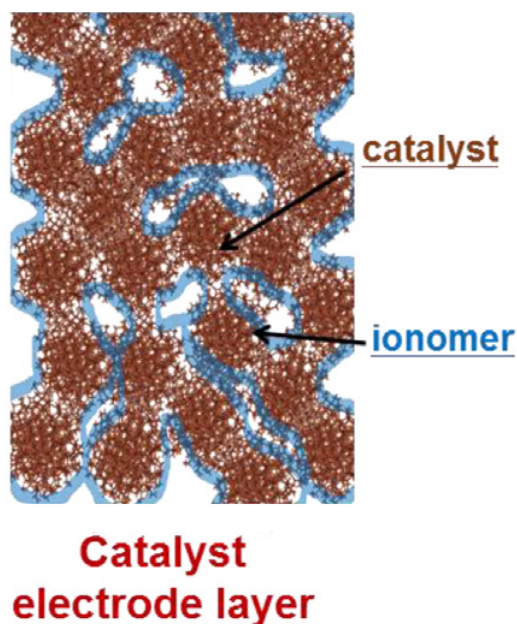
Figure 2.5: Exemplary structure of catalyst with ionomer binder. Based upon Artyushkova et al. [23]

point, a higher catalyst charge is not improving the efficiency anymore. Instead, catalyst material agglomerates and can even reduce the actual TPB area available. Binder is the mechanical support structure of the electrocatalyst and also serves as the connection of the catalyst particles to the membrane for the protons. Both the amount of catalyst and of binder influence the particle size, connectivity and mechanical stability. Careful evaluation of the optimized catalyst and binder charge has to be employed.

Kumar and Himabindu [24] found an anode charge of 0.2 to 0.8 mg/cm^2 platinum and a cathode charge of 1.0 to 3.0 mg/cm^2 iridiumoxides and rutheniumoxides including mixtures to be most commonly used for WE. Sambandam and Ramani [25] report an optimal Nafion$^®$ binder amount of 32 weight-% in the catalyst when dealing with most Nafion$^®$ membranes, depending on the equivalent weight, the mass of dry Nafion$^®$ per mole SO$_3^-$ when in acidic form. [26].

2.2.2 Reinforced Membranes for Fuel Cells and Electrolysis

In both FC and WE mode, thinner membranes do not only have disadvantages - the aforementioned mechanical stability and gas crossover -, but they also offer advantages

like lower ohmic resistance and lower material costs. For FC, they also offer an improved water transport. For WE, this is more of a disadvantage, since the supplied water might dissipate to the cathode in too large amounts.

Thinner membranes ($t_{\mathrm{m}} < 50$ µm) are especially asked for at high current densities, where the ohmic losses become more dominant over the activation losses caused by electrocatalysts. Membranes need to be improved against chemical, mechanical and thermal stresses. Chemical degradation results from free radicals and other reactive species, mechanical stresses from swelling by water content and variation in compression. Thermal stresses result from changes in the membrane temperature. All three effects, however, lead to issues with the mechanical stability, which can then lead to perforations, cracks, tears, or pinholes.

Several methods have been developed to increase the stability and durability of PE membranes: chemical cross-linking of the ionomer chains, chemical stabilization with additives to reduce chemical degradation, reinforcement with woven or expanded PTFE, other polymers or even inorganic fillers. [27]

Nafion® XL is a reinforced PFSA membrane with a microporous PTFE-rich reinforcement. This reinforcement layer still has a relatively high amount of Nafion® and has thin Nafion® layers on both sides which are dotted with silica particles. The total thickness is only $t_{\mathrm{m}} = 27.5$ µm which is significantly thinner than Nafion® 115 membranes at $t_{\mathrm{m}} = 127$ µm which are commonly used in WE. These reinforced membranes use both chemical additives (the silica particles for increased tensile strength) and a PTFE reinforcement layer for mechanical stability. The total contents are about 10% PTFE, 85% PFSA and 5% additive. An EW of 1100 g/mol is commonly used as well. [28]

Even though PTFE is not conductive for protons and is expected to have lower water uptake, the overall conductivity does not change significantly. The hydrogen crossover is slightly lower than for the thinner unreinforced Nafion® 211 membrane with a thickness of $t_{\mathrm{m}} = 25.4$ µm. The linear expansion due to water uptake is also lower. This can reduce stress during and between operation on the harnessed membrane, when the humidification level can change. The official datasheets for Nafion® XL and 211 are attached.

HAADF-STEM image of cross-sectioned MEA with Nafion XL membrane
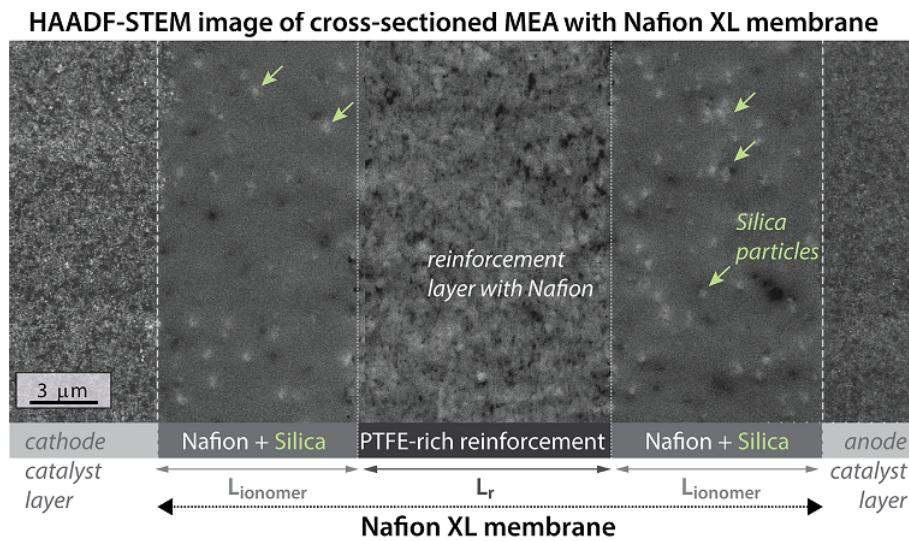
Figure 2.6: STEM image of Nafion® XL. [28] In this image, both the anode and the cathode catalyst layers are applied to the membrane. The microscope technique used is high-angle annular dark-field (HAADF) imaging with a scanning transmission electron microscope (STEM).

2.3 Water Management

Water transport through the PE membrane is mainly due to three different effects: electro-osmotic drag, transport due to pressure gradient and transport due to concentration gradient. The two major effects according to Medina and Santarelli [10] are electro-osmotic drag and pressure gradient, the concentration gradient was negligible in their experiments. However, to understand the details of water transport across the membrane, a closer look at the definitions of the important coefficients is necessary.

2.3.1 Definition of Transport Coefficients

Net water transport $\dot{m}_{\mathrm{net}}$ is described by the mass flows of the three effects according to equation (2.9). Usually a positive net mass flow means a flow direction from the anode to the cathode.

$$\dot{m}_{\mathrm{net}} = \dot{m}_{\mathrm{eo}} + \dot{m}_{\mathrm{p}} + \dot{m}_{\mathrm{co}} \,, \tag{2.9}$$

with $\dot{m}_{\mathrm{eo}}$ being the mass flow due to electro-osmotic drag, $\dot{m}_{\mathrm{p}}$ is the mass flow due to pressure gradient and $\dot{m}_{\mathrm{co}}$ is the mass flow due to concentration gradient.

The second important definition is that of the drag coefficient n_d. This value describes the amount of water molecules $\dot{n}$ transported through the membrane per proton. This covers all three transportation effects and is therefor based upon the net water transport and the amount of protons conducted through the membrane.

$$n_{\mathrm{d}} = \frac{\dot{n}_{\mathrm{H_2O}}}{\dot{n}_{\mathrm{H+}}} \,. \tag{2.10}$$

Another value that is close to the drag coefficient and often gets mixed up with it is the electro-osmotic drag coefficient n_{eo}. This value only covers the electro-osmotic drag and can behave differently from the drag coefficient with changing parameters. It contributes to the drag coefficient.

$$n_{\mathrm{eo}} = \frac{\dot{n}_{\mathrm{H_2O,eo}}}{\dot{n}_{\mathrm{H+}}} \,. \tag{2.11}$$

According to equation (2.3) the stoichiometry of H:O in the produced gas is 2:1. In theory, one could feed one mole of water into the electrolysis cell and receive two moles of atomar hydrogen (or one mole of molecular hydrogen) and one mole of oxygen (or half a mole of molecular oxygen). However, electrolysis cells are usually operated over-stoichiometric. The TPB needs not only to be supplied with water, but the PE membrane also has to be humidified. There are also imponderable flow effects through the electrodes of the MEA, mainly due to different mass flows through the bipolar plates, generated gas bubbles and inhomogeneous porous transport layers (PTL). The PTLs allow transport to and away from the TPB. On the cathode, they are often referred to as gas diffusion layers (GDLs), because in WE mode there are only gaseous participants in the reaction.

Inhomogeneous water distribution in the TPB can cause local starvation and therefor inhomogeneous current distributions. This can lead to local drying and potentially "hot spots" elsewhere in the membrane and mechanical stresses due to inhomogeneous swelling of the membrane. Electrolyzer failure is the worst case incident. To protect the PE membrane from these effects, there is more water fed into the anode side than is actually consumed in the reaction. [14] The factor is called water stoichiometry ξ:

$$\xi = \frac{\dot{m}_{\mathrm{H_2O,feed}}}{\dot{m}_{\mathrm{H_2O,cons}}} \,. \tag{2.12}$$

At the same time, though, the TPB is not to be fed with too much water. An increasing water velocity can not only increase pressure drop but even damage the MEA, the flow regime has a significant impact on the efficiency by changing the water access to the TPB. Higher velocities can therefor lead to lower efficiencies. [29]

Figure 2.7 shows the MEA including the in- and outlet flows, the relative concentrations at both electrodes (hydrogen at the cathode and oxygen at the anode) and the mass transport effects of water across the membrane. Note that especially the concentration of the gas-liquid-mixture can change depending on the water inflow and the amount of product gas. In industrial applications, there is usually no water inflow on the cathode side. This is included here because it is considered for the Re-Flex project.

2.3.2 Concentration Gradient

The different concentrations of water on the two sides of the membrane - cathode and anode - lead to the water transport mechanism due to a concentration gradient. Different concentrations always lead to a mass flow trying to achieve equilibrium, called diffusion. The mass flow $\dot{m}_{\mathrm{co}}$ can be described using Fick's first law of diffusion:

$$\dot{m}_{\mathrm{co}} = D_{\mathrm{w}} * \frac{C_{\mathrm{a}} - C_{\mathrm{c}}}{t_{\mathrm{m}}} * A * M_{\mathrm{H_2O}} \,, \tag{2.13}$$

with D_{w} being the dimensionless water diffusion coefficient, C_{a} and C_{c} the concentrations of water on the anode and cathode side respectively, t_{m} the membrane thickness, A the cell area and $M_{\mathrm{H_2O}}$ the molar mass of water.

The water diffusion coefficient D_{w} can be described following Dutta et al. [30] by:

$$D_{\mathrm{w}} = D_{\lambda} * e^{\left(2416\ \mathrm{K} * \left(\frac{1}{303\ \mathrm{K}} - \frac{1}{T_{\mathrm{cell}}}\right)\right)} \,, \tag{2.14}$$

where T_{cell} is the cell temperature and D_{λ} the diffusion coefficient of the membrane taking into account its dimensionless water content λ.
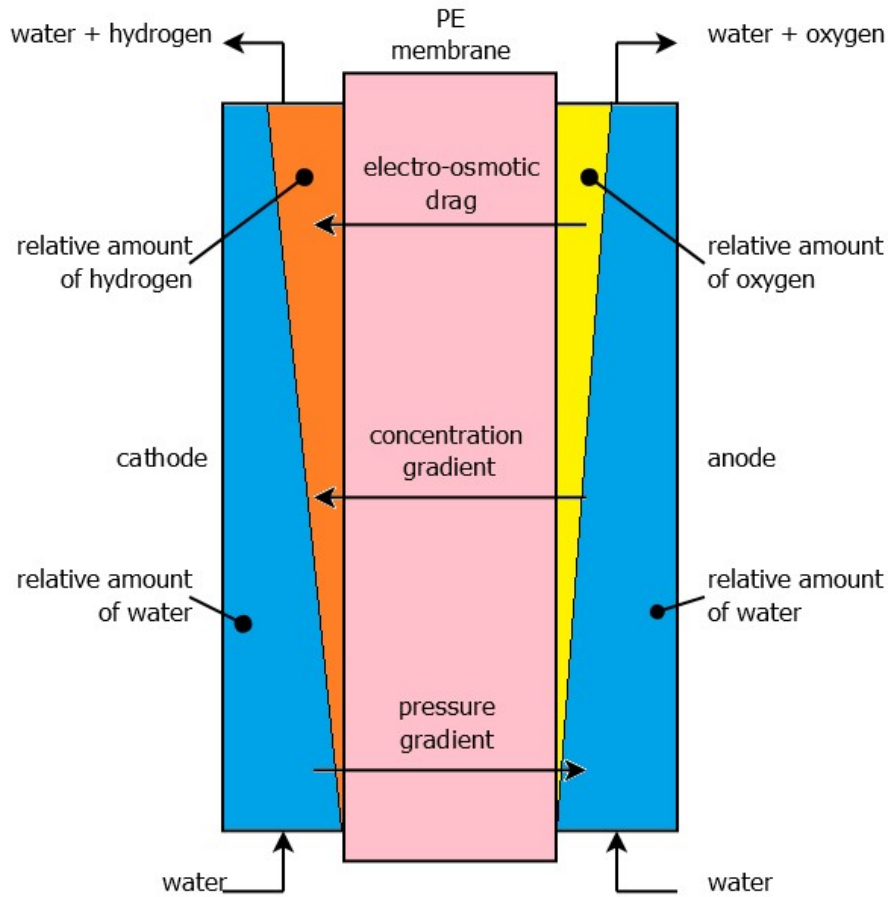
Figure 2.7: The water transport mechanisms including the relative concentrations of the supplied water and the product gases inside the electrodes. The direction of the electro-osmotic drag is fixed during WE, the transport due to pressure gradient too, since the pressure is amplified only on the cathode. The concentration gradient transport corresponds to the sketched relative concentrations, but this can change with the operating parameters.

After Dutta et al. [30], it can be calculated using:

$$D_\lambda = (m^2/s) \begin{cases} 10^{-10}, & \lambda < 2 \\ 10^{-10} * (1 + 2(\lambda - 2)), & 2 \leq \lambda \leq 3 \\ 10^{-10} * (3 - 1.67(\lambda - 3)), & 3 < \lambda < 4.5 \\ 1.25 * 10^{-10}, & \lambda \geq 4.5 \end{cases} . \tag{2.15}$$

The water content on both sides of the membrane is different, so the average value will be taken to calculate the diffusion coefficient of the membrane.

The concentrations C of water on the anode and cathode side also depend on the water content and are calculated using:

$$C = \frac{\rho_{\mathrm{m,dry}}}{M_{\mathrm{m,dry}}} * \lambda . \tag{2.16}$$

$\rho_{\mathrm{m,dry}}$ is the density of the dry membrane, $M_{\mathrm{m,dry}}$ the molar mass. Since the latter is a complex structure and depends on manufacturing processes, it is often substituted by EW. λ is the water content on both sides respectively and depends on the water activity a.

$$\lambda = \begin{cases} 0.043 + 17.81 * a - 39.85 * a^2 + 36 * a^3, & 0 < a \leq 1 \\ 14 + 1.4 * (a - 1), & a > 1 \end{cases} . \tag{2.17}$$

Water activity a above 1 indicates liquid water, below 1 indicates gaseous water content. The water activity a can be calculated using:

$$a = x_{\mathrm{w}} * \frac{p_{\mathrm{H_2O}}}{p_{\mathrm{s}}} \tag{2.18}$$

with $p_{\mathrm{H_2O}}$ being the partial water pressure and p_{s} the saturation pressure of water at the corresponding temperature T. x_{w} is the molar water content on the corresponding electrode.

There are many approximating equations for the saturation pressure, for example the Magnus equation:

$$p_{\mathrm{s}} = f(T) = 0.61094 \text{ kPa} * e^{\frac{17.625 * T}{T + 243.03 \text{ K}}} . \tag{2.19}$$

Here, the resulting value for the saturation water pressure is given in kPa and the temperature needs to be in °C.

The molar water content is described by:

$$x_\text{w} = \frac{\dot{n}_{\text{H}_2\text{O}}}{\dot{n}_\text{tot}} = \frac{\dot{n}_{\text{H}_2\text{O}}}{\dot{n}_{\text{H}_2\text{O}} + \dot{n}_\text{gas}} \,. \tag{2.20}$$

$\dot{n}$ is the molar flow of water or gas respectively. [10] The averages can be assumed here, when the gas generation and the water transport effects through the membrane are considered homogeneous over the area of the membrane.

Generally, the water activity a ranges from 0 to 1 when in contact with partly vaporous water. $a = 0$ means no water available, $a = 1$ means start of fully liquid water. The water content λ calculated by equation (2.17) results in a range of 0 to 14 respectively. However, when operated clearly above the condensing threshold - the partial pressure being larger than the saturation pressure and corresponding high water content x_w -, the water content λ in the membrane behaves differently, increasing more slowly. Evaluation of the exact state of water on the sides of the membrane has significant impact on the transport behavior, but is difficult to investigate.

It needs to be added that especially the formulae for the water diffusion coefficient D_w and the water content of the membrane λ are assumptions for Nafion® 115 membranes. [10]

2.3.3 Pressure Gradient

WE systems often apply an increased pressure level on the cathode side. Hydrogen is usually stored in pressurized vessels and electrical compression requires energy. Chemical compression has lower hindrances. Hydrogen evolves on the cathode side even at elevated pressures and can be directly stored or compressed electrically with less energy consumption. The anode, however, is usually kept at pressures close to atmospheric pressure. These two different pressure levels at cathode and anode create a pressure gradient over the membrane. Since membranes for WE are usually in the range of tens or hundreds of micrometers thick but the pressure gradient can be up to several tens

of bars, there is a strong hydraulic resistance for the water molecules moving with the protons.

The water percolation caused by a pressure gradient is described by Darcy's law:

$$\dot{m}_{\mathrm{p}} = \rho * A * \frac{K_{\mathrm{D}}}{\mu} * \nabla p \,. \tag{2.21}$$

In this formula, $\dot{m}_{\mathrm{p}}$ is the mass flow due to the pressure gradient, ρ the density of water, A the area of the cell, K_{D} the Darcy constant, μ the dynamic viscosity and ∇p the pressure gradient. Since the gradient is one-dimensional, ∇p is Δp, the pressure difference between cathode and anode $(p_{\mathrm{a}} - p_{\mathrm{c}})$. Therefor in this form, a positive water flow occurs from the anode towards the cathode.

The dynamic viscosity μ of water is only dependent on the temperature T based on Birgersson et al. [31]:

$$\mu = 0.6612 \,\mathrm{Pa} * \mathrm{s} * (T - 229 \,\mathrm{K})^{-1.562} \,. \tag{2.22}$$

The Darcy constant K_{D} describes the permeability of the membrane and is closely related to the porosity ϵ. Even though Nafion® membranes are not porous in general, they behave like porous materials when in contact with water. Oosthuizen et al. [32] have examined this correlation. For specific membranes, it might be necessary to extrapolate based on table 2.1 and the resulting fitting equation:

$$K_{\mathrm{D}} = 4.71 * 10^{-5} \,\mathrm{m}^2 * \epsilon^{37.39} \,. \tag{2.23}$$

porosity ϵ	[-]	0.05	0.4	0.6	0.66	0.7
permeability/K_{D}	[m^2]	10^{-53}	10^{-19}	10^{-13}	10^{-11}	10^{-10}

Table 2.1: The correlation between the porosity of the PE membrane and the permeability/Darcy constant K_{D} based on Oosthuizen et al. [32]

2.3.4 Electro-osmotic Drag

Electro-osmotic drag occurs when protons move through the humidified PE membrane. It is dependent on the humidification ratio of the membrane, which describes the ratio of SO_3^- groups and water molecules inside the membrane. The calculations assume a fully humidified membrane. This is the major difference to fuel cell systems - due to the

presence of liquid water in WE cells, the humidification of the membrane is higher and increases the number of water molecules dragged by the protons. Based on equation (2.11) the calculation can be expressed by:

$$n_{\text{eo}} = \frac{\dot{n}_{\text{H}_2\text{O,eo}}}{\dot{n}_{\text{H}^+}} = \frac{\dot{m}_{\text{H}_2\text{O,eo}} * M_{\text{H}^+}}{\dot{m}_{\text{H}^+} * M_{\text{H}_2\text{O}}} = \frac{\dot{m}_{\text{H}_2\text{O,eo}} * M_{\text{H}_2}}{\dot{m}_{\text{H}_2} * M_{\text{H}_2\text{O}}} \tag{2.24}$$

or using the definition based on the number of protons $\dot{n}_{\text{H}^+}$, the mass flow of water by electro-osmotic drag:

$$\dot{m}_{\text{eo}} = n_{\text{eo}} * M_{\text{H}_2\text{O}} * \dot{n}_{\text{H}^+} \,. \tag{2.25}$$

Here $\dot{n}$ is the molar flow and $\dot{m}_{\text{eo}}$ the mass flow of water through the membrane due to electro-osmotic drag, with $M_{\text{H}_2\text{O}}$ being the molar mass of water. n_{eo} describes a factor as mentioned in equation (2.11) and is usually found experimentally as will be further shown in chapter 2.3.5.

The flow can only move with the protons - during WE from the anode to the cathode.

2.3.5 State of the Art

Currently, the water behavior in fuel cells is well researched, mainly due to its high relevance in transportation systems. [33–35] For water electrolysis, however, there are fewer studies available and often not as detailed. WE usually operates in stationary systems at high power and the water management is not the biggest price driver. Water management can play an important part in reaching highest efficiencies though.

Onda et al. [12] analyzed the electro-osmotic drag experimentally by varying the membrane temperature T at a constant current density i. Pressure is set as atmospheric. Water is fed only to the anode. They did not go into details of their analyses and stated a formula for the electro-osmotic drag:

$$n_{\text{eo}} = 0.0134 * T + 0.03 \,. \tag{2.26}$$

Awasthi et al. [15] developed a model and simulated different operating conditions for a PEM water electrolyzer. The drag coefficient n_d is one result of their simulation. Temperature T varies between 40 and 80 °C and cathode pressure p_{c} between 1 MPa and 10 MPa.

$$n_d = 5 \,. \tag{2.27}$$

Medina and Santarelli [10] did the most extensive research on water management and electro-osmotic drag in WE mode so far. Several papers refer to their solutions. They did an experimental research and measured water flows at different cathode pressures p_c, current densities i and temperatures T. This way they developed a sophisticated model for the total drag coefficient n_d and the electro-osmotic drag coefficient n_{eo}:

$$\begin{aligned} n_d =& 2.27 - 0.70 \ (\mathrm{A/cm}^2)^{-1} * i - 0.02 \ \mathrm{bar}^{-1} * p_c + 0.02 \ (\mathrm{bar} * \mathrm{A/cm}^2)^{-1} * i * p_c + \ ... \\ & ... \ + 0.003 \ {}^\circ\mathrm{C}^{-1} * T + 0.005 \ ({}^\circ\mathrm{C} * \mathrm{A/cm}^2)^{-1} * i * T - 0.0002 \ ({}^\circ\mathrm{C} * \mathrm{bar})^{-1} * T * p_c \,. \end{aligned} \tag{2.28}$$

$$n_{eo} = 0.0252 \ \mathrm{bar}^{-1} * p_c - 1.9073 \ (\mathrm{A/cm}^2)^{-1} * i + 0.0189 \ \mathrm{K}^{-1} * T - 2.7892 \,.^3 \tag{2.29}$$

There are still several limitations to their model. First, they only varied temperature T between 45 and 55 °C, the pressure p_c between 7 and 70 bar and the current density i between 0.25 and 1 A/cm². Also, they assumed a linear behavior between each of these two measurement points. The validity especially outside of the limits of their application is to be considered carefully.

Assuming for example one use case for the Re-Flex project in table 2.2. While the result for the drag coefficient n_d seems possible, the electro-osmotic drag coefficient n_{eo} is obviously incorrect. It can only be positive by definition. Especially the high current density does not comply with the use limits of these models and therefor needs another, more detailed look for proper water management.

Another important note ist, that according to their findings the electro-osmotic drag coefficient is anti-proportional to the current density, indicated by the negative factor in equation (2.29). This might seem counter intuitive at first, but it needs to be remembered that this is only the amount of water molecules per proton. Since the amount of protons still increases with higher current densities, the net amount of water dragged by electro-osmosis might still increase. A possible explanation is the hindrance of water molecules being dragged by the protons because there are too many protons in the membrane. If this behavior is assumed to be linear, obvious errors as in table 2.2 can occur.

---

[3]Formula taken from Ommi et al. [13], data originates from Medina and Santarelli [10].

parameter	abbr.	unit	value
cathode pressure	p_c	bar	6
membrane temperature	T	K	353.15
current density	i	A/cm^2	3
drag coefficient	n_d	-	1.75
electro-osmotic drag coefficient	n_eo	-	-1.69

Table 2.2: Calculation of drag coefficient n_d and electro-osmotic drag coefficient n_eo for an extreme use case according to the Re-Flex project, taken from the project application. The formulae used are equations (2.28) and (2.29).

A non-linear relationship of the electro-osmotic drag coefficient is possible and will be examined at high current densities of up to 5 A/cm^2 in this work.

3 Test Setup

In this chapter the test stand and the general setup are described. The test stand is developed to allow an upgrade to consecutive FC and WE mode, while for this work the test stand only operates in WE mode. A flow chart for the complete test stand is attached.

3.1 Test Stand

Figure 3.1 shows the flowchart of the test stand. It consists of a quick connecting system[4] which has a cell holding including MEA, flowfields, sealing, in- and outlet and possibly a connection for a cooling circuit and an electrical heater. The cells can be prepared in quick connectors which can then for the tests be inserted into the quick connecting system. There, a piston driven by pressurized air holds the quick connector with the cell and guarantees water-tightness. The in- and outlet tubes and the electrical cables can remain connected to the quick connecting system, only the sense cables for measuring the actual voltage and current have to be linked. Detailed pictures of the test stand including the descriptions are attached.

The hydrogen side - during WE acting as the cathode - has a supply of water. Since the cathode side is not splitting water into its atoms, this is mainly to keep the membrane moistened and is rather low. A small dosing pump, which controls the amount of strokes per minute with a defined volume, acts as the supplier and the flow meter at the same time. The water supply comes from the bottom of the cell.

The outlet of the produced hydrogen - along with the water from the supply and from the anode side through the membrane - is at the top side. This way interference of the hydrogen outflow with gravity is to be minimized: Gases need to exit at the top.[5] The hydrogen gas flows to a back pressure regulator which controls the cathode pressure and

---

[4]Delivered by balticFuelCells GmbH, Germany.

[5]The same goes vice versa for FC mode, where the excess water - fed with both hydrogen and oxygen to humidify the membrane - needs to flow out at the bottom of the cell.
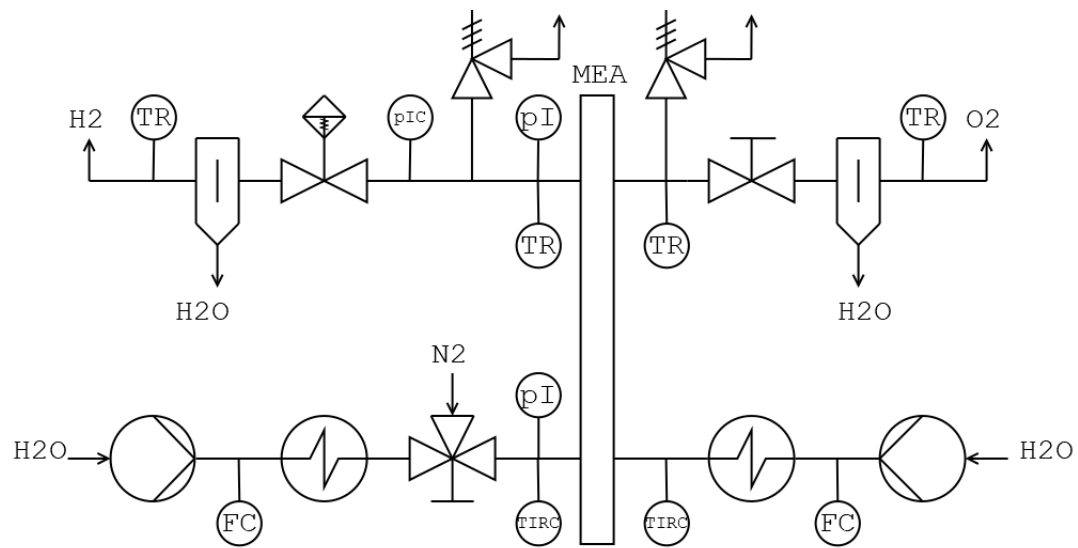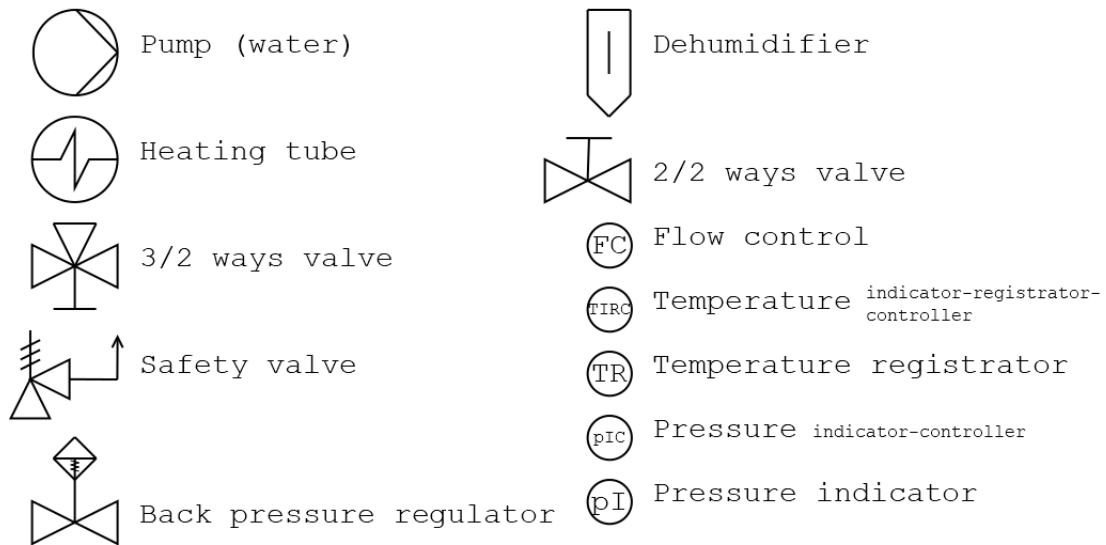
Figure 3.1: Flowchart of the test stand for WE. The MEA is shown in the middle, the liquid inflows are on the lower part of the cell and the gaseous outflows at the top. Only the cathode side is kept under pressure by the back pressure regulator. Information connectors are not included for clarity reasons.

reduces it to roughly atmospheric pressure. Afterwards the hydrogen gas flows into a phase-separating dehumidifier and is released into the fume hood.

The oxygen side - during WE mode the anode - is also supplied by water at the bottom of the cell. Since the anode side is run at near atmospheric pressure, a peristaltic pump is being used. This pump works with a flexible tube which gets contracted by rotating "shoes" and displaces a specific amount of water per turn. It can not apply the pressures of a dosing pump, but the output is smoother and can be varied over a broader range. Since this pump also moves a specific amount of water per turn, an external flow meter is not needed.

The outflow of the anode consists of a phase-separating dehumidifier after which the oxygen is also released into the fume hood.

Both the inflows are also running through heating tubes. Since the temperature of the process is to be controlled and the electric heater of the quick connecting system alone might not result in a homogeneous temperature distribution over the MEA, both water supplies are preheated right before entering the cell.

The nitrogen is for purging to ensure reproducible test conditions. Deionized (DI) water is used to prevent degradation of the electrocatalysts and the PE membrane. While tap water generally has a conductivity of about 0.005 to 0.05 S/m, the tap water used is deionized to achieve a conductivity below 7.0 µS/m.

For safety reasons, two remarks have to be added: First, the amounts of hydrogen and oxygen are very small according to the values described in the following section 3.1.1 and even though both hydrogen and oxygen are released into the fume hood,an explosion due to a critical atmosphere is not likely to happen.

Second, whereas it is planned to only run the cathode side at a higher pressure, pressure relief valves are added to both sides in case of malfunctioning control valves. This prevents over-pressure and damage to the membrane and the quick connecting system.

The measured values and the corresponding measurement devices can be seen in table 3.1. Whereas temperature, pressure, current (or voltage) and water inflows are set to fixed values during experiments, voltage (or current) and the outflows of water, hydro-

monitored parameter	abbreviation	measurement devices
temperature membrane	T	T-sensor quick connecting system
pressure cathode	p_c	back pressure regulator (or p-gauge)
water flow anode inlet	$\dot{m}_\mathrm{a,in}$	peristaltic pump
water flow cathode inlet	$\dot{m}_\mathrm{c,in}$	dosing pump
water flow anode outlet	$\dot{m}_\mathrm{a,out,l}$	water storage behind dehumidifier
water flow cathode outlet	$\dot{m}_\mathrm{c,out,l}$	water storage behind dehumidifier
water content H_2 outflow	$\dot{m}_\mathrm{c,out,g}$	temperature sensor dehumidifier
water content O_2 outflow	$\dot{m}_\mathrm{a,out,g}$	temperature sensor dehumidifier
voltage	U	potentiostat
current	I	potentiostat

Table 3.1: The necessary values including the measurement positions or measurement for the calculation. The gas flows can be calculated using current and voltage according to equations (3.3) and (3.4).

gen and oxygen are the relevant measured values. The water is split into a liquid and a gaseous part in the dehumidifiers. The liquid part can be gathered in the dehumidifier and a storage basin, the gaseous part is released into the fume hood together with the gas it is soluted in (hydrogen or oxygen, respectively).

3.1.1 Calculation of the Design Mass Flows

For choosing pumps, tubes and the whole water analysis, the relevant mass flows (water at in- and outlet, hydrogen outlet and oxygen outlet) have to be determined. The gas production can be calculated using Faraday's second law:

$$m = \frac{I * t * M}{\mathrm{F} * k}, \tag{3.1}$$

with m being the mass of the produced substance, I the current, t the time span, M the molar mass of the produced substance, F the Faraday constant (F = 96485.33 C/mol) and k the number of participating electrons in the reaction (according to section 2.1: $k = 2$). The Faraday efficiency is assumed to be unity, which is reasonable according to Tijani and Rahim [20] at high current densities, low electrode pressures and thick PE membranes.

Since the current density i is a relevant parameter to be changed and the area A is known, the current I can be calculated. For the maximum current density $i_{\max} = 5$ A/cm^2 the result is:

$$I = i * A \Rightarrow I_{\max} = i_{\max} * A = 5 \text{ A/cm}^2 * 4 \text{ cm}^2 = 20 \text{ A} \,, \tag{3.2}$$

Over the time span of one hour $t = 3600$ s, the following mass of hydrogen ($M_{\mathrm{H_2}} = 2.02$ g/mol) would therefor be generated:

$$m_{\mathrm{H_2}} = \frac{I * t * M_{\mathrm{H_2}}}{\mathrm{F} * k} = \frac{20 \text{ A} * 3600 \text{ s} * 2.02 \text{ g/mol}}{96485.33 \text{ C/mol} * 2} = 0.75 \text{ g} \,, \tag{3.3}$$

For oxygen ($M_{\mathrm{O_2}} = 32.00$ g/mol) the result needs to be divided by an additional factor of $f = 2$, because also according to section 2.1 the chemical reaction only generates half a molecule O_2:

$$m_{\mathrm{O_2}} = \frac{I * t * M_{\mathrm{O_2}}}{f * \mathrm{F} * k} = \frac{20 \text{ A} * 3600 \text{ s} * 32.00 \text{ g/mol}}{2 * 96485.33 \text{ C/mol} * 2} = 5.97 \text{ g} \,, \tag{3.4}$$

The same formula applies for the consumed water $m_{\mathrm{H_2O,cons}}$ with $M_{\mathrm{H_2O}} = 18.02$ g/mol:

$$m_{\mathrm{H_2O,cons}} = \frac{I * t * M_{\mathrm{H_2O}}}{\mathrm{F} * k} = \frac{20 \text{ A} * 3600 \text{ s} * 18.02 \text{ g/mol}}{96485.33 \text{ C/mol} * 2} = 6.72 \text{ g} \,, \tag{3.5}$$

However, this is not the total mass of water needed at the anode. According to section 2.3, the water transported through the membrane according to the drag coefficient n_{d} as well as the amount to secure full humidification of the membrane following the stoichiometry ξ needs to be added. The worst case for the drag effect in the analyzed literature is set by Awasthi et al. [15]:

$$n_{\mathrm{d}} = 5 \,. \tag{3.6}$$

This is the amount of water molecules dragged per proton according to equation (2.10). Per hydrogen molecule H_2 the value has to be doubled. This can become useful in WE, because hydrogen molecules get pushed through the membrane as the gas crossover. Also the amount of moles of water per hydrogen molecule is the same.

For the stoichiometry of water ξ Ito et al. [29] recommends a value of:

$$\xi = 5 \,. \tag{3.7}$$

This way the worst case scenario for the needed water supply on the anode side can be calculated as:

$$m_{\mathrm{H_2O,tot}} = m_{\mathrm{H_2O,cons}} * (2 * n_d) * \xi = 6.72 \text{ g} * (2 * 5) * 5 = 336.18 \text{ g} \qquad (3.8)$$

or as the mass flow $\dot{m}_{\mathrm{H_2O,tot}}$:

$$\dot{m}_{\mathrm{H_2O,tot}} = \frac{m_{\mathrm{H_2O,tot}}}{t} = \frac{336.18 \text{ g}}{3600 \text{ s}} = 336.18 \text{ g/h} = 5.60 \text{ g/min} = 0.09 \text{ g/s}. \qquad (3.9)$$

Most likely his value is not the actually needed water mass flow at the anode. Several papers suggest a lower drag coefficient n_d and the stoichiometry ξ also includes a safety factor. However, the pump needs to be designed for the worst case scenario and therefor the maximum amount of water until this work can give a more detailed prediction of the water management necessary in the relevant state of operation.

3.1.2 Calculation of Heating Tube Power

The test stand uses DI water with low conductivity stored in a storage tank. The water can therefor be assumed to have room temperature $T_{\mathrm{in}} = T_{\mathrm{r}} \approx 20\,^\circ\mathrm{C}$. The desired water temperature T_{out} is set to be up to $80\,^\circ\mathrm{C}$. The heating tubes are supposed to preheat the water to this value. The heat capacity of DI water is almost the same as of mineralized water, $c_{\mathrm{p}} \approx 4184 \text{ J/(kg} * \text{K)}$. The necessary heating power $\dot{Q}$ can be calculated using:

$$\dot{Q} = \dot{m} * c_{\mathrm{p}} * \Delta T = \dot{m} * c_{\mathrm{p}} * (T_{\mathrm{out}} - T_{\mathrm{in}}). \qquad (3.10)$$

With the expected maximum mass flows from section 3.1.1 the power necessary for both the anode and cathode supply can be calculated. For the anode:

$$\begin{aligned}
\dot{Q}_{\mathrm{H_2O,a}} &= \dot{m}_{\mathrm{a}} * c_{\mathrm{p}} * (T_{\mathrm{out}} - T_{\mathrm{in}}) \\
&= 336.18 \text{ g/h} * 4184 \text{ J/(kg} * \text{K)} * (80 - 20) \text{ K} = 23.44 \text{ W} \qquad (3.11)
\end{aligned}$$

is used and for the cathode:

$$\begin{aligned}
\dot{Q}_{\mathrm{H_2O,c}} &= \dot{m}_{\mathrm{c}} * c_{\mathrm{p}} * (T_{\mathrm{out}} - T_{\mathrm{in}}) \\
&= 10 \text{ g/min} * 4184 \text{ J/(kg} * \text{K)} * (80 - 20) \text{ K} = 41.84 \text{ W}. \qquad (3.12)
\end{aligned}$$

Heating tubes are usually classified in power per meter (W/m) and range from $100 - 120$ W/m. An exemplary data sheet is included in the attachments. Since the tubes are

also used for flexible connection of the water pumps to the cell quick connector, a length of one meter is chosen.

This way, the internal heater of the quick connector system only has to provide necessary heat for holding the temperature level.

3.2 Membrane Electrode Assembly

An MEA with an area of 4 cm^2 is used. This poses the question whether the efficiencies and the water management effects of small cells will be comparable to bigger cells. Many researches are using bigger areas of 25 cm^2 or even 160 cm^2 [10]. There are few results concerning water management comparing smaller and bigger MEAs. However, there are researches dealing with efficiencies of MEAs with different sizes. Usually the bigger the area, the higher the efficiency becomes. It is interesting to note that stacks also seem to become more efficient the more cells are built in series. [36] Larger areas reduce the inhomogeneous MEA parts at the edges of the MEA. Stacks might benefit from improved heat usage and lower contact resistance. Since this work does not focus on efficiency analysis, the effect has to be remarked but does not necessarily influence the results.

Since this work deals with high current densities and low pressure gradients (only pressure losses from the tubes and auxiliaries), thinner membranes are used. Nafion$^®$ 211 is chosen, with the equivalent weight $EW = 1100$ g/mol and the thickness $t_m = 1$ µin $\approx$ 25.4 µm.

On the cathode side, a platinum covered carbon paper GDL is used. This allows hydrogen to access the membrane surface as well as leaving it and has a low electrical resistance. The used GDL delivered by Paxitech[6] is already charged with the elctrocatalyst platinum. The amount is 0.5 mg of platinum per cm^2.

On the anode side, a porous transport layer (PTL)[7] made from titan fleece is implemented. During electrolysis carbon would degrade quickly forming carbon dioxide due to occurring high potentials (>1.8V). [37] Porous titanium layers made from micro fibers

---

[6]Paxitech SAS, insolvent since 2017 as of 06.09.2019.
[7]PTLs include GDLs, but the latter is generally specified for gases.
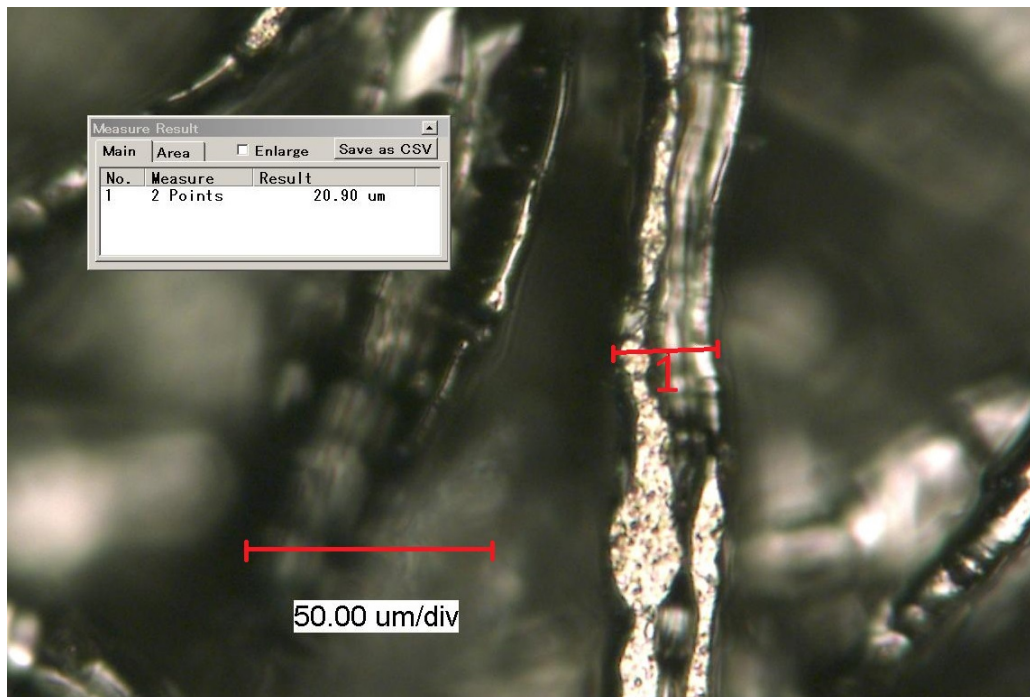
Figure 3.2: Microscopic shot of the surface of the used titanium fleece. An exemplary fiber diameter is shown, the scale bar is 50 µm long.

allowwater and oxygen to cross and have a low electrical resistance while being chemically stable. The commercially available PTL[8] used has a thickness of $t_{\mathrm{PTL}} = 1$ mm and a porosity of $\epsilon = 56$ %. Figure 3.2 shows a microscopic view of this titanium fleece. Most fiber diameters range around 20 µm.

The PTL on the anode side has no pre-charge of electrocatalyst. The membrane needed to be covered by it. Iridium dioxide is used with a Nafion® binder. After drying this allows the electrocatalyst on the membrane surface to develop a large surface for the fuel water and contact to both the membrane material for high TPB area as well as to the electrode for proper electrical connection.

The flowfields on both sides are milled into the titanium electrical contact surfaces. A counter flow of water is usually preferable due to better educt concentration distribution. The test stand is supposed to get upgraded to consecutive WE and FC mode. During FC mode, water stagnation especially in the anode can become problem. Therefor a

---

[8]2GDL40-1,0, NV Bekaert NA, www.bekaert.com

parallel flow is being used allowing liquid water to flow out more easily during FC mode and gas (hydrogen and oxygen) to exit at the top.

3.2.1 Preparation of the Membrane Electrode Assembly

The MEA only needs catalyst on the anode side. The catalyst with Nafion® binder material is sprayed onto the PE membrane. For this, the catalyst with binder needs to be in a liquid solution. The proper amount of catalyst is mixed with the Nafion® binder and with a water-isopropanol solution of about 7 parts water and 1 part isopropanol. Isopropanol acts as a dispersant for the iridiumoxide. It then needs to be homogenized by dispersing in an ultrasonic bath for up to one hour, then the mixture is left on a magnetic stirrer over night.

The next day, the now homogenized ink is filled into a spraygun. The sprayer works with argon as a carrier gas which sucks the ink from the container and sprays it as a very thin film onto the PE membrane. The membrane is fixed with a mask on a heated plate and an infrared light is set above the membrane. The heating and the infrared light are supposed to dry out the membrane between each sprayed layer to avoid too high humidification of the membrane which would then deform and lead to inhomogeneous catalyst distribution. The mask defines the catalyst area, 2.6 cm times 2.6 cm in this case for a 4 cm^2 area to be tested. This allows some flexibility to place the membrane on the electrodes. The ink is sprayed in several thin layers until the whole material is used up.

The calculation of the catalyst loading is then done using a reference membrane. A small reference membrane is cut, measured and weighed and then set next to the PE membrane to be sprayed. It is covered in roughly the same way as the PE membrane. After the spraying and a one hour drying process, the reference membrane is weighted again and the difference in weight corresponds to the catalyst and binder mass.

$$m_{\mathrm{IrOx,ref}} = (m_{\mathrm{after}} - m_{\mathrm{before}}) * f_{\mathrm{w-\%,IrOx}} . \tag{3.13}$$

The masses m are weighed before and after the full spraying process. $f_{\mathrm{w-\%,IrOx}}$ is the percentage of iridiumoxide in the catalyst-binder material, 1 minus the defined binder weight percentage:

ingredient	amount
iridiumoxide (99.99 %)	0.0718 g
Nafion® binder	0.1919 g suspension, 0.0109 g solid
H$_2$O	3 ml
$1:1-$ isopropanol : H$_2$O	1 ml

Table 3.2: Exemplary ingredients resulting in an ink for $\rho_{\mathrm{A,IrOx}} = 1.06$ mg/cm^2 iridiumoxide, 87 weight-% iridiumoxide and about 13 weight-% Nafion® binder on the sprayed PE membrane.

$$f_{\mathrm{w-\%,IrOx}} = 1 - f_{\mathrm{w-\%,binder}} \, . \tag{3.14}$$

This results in the real mass of iridiumoxide on the reference area $m_{\mathrm{IrOx,ref}}$. The area is not equal to the sprayed membrane area and the charge is usually defined as a value per area. Dividing the reference mass of iridiumoxide by a defined area gives the specific loading per area:

$$\rho_{\mathrm{A,IrOx}} = \frac{m_{\mathrm{IrOx,ref}}}{A_{\mathrm{ref}}} \tag{3.15}$$

with the reference area A_{ref}.

An exemplary calculation of the ink's ingredients for $\rho_{\mathrm{A,IrOx}} = 1.06$ mg/cm^2 iridiumoxide and about 13 weight-% Nafion® binder catalyst coated membrane is shown in table 3.2. The spraying process takes about 35 minutes.

The process, however, is not very accurate and difficult to reproduce. The spraying process is done manually and therefor prone to systematic errors. The amount lost on the mask is estimated based on experience. This makes it necessary to record the catalyst charge very carefully and adjust it if necessary even with a second spraying process.

4 Experimental Procedure

The test stand allows variation of several parameters of the operation. The heating tubes allow setting temperature, the back pressure regulator the cathode pressure and the potentiostat the current density. Both water pumps - anode and cathode supply - can be set to a defined volume flow. Since the transported medium is liquid water, the volume flow directly corresponds with the mass flow regarding constant density. It is therefor possible to analyze the effects of different water feed flows to the cell in two major ways: one being the change to the polarization curves and the second being the three major transportation effects across the membrane. Polarization curves should show reduced voltages at the same current densities.

If not stated otherwise, the following focus will lie upon WE mode. Measuring polarization curves (voltage-current-curves) is a major analysis tool to evaluate efficiencies of MEAs. They are measured by applying different currents and the measuring the voltage across the MEA using the potentiostat. Starting with the maximum current density of up to 5 A/cm^2 and waiting for steady state operation, then gradually decreasing it to the minimum values of around 0.1 A/cm^2 shows decreasing voltages and therefor decreasing losses. Starting with a high current density ensures stable operation when occurring transport effects - inhomogeneous humidification of the membrane, gas bubbles hindering access of water to the TPB, etc. Each voltage step operates for $t = 30$ s until the next voltage step occurs. This can be controlled and measured by the controlling software of the potentiostat. The average current density and voltage is calculated from the last $t = 10$ s and serves as the measured value for the polarization curve.

4.1 Measures to Enable High Current Densities

There are three major overpotentials to be worked on to enable high current densities:

1. the activation overpotential caused by the electrocatalyst,

2. the ohmic overpotential mainly caused by proton transport in the membrane and electrocatalyst as well as the contact resistances of the cell,

3. the transport overpotential mainly influenced by water and gas transport in the PTL (anode: water and oxygen) and GDL (cathode: hydrogen, possibly water due to transport effects through the membrane).

The transport overpotential is increasing at increased current densities. It needs to be observed whether this occurs in the range of these experiments. Improved porosity of the titanium fleece PTL and optimization of the flow field - mainly the diameters of in- and outlet - are possible improvements. Changing the porosity of the PTL can have positive and negative effects: A higher porosity increases the transport rate of water and oxygen in the PTL, but reduces the electrical conductivity.

Ohmic overpotentials result in heat losses and will be analyzed conducting experiments with MEAs using thinner membranes to reduce the proton conductivity overpotential. The contact pressure of the quick connecting system is also optimized to reduce contact resistance between the flowfield, the titanium fleece PTL and the electrocatalyst sprayed onto the membrane.

To reduce the activation overpotential, several loadings of electrocatalysts are tested with the same binder amount. It has to be considered that the electrocatalyst is a major factor in investment costs of WE systems, so low amounts are preferable.

4.1.1 Optimizing Ohmic Losses

Ohmic losses increase linearly with the current according to Ohm's law. Ohmic losses are the dominating overpotential in the region after the activation losses (see figure 2.2). Reducing ohmic losses lowers the slope and reduces the voltage needed for set current densities.

Two major measures are tested in this work: First, thin membranes are used for WE. Thin membranes have an increased proton conductivity due to lower distance needed to travel and therefor a lower ohmic resistance. However, they also have an increased gas crossover due to the same reason - this might lead to problems at elevated pressures on the cathode side and even create dangerous gas mixtures when hydrogen gets pushed through the membrane into the oxygen gas stream in industrial operation. The Faraday efficiency would also decrease. For these measurements, however, the product gas would

need to be gathered and analyzed (hydrogen and/or oxygen), which is currently not possible with the test stand.

The second major influence is the contact pressure of the cell fixture described in section 3. Increasing the pressure on the contact stamp lowers contact resistance and therefor the overpotential by pressing the contacting flow field to the titanium fleece to the membrane. However, this is only possible up to a certain amount until the full area is contacted and the membranes does not break. The possible contact pressure therefor depends on the physical stability of the membrane.

4.1.1.1 Nafion® 211

The first membrane to be analyzed is the Nafion® 211. It is a second generation Nafion® membrane with equivalent weight $EW = 1100$ g/mol and a thickness of $t_m = 25.4$ µm. So far, it is mainly used for FC operation. Extremely low thickness enables high efficiency and because both educt gases are usually not under pressure in FC mode, the gas crossover of the membrane is negligible. The physical stability concerning a pressure gradient is also usually negligible.

In WE mode, however, the gas crossover can become a major problem at elevated cathode pressures as described before (see chapter 2.1.2). The second major issue is the physical stability: In FC mode, both electrodes can operate with carbon-based GDLs, since no voltages above 1.8 V occur. These high voltages may lead to a quick degradation of the carbon fibers. In WE mode, the anode - the side where oxygen is produced from liquid water - needs a titanium fleece for long-term stability. Elevated pressures applied during WE can also be a problem and damage the membrane.

The first Nafion® 211 membranes are prepared following section 3.2.1. The amount of iridiumoxide is set to be $\rho_{A,IrOx} \approx 0.7$ mg/cm² and the Nafion® binder amount to $f_{w-\%,binder} \approx 12$ weight $- \%$. The MEA is then put into the cell fixture between the carbon GDL on the cathode and the titanium fleece PTL on the anode. This assembly is then set into the test stand and pressed together by the contacting stamp and the potentiostat applies a low voltage.

First, stable operation at a voltage of $U = 2$ V was sought. Polarization curves are measured and serve as the main criterium for efficiency: Decreasing voltages at set current

densities indicate higher efficiency. At fixed voltage, the contact pressure is varied. The current density changes with the contact pressure and is measured.

4.1.1.2 Nafion® XL

The second membrane analyzed is the Nafion® XL, a reinforced membrane using a sandwich structure. Two thin Nafion® sheets lie on the sides of a PTFE-rich sheet. This is supposed to increase the physical stability significantly while hardly lowering the proton conductivity. The total thickness is $t_{\mathrm{m}} = 27.5$ µm. The equivalent weight is inhomogeneous according to Böhm et al. [40] The Nafion® sheets have a lower $EW \approx 970$ g/mol, the PTFE a significantly higher $EW \approx 2000$ g/mol. For this work, $EW \approx 1100$ g/mol is assumed. The membranes are prepared in the same spraying process described in section 3.2.1 and built into the cell fixture.

The reinforced Nafion® XL has not yet been tested in WE mode. It is designed for durable FC operation. However, to achieve high current densities during WE mode at low voltages, thin membranes are promising to achieve this goal due to their reduced ohmic losses. As mentioned before, the gas crossover needs to be considered before industrial operation though. A high gas crossover reduces the produced gas and therefor the overall efficiency, making an optimization process needed.

As before, stable operation at a voltage of $U = 2$ V was the first objective. Then polarization curves, if possible at current densities up to $i = 5$ A/cm^2, are measured and compared with literature values.

4.1.1.3 Optimizing Contact Resistance

The contact resistance is another major parameter influencing the ohmic overpotential. It describes the ohmic resistance between the stamp - the flow field, which serves as the anode -, the titanium fleece PTL and the membrane on both the anode and cathode sides, where the actual reaction takes place at the elctrocatalyst.

The next step is varying the contact pressure of the cell fixture stamp. BalticFC provided the calculation sheet and the needed data of the compacting pressure depending on the air pressure connected to the cell fixture. The relationship is:

air pressure p_{cylinder}	contact pressure p_{stamp}
bar	bar
0	0
1	19.63
2	39.28
3	58.90
4	78.54
5	98.17

Table 4.1: Table showing the relation of air pressure p_{cylinder} to contact pressure p_{stamp}. The calculation is shown in equation (4.1).

$$p_{\text{stamp}} * A_{\text{cell}} = p_{\text{cylinder}} * A_{\text{cylinder}}$$

$$\Leftrightarrow \ p_{\text{stamp}} = p_{\text{cylinder}} * \frac{A_{\text{cylinder}}}{A_{\text{cell}}} \ , \tag{4.1}$$

with p_{stamp} being the compacting pressure of the stamp, p_{cylinder} the pressure in the cylinder (the air pressure), A_{cell} the cell area and A_{cylinder} the area inside the cylinder. With the known values for the areas - $A_{\text{cell}} = 4 \text{ cm}^2$ and $A_{\text{cylinder}} = 78.54 \text{ cm}^2$ - and the adjustable air pressure inside the cylinder - initially $p_{\text{cylinder}} \approx 3$ bar -, the pressure on the membrane can be calculated:

$$p_{\text{stamp}} = 3 \text{ bar} * \frac{78.54 \text{ cm}^2}{4 \text{ cm}^2} = 58.90 \text{ bar} \,. \tag{4.2}$$

Table 4.1 shows the results for relevant pressures to be analyzed.

4.1.2 Optimizing Activation Losses

Activation losses are mainly an issue with the electrocatalyst. Side reactions and gas crossover also take part in the overpotential. Especially at small cells like the used one - with an area of $A = 4 \text{ cm}^2$ -, the side reactions can have a higher influence as well as the gas crossover due to thin membranes. The results in this work should therefor be primarily compared to each other, because literature values often refer to larger areas.

Since the spraying process is not an accurately predictable process, it has been improved to result in several membranes with almost linear differences in catalyst loading. Four membranes are put into a harness and sprayed simultaneously - but each spraying pro-

spraying step	membrane 1	membrane 2	membrane 3	membrane 4
1	x	x	x	x
2	x	x	x	
3	x	x		
4	x			

Table 4.2: Table showing the spraying process for four linearly spaced electrocatalyst loadings. x indicates spraying in the spraying step, otherwise the membrane is covered. This process repeats until the sprayed ink is completely distributed.

cess, a cover is shifted preventing any spraying on the membrane. With the pattern shown in table 4.2, the loadings should result in an almost linear relationship of electrocatalyst loading depending on how often the membranes were covered.

This way the membrane 1 has the highest loading, membrane 2 has 75 % of membrane 1, membrane 3 has 50 % of membrane 1 and membrane 4 has 25 % of membrane 1. The total ink amount therefor needs to be about the 2.5-fold of the ink for the high loading of membrane 1. There is no reference membrane needed anymore, because the membranes themselves are weighed before and after the spraying process.

The membrane type used is chosen based upon the previous experiments. The maximum loading of membrane 1 is aimed to be about $\rho_{\mathrm{A,IrOx}} \approx 1$ mg/cm^2, the binder $f_{\mathrm{w-\%,binder}} \approx 30$ weight $-$ %. All four membranes are afterwards tested with the test stand and polarization curves are measured after achieving stable operation. The polarization curves are measured starting from the higher current density $i_{\mathrm{max}} = 2$ A/cm^2 since stable operation is most critical there. The water flow can be adjusted for stable operation there and is then no issue for the lower current densities.

The four loaded membranes are then compared to each other and the optimal one is chosen for further testing.

4.2 Analysis of Water Transport Effects

The second major objective is to determine the necessary water amount for stable operation and to give an estimation of the values of the transport effects at higher current densities. According to section 2.3.5, the optimal stoichiometric values are not very

clearly determined and vary from 5 to 50 depending on the literature source and its definition of the transport coefficients. Also, the hypothesis of decreased electro-osmotic drag coefficient at higher current densities needs to be examined. [10]

4.2.1 Estimation of the Electo-osmotic Drag

The electro-osmotic drag is the transport effect only based on the moving protons inside the PE membrane carrying water molecules. Medina and Santarelli [10] found a lower electro-osmotic drag coefficient at higher current densities. This is to be analyzed using this estimation.

Transport mechanisms due to concentration and pressure gradient add or subtract another water amount respectively. Transport effect values due to pressure gradient and concentration gradient are difficult to evaluate with the test stand due to the dampening dehumidifiers. Those containers collect the water flows and release surges due to a small opening of the water exit. This makes low volume flows difficult to measure accurately or a long test duration needed. Both the transport mechanisms are expected to be low though, shown by the following calculations. These calculations include several assumptions and should be evaluated carefully.

Starting with the concentration transport, assuming for example:

- $T = 353.15$ K, therefor water saturation pressure $p_\mathrm{s} \approx 48.05$ kPa,

- $p = 1$ bar,

- molar water content on the anode unity (no gas flow) $x_\mathrm{w,a} = 1$,

- membrane thickness $t_\mathrm{m} = 27.5$ μm.

- the average molar water flow of water in the cathode five times higher than the gas flow $\dot{n}_{\mathrm{H_2O}} = 5 * \dot{n}_{\mathrm{H_2}}$. This also reduces the partial pressure of water on the cathode to $p_{\mathrm{H_2O}} = \frac{5}{6} * p$.

The molar mass of water is $M_{\mathrm{H_2O}} = 18.015$ g/mol. Then the resulting water flow through the membrane due to the concentration gradient is according to section 2.3.2:

$$
\begin{aligned}
\dot{m}_{\mathrm{co}} =& D_{\mathrm{w}} * \frac{C_{\mathrm{a}} - C_{\mathrm{c}}}{t_{\mathrm{m}}} * A * M_{\mathrm{H_2O}} \\
=& 3.88 * 10^{-6} \ \mathrm{m^2/s} * \frac{2.82 * 10^{-2} \ \mathrm{mol/cm^3} - 2.66 * 10^{-2} \ \mathrm{mol/cm^3}}{27.5 \ \mathrm{\mu m}} * \ \ldots \\
& \ldots \ * 4 \ \mathrm{cm^2} * 18.015 \ \mathrm{g/mol} \\
=& 1.65 * 10^{-4} \ \mathrm{g/s} \,.
\end{aligned}
\tag{4.3}
$$

Over one full day, this would result in:

$$
m_{\mathrm{co}} = \dot{m}_{\mathrm{co}} * t = 1.65 * 10^{-4} \ \mathrm{g/s} * 1 \ \mathrm{d} * 24 \ \mathrm{h/d} * 3600 \ \mathrm{s/h} \approx 14.21 \ \mathrm{g}.
\tag{4.4}
$$

The transport due to pressure is even lower, even at highly elevated pressures. It an be calculated using:

- $T = 353.15$ K, therefor dynamic viscosity of water $\mu \approx 3.54 * 10^{-4} \ \mathrm{N} * \mathrm{s/m^2}$,

- porosity $\epsilon \approx 0.3$ [10], therefor Darcy constant $K_D \approx 1.32 * 10^{-24}$,

- cathode pressure (gauge) $p_{\mathrm{c}} = 6 \ \mathrm{bar(g)}$, anode pressure (gauge) $p_{\mathrm{a}} = 0 \ \mathrm{bar(g)}$,

- membrane thickness $t_{\mathrm{m}} = 27.5 \ \mathrm{\mu m}$.

Using the formulae from section 2.3.3, this yields:

$$
\begin{aligned}
\dot{m}_{\mathrm{p}} =& \rho * A * \frac{K_{\mathrm{D}}}{\mu} * (p_{\mathrm{a}} - p_{\mathrm{c}}) \\
=& 992 \ \mathrm{kg/m^3} * 4 \ \mathrm{cm^2} * \frac{1.32 * 10^{-24} \ \mathrm{m^2}}{3.54 * 10^{-4} \ \mathrm{N} * \mathrm{s/m^2}} * (0 \ \mathrm{bar(g)} - 6 \ \mathrm{bar(g)}) \\
=& 3.23 * 10^{-8} \ \mathrm{g/s} \,,
\end{aligned}
\tag{4.5}
$$

over a period of one day:

$$
m_{\mathrm{p}} = \dot{m}_{\mathrm{p}} * t = 3.23 * 10^{-8} \ \mathrm{g/s} * 24 \ \mathrm{h} * 3600 \ \mathrm{s/h} \approx 2.79 \ \mathrm{mg}.
\tag{4.6}
$$

Both values are expected to play a minor role compared to the electro-osmotic drag. Long-term measurements have to be conducted to support this. This thesis focuses on measurements on the electro-osmotic drag. According to Medina and Santarelli [10], the water transport due to electro-osmotic drag calculates using the following assumptions:

- $T_{\mathrm{cell}} = 353.15$ K,

- $p_{\mathrm{c}} = 6 \ \mathrm{bar(g)}$,

- $i = 1 \text{ A/cm}^2$.

according to sections 2.3.4 and 3.1.1 to:

$$
\begin{aligned}
\dot{m}_{\text{eo}} &= n_{\text{eo}} * M_{\text{H}_2\text{O}} * \dot{n}_{\text{H}^+} \\
&= n_{\text{eo}} * M_{\text{H}_2\text{O}} * \frac{i}{F} * A * n \\
&\approx 2.13 * 18.015 \text{ g/mol} * 1 \text{ A/cm}^2 * 4 \text{ cm}^2 * 2/(96485.33 \text{ C/mol}) \\
&= 3.55 * 10^{-4} \text{ mol/s} = 6.40 * 10^{-3} \text{ g/s} ,
\end{aligned} \tag{4.7}
$$

or over a whole day:

$$
m_{\text{eo}} = \dot{m}_{\text{eo}} * t = 6.40 * 10^{-3} \text{ g/s} * 24 \text{ h} * 3600 \text{ s/h} \approx 553.21 \text{ g} . \tag{4.8}
$$

This is one order of magnitude larger than the amount transported by concentration and several orders of magnitude larger than the flow by pressure gradient. Reducing these two effects by closing the cathode's bottom opening and letting water gather there and limiting the pressure difference to the natural resistance of the tubes and flow devices, the difference should increase even more.

When both the anode and cathode pumps are running and the cathode is left at almost atmospheric pressure, the main contributor to the water transport during operation is the current and therefor electro-osmotic drag. The peristaltic pump pushes a defined amount of water through the anode, a part is consumed and a part leaves with the product gas. The rest is gathered in the outflow container of the dehumidifier and the weight difference over a specific interval is measured. The water amount is measured to evaluate the outflow and to be able to evaluate the transport effects through the membrane.

The current density is set to a fixed value using the potentiostat which can control the total current delivered to the cell. Since the area is known ($A = 4cm^2$), the current density can be calculated using equation (3.2). The low current density is $i_1 = 2 \text{ A/cm}^2$, the high value $i_2 = 5 \text{ A/cm}^2$ or $I_1 = 8 \text{ A}$ and $I_2 = 20 \text{ A}$ respectively.

Electrical current has its main effect on the electro-osmotic drag. While the total water transport is expected to increase with higher currents, the ratio of water molecule to the current is said to decrease due to transportation hindrances inside the membrane. [10]

Running a WE cell at higher current densities might therefor improve the running costs by decreasing the ratio of necessary DI water.

To analyze this behavior, two experiments are conducted: First, water is set to flow the anode to ensure high water concentrations. The cathode pressure is set to zero bar(g) and water is left inside the cathode. The water mass flow through the anode for i_1 is set to $\dot{m}_{H_2O} \approx 2.6$ g/min. For i_2, the water mass flow through the anode is set to $\dot{m}_{H_2O} \approx 3.9$ g/min. The measured water amount flowing through the anode is measured. No water is consumed and no gas exits the cell. Over a set time Δt, the mass is collected and the difference weighed $\Delta m_{nocurrent}$. This is measured at the anode, since no water should cross the membrane to the cathode due to no pressure or concentration gradient and no current flowing. This results in a reference mass flow $\dot{m}_{nocurrent}$, where no water is expected to cross the membrane, gets consumed by WE or is lost in gaseous flows:

$$\dot{m}_{nocurrent} = \frac{\Delta m_{nocurrent}}{\Delta t} \ . \tag{4.9}$$

Then the potentiostat is set to apply the corresponding current. Now not only water is consumed at the anode and dragged through the PE membrane by the protons, but also gas with dissolved water exits. The latter can be calculated using the temperature and the first using the current density. The dragged water mass flow can therefor be calculated. Since the concentration and pressure gradient are almost zero, the electro-osmotic drag water mass flow $\dot{m}_{eo}$ can be estimated using:

$$\dot{m}_{eo} \approx \dot{m}_{net} = \dot{m}_{nocurrent} - (\frac{\Delta m_i}{\Delta t} + \dot{m}_{H_2O,cons} + \dot{m}_{a,out,g}) \ . \tag{4.10}$$

$\dot{m}_{net}$ is the net water mass flow through the membrane, Δm_i the mass difference in the container over time Δt at current density i, $\dot{m}_{cons}$ the consumed water mass due to WE according to equation (3.5) and $\dot{m}_{a,out,g}$ the gaseous part of the anode water outflow. The relationship will be further explained in the following section.

With no current flowing, the water mass flow is the reference water mass flow at no current $\dot{m}_{nocurrent}$. Applying current lowers the water outflow by the consumed part $\dot{m}_{cons}$, the gaseous outflow of water with the hydrogen gas $\dot{m}_{a,out,g}$ and the net water mass flow across the membrane $\dot{m}_{net}$. Since the concentration and pressure gradients are low, their transport effects are low and the net water mass flow across the membrane $\dot{m}_{net}$ is approximately the water mass flow due to the electro-osmotic drag $\dot{m}_{eo}$.

The water exits the dehumidifiers in surges - in varying size and time inbetween. This is probably due to a too small tube and cohesive forces in the water being too high until, at some point, the gravitational force of the water mass above the exit becomes too large and pushes the water out. The variation is probably based on gas bubbling or other irregularities. The mass is therefor always measured after a surge - then the water level inside the dehumidifiers is assumed to be comparable.

4.2.1.1 Calculation of Net Water Mass Flow

Figure 4.1 shows the relevant water flows in anode and cathode respectively. $\dot{m}_{\text{net}}$ is the net water mass flow across the membrane defined according to equation (2.9), $\dot{m}_{\text{a}}$ and $\dot{m}_{\text{c}}$ the mass flows entering the electrodes. $\dot{m}_{\text{a,out}}$ and $\dot{m}_{\text{c,out}}$ are the mass flows exiting the electrodes, $\dot{m}_{\text{H}_2\text{O,cons}}$ the consumed water amount by electrolysis calculated using equation (3.5). The mathematical relationships are therefor:

$$\dot{m}_{\text{a}} = \dot{m}_{\text{a,out}} + \dot{m}_{\text{net}} + \dot{m}_{\text{H}_2\text{O,cons}} \text{, and} \tag{4.11}$$

$$\dot{m}_{\text{c}} = \dot{m}_{\text{c,out}} - \dot{m}_{\text{net}} . \tag{4.12}$$
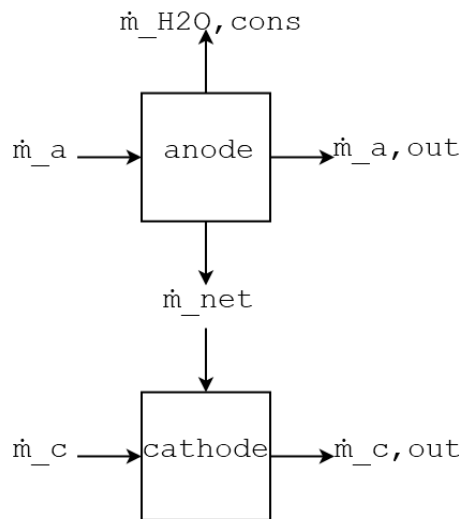

Figure 4.1: Balance of water mass flows at the anode and the cathode.

The exiting mass flows can be calculated using:

$$\dot{m}_{\text{a,out}} = \dot{m}_{\text{a,out,l}} + \dot{m}_{\text{a,out,g}} . \tag{4.13}$$

$\dot{m}_{\text{a,out,l}}$ is the liquid mass flow measured by weight difference of the container at the anode outflow, $\dot{m}_{\text{a,out,g}}$ the gaseous part in the product gas. The liquid part can be measured with the weight difference of the container $\Delta m_{\text{a,out,l}}$ over time Δt:

$$\dot{m}_{\text{a,out,l}} = \frac{\Delta m_{\text{a,out,l}}}{\Delta t} \,. \tag{4.14}$$

This way the net mass flow across the membrane $\dot{m}_{\text{net}}$ calculates as follows:

$$\dot{m}_{\text{net}} = \dot{m}_{\text{a}} - \frac{\Delta m_{\text{a,out}}}{\Delta t} - \dot{m}_{\text{H}_2\text{O,cons}}$$
$$= \frac{\Delta m_{\text{c,out}}}{\Delta t} - \dot{m}_{\text{c}} \,. \tag{4.15}$$

The measured water mass consists of the liquid water outflow which is measured by weighing the water storage containers collecting the outflow of the dehumidifier and of the gaseous content in the educt gas flows, being hydrogen and oxygen respectively.

Since the concentration and pressure transport is expected to be small compared to the electro-osmotic drag, the net water mass flow corresponds to the mass flow due to electro-osmotic drag:

$$\dot{m}_{\text{net}} \approx \dot{m}_{\text{eo}} \tag{4.16}$$

and using equation (2.24) and the fixed current, the electro-osmotic drag coefficient n_{eo} can be calculated based on equations (2.24) and (3.3):

$$n_{\text{eo}} = \frac{\dot{m}_{\text{H}_2\text{O,eo}} * M_{\text{H}_2}}{\dot{m}_{\text{H}^+} * M_{\text{H}_2\text{O}}} \tag{4.17}$$

$$= \frac{\dot{m}_{\text{H}_2\text{O}}}{M_{\text{H}_2\text{O}}} * \frac{F * k}{i * A} \,. \tag{4.18}$$

This is expected to be only an estimation to verify the findings from Medina and Santarelli [10]: The calculations leading to the dominant electro-osmotic drag use several assumptions for Nafion® 115 membranes, which are significantly thicker. Concentration and pressure gradient water transport is neglected. Nafion® XL has an inhomogeneous structure and therefor *EW* and possibly a different porosity equivalent than Nafion® 115 used by Medina and Santarelli. Also, the Faraday efficiency η_{F} is neglected, because the test stand can not measure the amount of product gases. The results have to be

considered carefully. The main objective to verify smaller electro-osmotic drag at higher current density can be supported by the findings.

4.2.1.2 Calculation of Gaseous Water Losses with Product Gases

It is possible to calculate the amount of water soluted in the gas streams. A relative humidity of $rH = 100\,\%$ can be assumed, because the educt gases move through liquid water in the dehumidifier where they get cooled. For this, the mixing ratio X is used, which describes the ratio of water vapor mass to the mass of the dry gas. The dry gas is oxygen in this case: [41]

$$
\begin{aligned}
X_{O_2} &= \frac{m_{H_2O,g}}{m_{O_2}} = \frac{\dot{n}_{H_2O,g} * M_{H_2O}}{\dot{n}_{O_2} * M_{O_2}} \\
&= B_{O_2} * \frac{p_{H_2O}}{p_{tot} - p_{H_2O}} \,,
\end{aligned}
\tag{4.19}
$$

with p_{H_2O} being the water (vapor) pressure and p_{tot} the total pressure. The constant B_{O_2} is a ratio calculated using the molar mass of water is $M_{H_2O} = 18.02$ g/mol and that of oxygen $M_{O_2} = 32.00$ g/mol:

$$
B_{O_2} = \frac{M_{H_2O}}{M_{O_2}} \,.
\tag{4.20}
$$

The water vapor pressure p_w can be assumed to be the saturation water pressure p_{ws} since $rH = 100\,\%$ is expected. The dehumidifier is on atmospheric pressure $p_{tot} = 1$ bar. The measured temperature at the dehumidifier T_{dh} allows the calculation of the mixing ratio X_{O_2} using the corresponding saturation water pressure p_s. The saturation water pressure is calculated using equation (2.19).

The gaseous water mass flow $\dot{m}_{a,out,g}$ in the oxygen gas outflow can therefor be calculated using:

$$
\dot{m}_{a,out,g} = X_{O_2} * \dot{m}_{O_2} = \frac{M_{H_2O}}{M_{O_2}} * \frac{p_{H_2O}}{p_{tot} - p_{H_2O}} * \dot{m}_{O_2}
\tag{4.21}
$$

with the corresponding mixing ratios and mass flows of hydrogen and oxygen calculated in section 3.1.1.

4.2.2 Current Density Depending on Anode Water Flow

The total water amount needed for stable operation of a PEM WE cell can be estimated observing the current density at a fixed cell voltage while varying the water flow through the anode. Applying a fixed voltage results in a corresponding current density across the membrane. The water flow can be set according to the expected current. Beginning at stoichiometry of $\xi = 5$ and decreasing it until we reach non-stable operation and back up again allows an estimation of the total water stoichiometry - excess water for full humidification and transported water included in this definition according to equation (2.12).

Table 4.3 shows the anode water inflows $\dot{m}_a$ at different voltages $U_1 \approx 2.0$ V and $U_2 \approx 1.9$ V which are expected to correspond to the current densities $i_1 = 2$ A/cm^2 and $i_2 = 1$ A/cm^2 respectively according to previous measurements. The voltages can be corrected if the current density differs too greatly over the course of one experiment. This can happen because of degradation effects, agglomeration of electrocatalyst or other structural changes of the electrocatalyst-binder layer. For the final stoichiometry calculations, the actual mean current density needs to be determined. The minimum water mass flows are calculated following sections 2.3.1 and 3.1.1 and gradually increased stoichiometry ξ. The voltages need to be set accordingly following previous experiments. The anode water flows do therefor not correspond exactly to the multiplied stoichiometries, since the current density varies over the duration of the experiment.

stoichiometry	$\dot{m}_a$ at U_1	$\dot{m}_a$ at U_2
-	g/min	g/min
1	0.04	0.02
2	0.09	0.04
3	0.13	0.07
4	0.18	0.09
5	0.22	0.11

Table 4.3: Table to determine an estimation for the optimal anode water flow using IV-curves. The voltages are $U_1 = 2$ V ($\hat{=}$ $i_1 = 2$ A/cm^2) and $U_2 = 1.9$ V ($\hat{=}$ $i_1 = 1$ A/cm^2). The stoichiometry is therefor not precisely the stoichiometry value, since the current density varies.

In general, it is also possible to set a fixed current density and measure the voltage across the PE membrane over the anode water flow. In first experiments, this lead to

quick total breakdowns of the operation due to the voltage exceeding the limits of the potentiostat. Therefor no measurements could be conducted. The voltage increased drastically over very short periods of time and exceeded the limits of the potentiostat ensuring safe operation. Figure 4.2 shows this behavior exemplary.
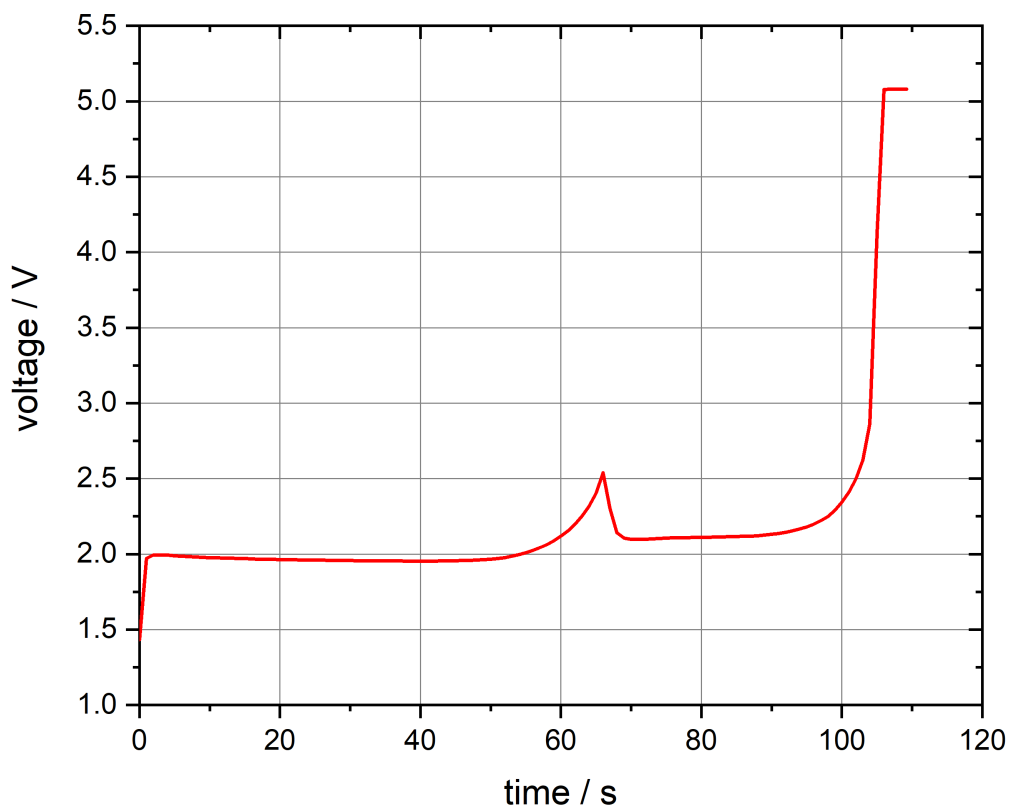
Figure 4.2: Exemplary behavior of the MEA under fixed current density $i = 2$ A/cm^2 and stoichiometry $\xi = 2$. After a short increase probably due to a small gas bubble, the voltage increases drastically due to a larger gas bubble.

This is most likely due to the small area of the tested membrane: On larger membranes, a low water amount leads to an inhomogeneous water distribution over the area of the cell. Some areas lack water and contribute less to the WE, while others need to conduct

the set current. These have therefor increased current densities and result in larger voltage. This can be used as a criterium for proper on improper anode water flow.

On a smaller cell area as ours, a low anode water flow might not only lead to a partially dried membrane, but potentially to a single gas bubble or layer covering the whole surface. At a fixed current density, the resistance would therefor increase drastically and therefor the voltage. With a set voltage, the current can vary over a wide range and even drop to zero if the resistance would become too high. It requires careful evaluation of the stoichiometry though: The stoichiometry of the currently set anode mass flow always needs to be recalculated from the current density.

5 Results

Using the test stand described in chapter 3 and the procedures in chapter 4, the different experiments are conducted to analyze the measures to enable high current densities and to determine the optimal water flow through the anode during WE.

5.1 Outcome of measures to Enable High Current Densities

High current densities are important to achieve high hydrogen production at low investment costs. Ohmic and activation losses are looked at in the following experiments.

5.1.1 Reducing Ohmic Losses in MEAs

Ohmic losses dominate the increasing current region after the sharp increase of activation losses (see figure 2.2). They behave linearly following Ohm's law. Improvements on proton conductivity through membranes and reducing the contact resistances are major factors in the optimization process. Thin reinforced membranes offer a chance comparing to thin non-reinforced membranes. Two Nafion® membranes are analyzed: the un-reinforced Nafion® 211 and the reinforced Nafion® XL.

5.1.1.1 Nafion® 211

Nafion® 211 membranes are cut, sprayed with iridiumoxide as the electrocatalyst for OER on the anode and examined using the cell fixture of the test stand. titanium fleece PTLs and carbon based GDLs with platinum electrocatalyst for the cathode are used. The water flow is set high enough to safely ensure stable operation, the water mass flow through the anode is $\dot{m}_a = 4.3$ g/min.

The first experiments fail because of high currents even at low voltages of $U = 1.5$ V. Figure 5.1 shows a typical behavior. Examining the MEAs show clear indicators of high heat influence hinting towards short circuits between the electrodes through pinholes.
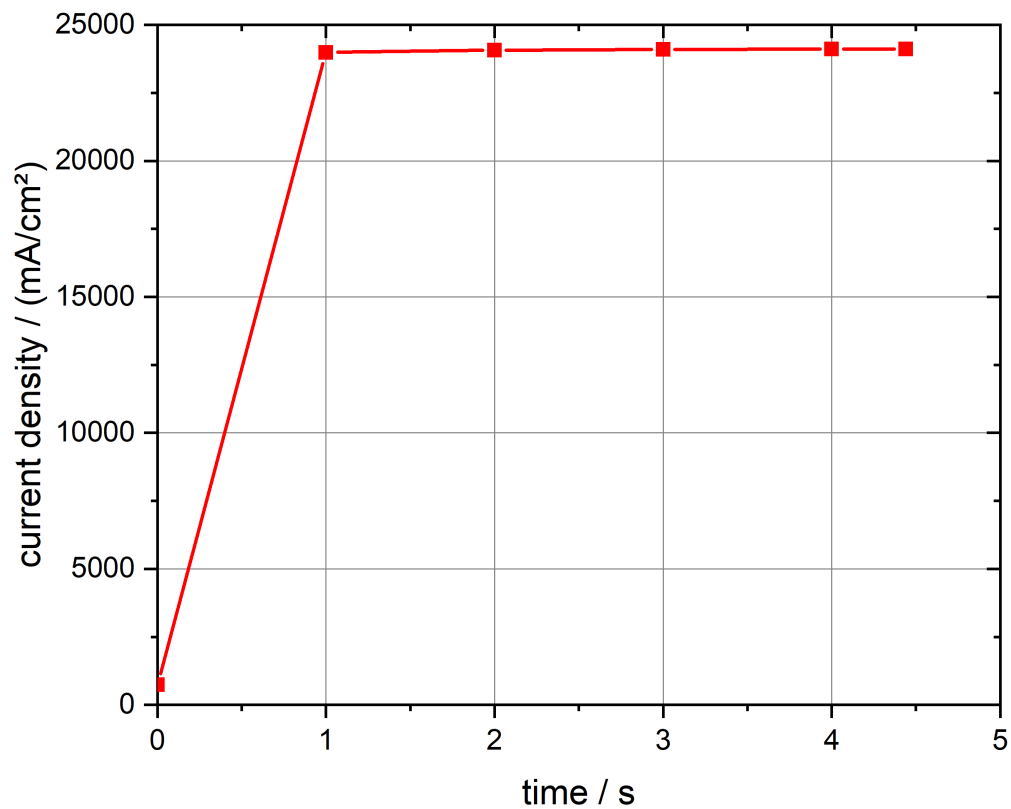
Figure 5.1: Exemplary behavior of the MEA with Nafion® 211. The applied cell voltage is $U = 1.5$ V. The lines are not measured and are included for visibility.

This could be explained by damaged membranes and GDL and PTL touching and leading to low resistances and therefor high currents.

Damage to the membranes can have several causes: pinholes by PTLs/GDLs damaging the membrane, damage by gas bubbles evolving under high pressure, heat transfer problems by too thin membranes are just the most relevant options in our case. Gas bubbles are not very likely, because the failing high current occurs almost instantaneously after activating the cell and only few gas can have evolved yet.

Figure 5.2 shows a macroscopic picture of the MEA and the titanium fleece PTL. The latter was folded off the membrane, the gray colorized parts were therefor at the same

Figure 5.2: Exemplary macroscopic pictures of two MEAs with Nafion® 211. The titanium fleece PTLs have been flipped over off the membrane. They have the same edge length of $l = 2$ cm. The colorization has therefor been at the same spot initially. a) and c) show the titan fleece PTLs, b) and d) the membranes with electrocatalyst.

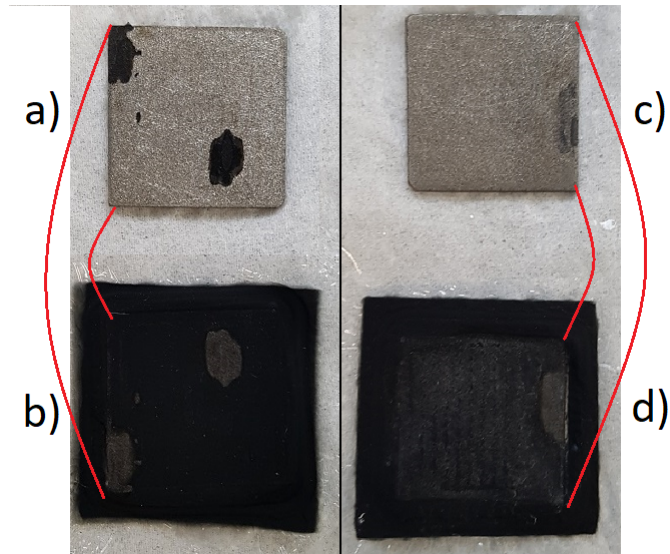place. The right one - c) and d) - only shows a colorization due to some degradation in c), the left - a) and b) - shows the membrane molten to the titanium fleece PTL in a) and got ripped apart during disassembly. This indicated a major heat influence on these small areas with diameters of less than $d < 0.5$ cm.

Figure 5.3 shows the titanium fleece PTL and the ripped-off part of the membrane under a microscope with magnification factor 100. The damage to the membrane can clearly be seen, but it is not possible to see the fused spot without damaging membrane during disassembly and therefor also the PTL.

However, figure 5.4 shows one titanium fleece PTL where the membrane did not fuse to the PTL material: The thermal influence can be seen in the blue colorized circle.

The assumed short circuit spots are also usually distributed differently on each MEA. Sometimes there is only one spot, sometimes two, rarely more. That leads to the assumption that the problem did not lie with the cell fixture itself. The next step is a test with a carbon PTL similar to the GDL just without electrocatalyst which is still the
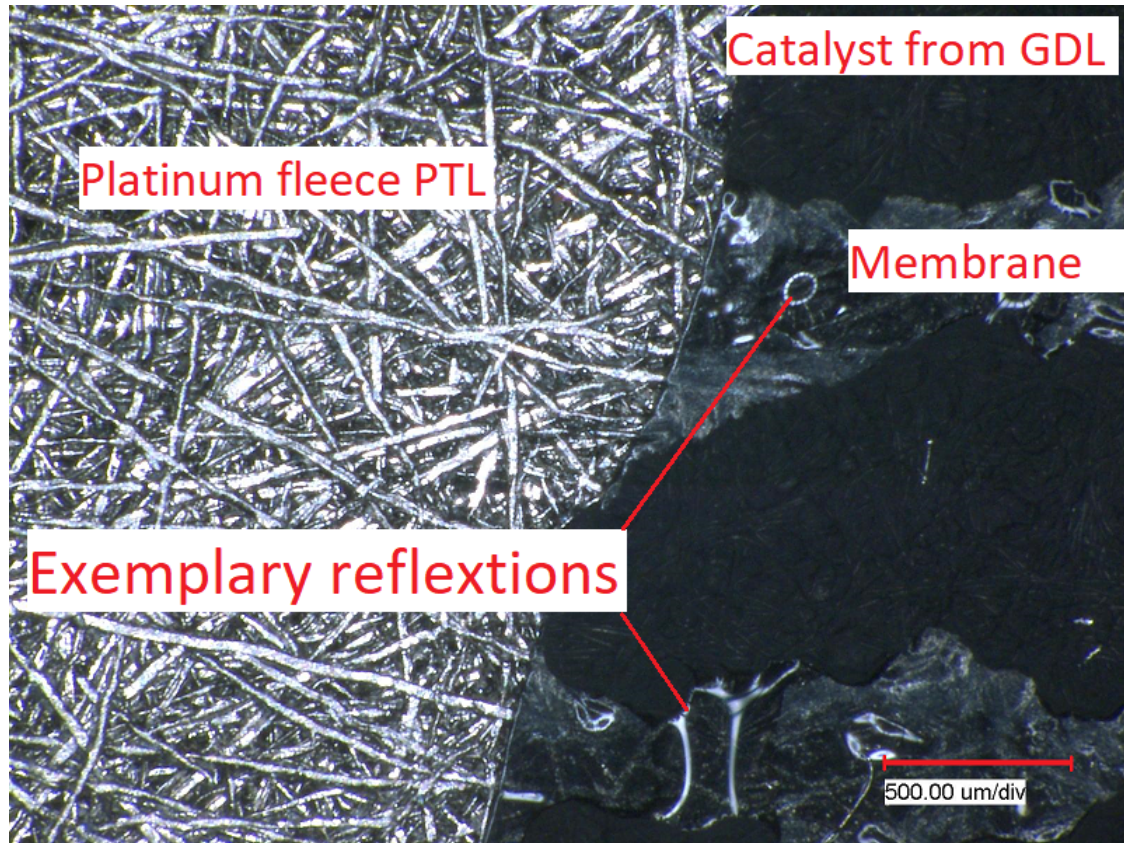
Figure 5.3: Exemplary microscopic picture of one MEA with Nafion® 211. Shown is the titanium fleece PTL and the ripped-off part of the membrane due to thermal link. The membrane also shows reflections of the microscope's lights due to humidification s well as dark parts probably of the carbon GDL and/or its platin catalyst layer.

same iridiumoxide-binder-mixture sprayed on the membrane as before. These carbon PTLs are usually used for FCs, since they degrade quickly at higher voltages occurring during WE. However, this does not happen too quickly and allows conclusions on potentially problematic titanium fleece PTLs. This experiment ran without major problems. The titanium fleece PTL can therefor be considered problematic, because the fibers can damage the membrane.

The next parameter to be influenced is the compacting pressure described by the pressure on the cylinder $p_{cylinder}$. Yet, even with very low air pressures on the cylinder - $p_{cylinder} \approx 1$ bar - and therefor low pressure on the cell - $p_{stamp} \approx 19.63$ bar according to equation (4.1) -, the membrane broke regularly. Figure 5.5 shows the behavior
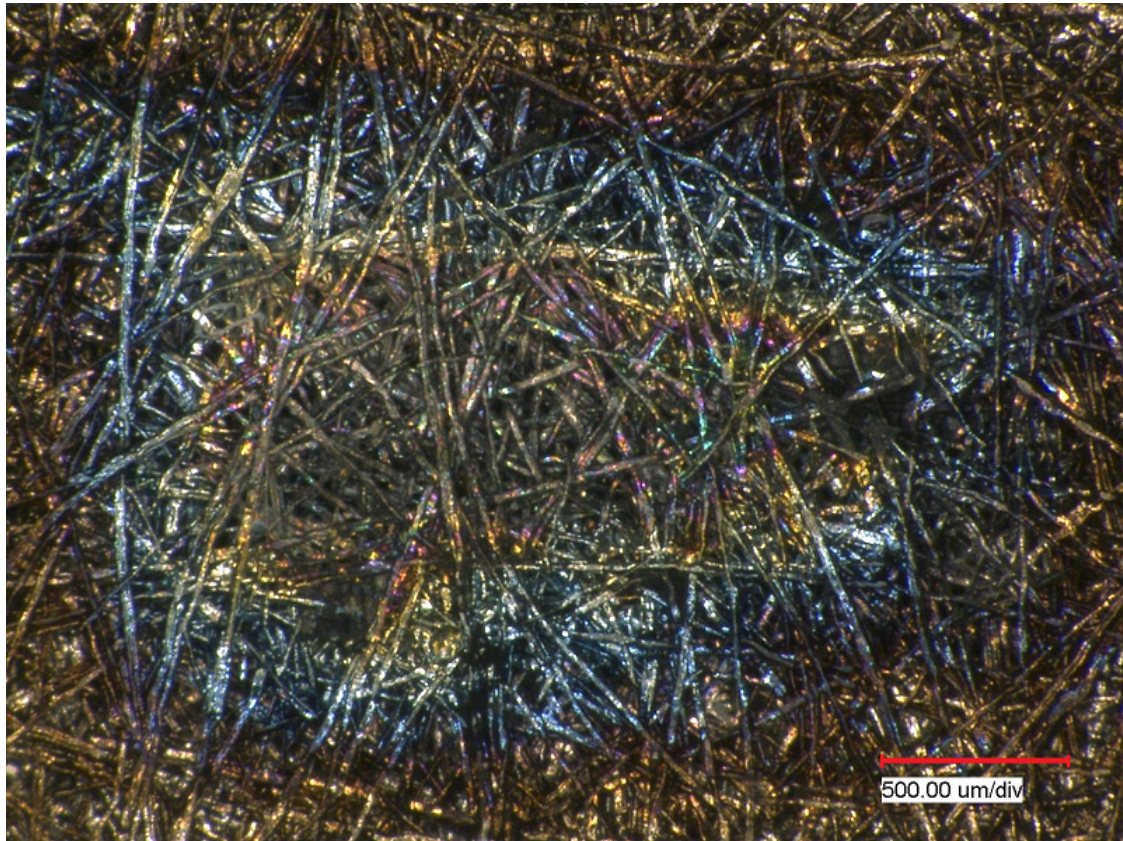
Figure 5.4: Exemplary microscopic picture of one MEAs with Nafion® 211. Shown is the titanium fleece PTL with a clear colorization in the middle due to thermal influence. The titanium fibers show a non-homogeneous surface.

of the current over time at fixed voltage $U = 1.5$ V and varying compacting pressure $1 \, bar \leq p_{\text{cylinder}} \leq 3$ bar. Most likely, the titanium fibers of the PTL press through the thin membrane and connect to the carbon GDL creating a short circuit. At the same time, the contact resistance increases with lower compacting pressures increasing the ohmic resistance (the details of the optimal compacting pressure will be shown in the upcoming sections). With the currently available titanium fleece PTL, the Nafion® 211 does not seem to work properly.

5.1.1.2 Nafion® XL

The second analyzed membrane is the Nafion® XL, a reinforced membrane using a sandwich structure with a PTFE-rich backbone. Its thin structure makes it appealing due to
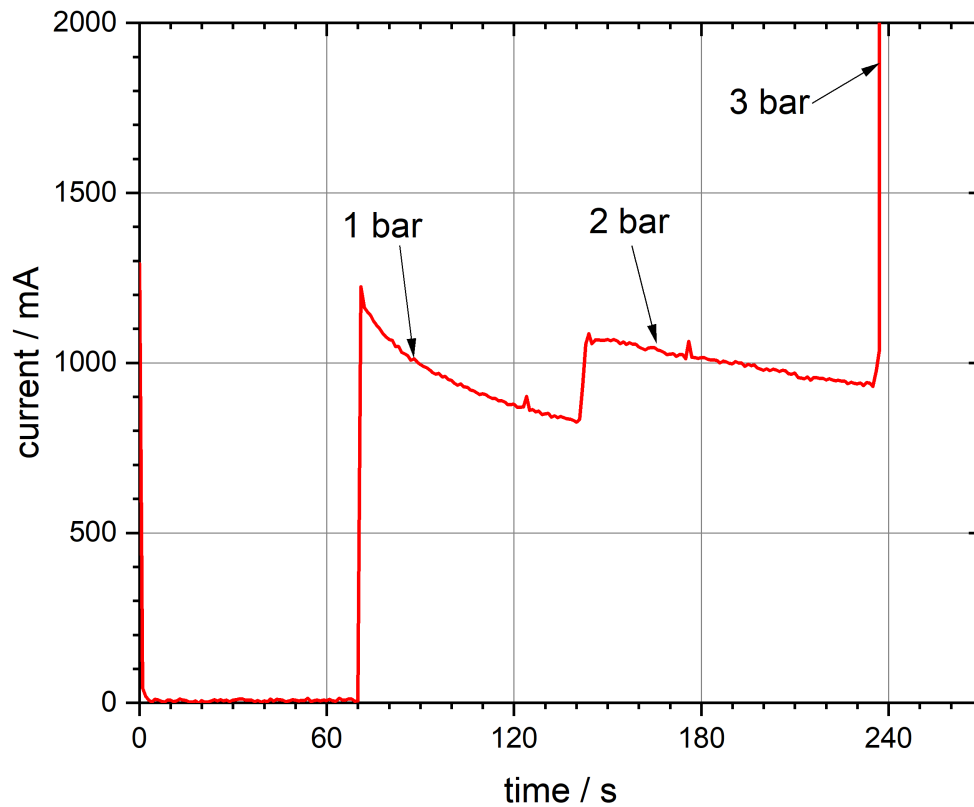
Figure 5.5: Current curve over time of a Nafion® 211 MEA under increasing pressure. After stable process at low voltage and pressure ($U = 1.5$ V, $p_{\text{cylinder}} \approx 0$ bar), the air pressure is increased. At $p_{\text{cylinder}} \approx 3$ bar, the membrane breaks.

low expected ohmic resistance, and its sandwich structure might have positive influences on the gas crossover. The latter will not be discussed in these experiments though and need to be analyzed in further works.

After the same preparations of the membrane, the MEAs are tested under constant voltage until reaching stable operation. The MEAs with the reinforced Nafion® XL membrane did not break even under elevated compacting pressures of up to 5 bar. Figure 5.6 shows the first MEA tested with the reinforced membrane. Stable operation is always reached after about one hour at first operation, quicker in following tests (usu-

ally about 5 minutes). This is most likely due to impurities on the membrane resulting from the spraying and installation process which are flushed away during first operation. Other possible reasons include evolution of surface structures and activation and conditioning of the electrocatalyst's surface. Whereas the reinforced MEAs do seem to have the necessary physical stability towards the compacting pressure and on the other hand gas bubbles did not seem to be the problem with the Nafion® 211 membranes, it was started with low voltages and gradually increased. The compacting pressure is set to a comparably low air pressure $p_{\text{cylinder}} = 1$ bar.

The efficiency is not high though. At a voltage of $U = 2$ V, one usually expects current densities of above $i > 1$ A/cm². The low current density of $i \approx 520$ A/cm² can be caused by: not optimal electrocatalyst and/or binder amount, increased contact resistance, resistances due to the membrane and possibly humidification issues. Humidification issues can be low or inhomogeneous humidification levels of the membrane. The latter is less likely due to a high water mass flow through the anode, but might be caused by the newly used Nafion® XL membrane.

Nonetheless, two polarization curves are measured. The first one is shown in figure 5.7. Comparing the polarization curves of decreasing and increasing current densities yields conclusions about the polarization of the MEA - if the polarization curve decreasing would be significantly higher than the increasing one, a major influence of imaginary power could be the reason for this. The MEA would partly act as a condensator, hindering power adaptations. In this case, however, due to a small membrane probably, the influence is negligible.

The second polarization curve in figure 5.8 is supposed to allow conclusions about the electrocatalyst. The polarization curves bend towards lower voltages at low currents which is the expected behavior in the region dominated by activation losses. if there was too few or too many iridiumoxide on the membrane or the structure would be problematic (e.g. agglomerations), the decrease in voltage would happen at higher current densities already. Optimization is still possible and will be analyzed in the following sections.
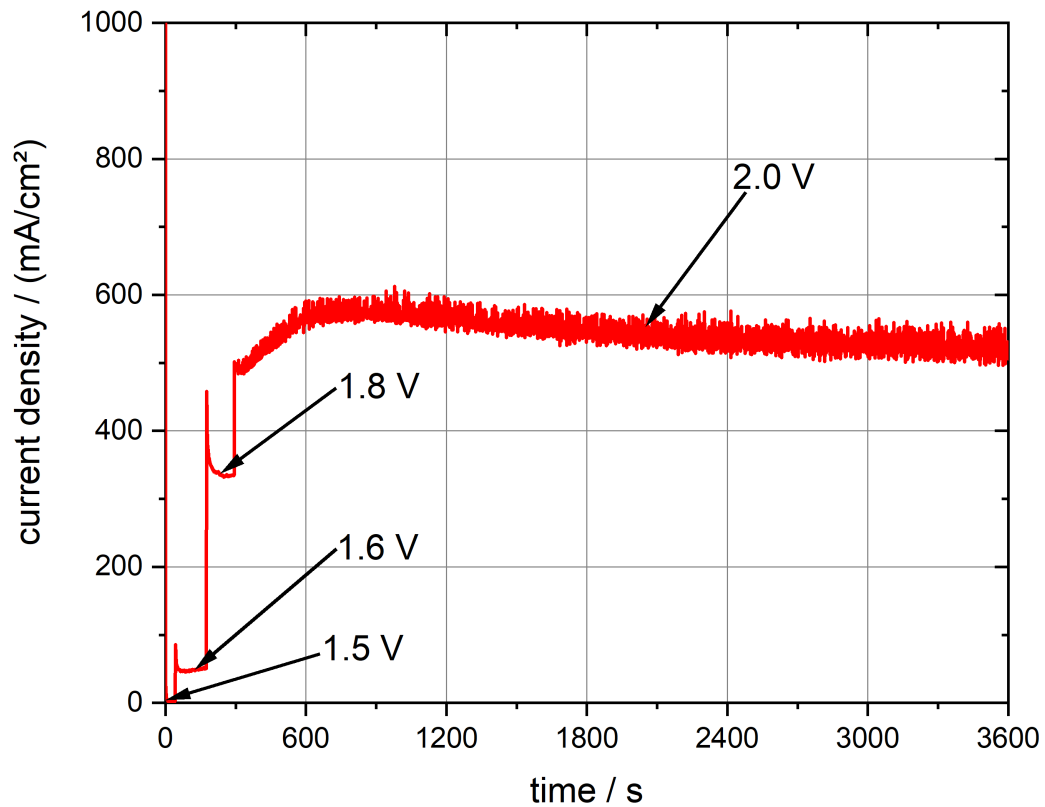
Figure 5.6: Current curve over time of a Nafion® XL MEA with electrocatalyst mass $\rho_{\text{A,IrOx}} = 0.38$ mg/cm², and binder mass percentage $f_{\text{w}-\%,\text{binder}} = 12$ weight $- \%$ under increasing voltage. The voltages were increased gradually and after reaching a voltage of $U = 2$ V, stable operation was waited for. This happend after around one hour.

The main problems with the efficiency of this MEA therefor lies most likely not with the electrocatalyst/binder, and neither with humidification issues. The next step is to analyze the contact resistance due to influence of the air pressure on the stamp p_{stamp}.

5.1.1.3 Optimizing Contact Resistance

As mentioned, the compacting pressure of the stamp p_{stamp} is a major problem for the thin Nafion® 211 membranes. The first tests for the Nafion® XL membranes are therefor

Figure 5.7: Polarization curve of a Nafion® XL with electrocatalyst mass $\rho_{A,IrOx} = 0.38$ mg/cm², and binder mass percentage $f_{w-\%,binder} = 12$ weight $- \%$. The measurement started at high current density, first gradually decreasing, then increasing. The thermoneutral voltage E^0 is shown as reference. The lines are not measured and are included for visibility.

conducted under a lower pressure of about $p_{stamp} \approx 20$ bar caused by an air pressure of $p_{cylinder} \approx 1$ bar. In the following, the air pressure will be the main reference for the compacting pressure, since this is the value influenceable by the test stand.

Figure 5.9 shows the previously used Nafion® XL MEA under elevating pressures. First, stable operation is sought at the initial low compacting pressure and at a voltage of $U = 2$ V. The current density is measured and the compacting pressure increased. The steps from $p_{cylinder} = 1$ to 2 and from 2 to 3 bar show significant improvement of the current density. The step to 4 bar shows a significantly smaller increase and does not
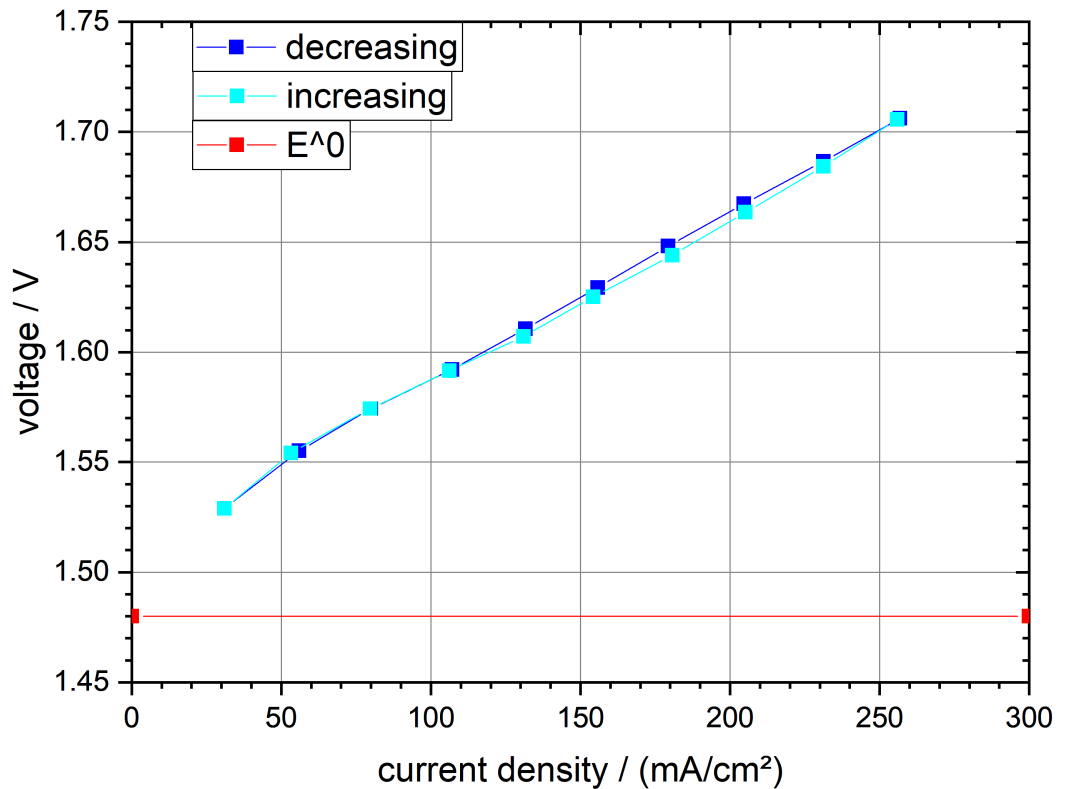
Figure 5.8: Polarization curve of a Nafion® XL with electrocatalyst mass $\rho_{A,IrOx}$ = 0.38 mg/cm², and binder mass percentage $f_{w-\%,binder}$ = 12 weight − %. The measurement started at high current density and focussed on very low current densities to show the activation losses. The lines are not measured and are included for visibility.

achieve stable operation quickly. The step to 5 bar was only conducted to show the high mechanical stability of the MEA. Increasing the compacting pressure offers significant influence on the efficiency.

Interesting to mention is the step down to 2 bar. It is significantly higher than before: before it is at $i \approx 3.1$ A/cm², after the compression and release the value is $i \approx 3.4$ A/cm². This increase is probably due to the contact areas being pressed together by previous
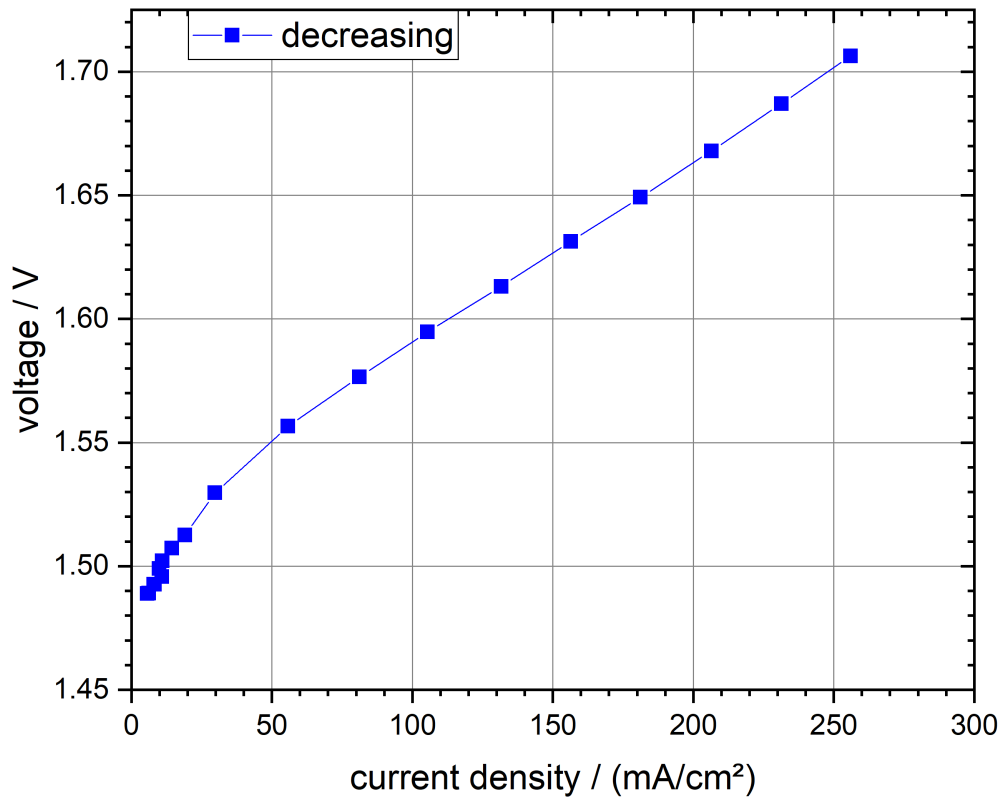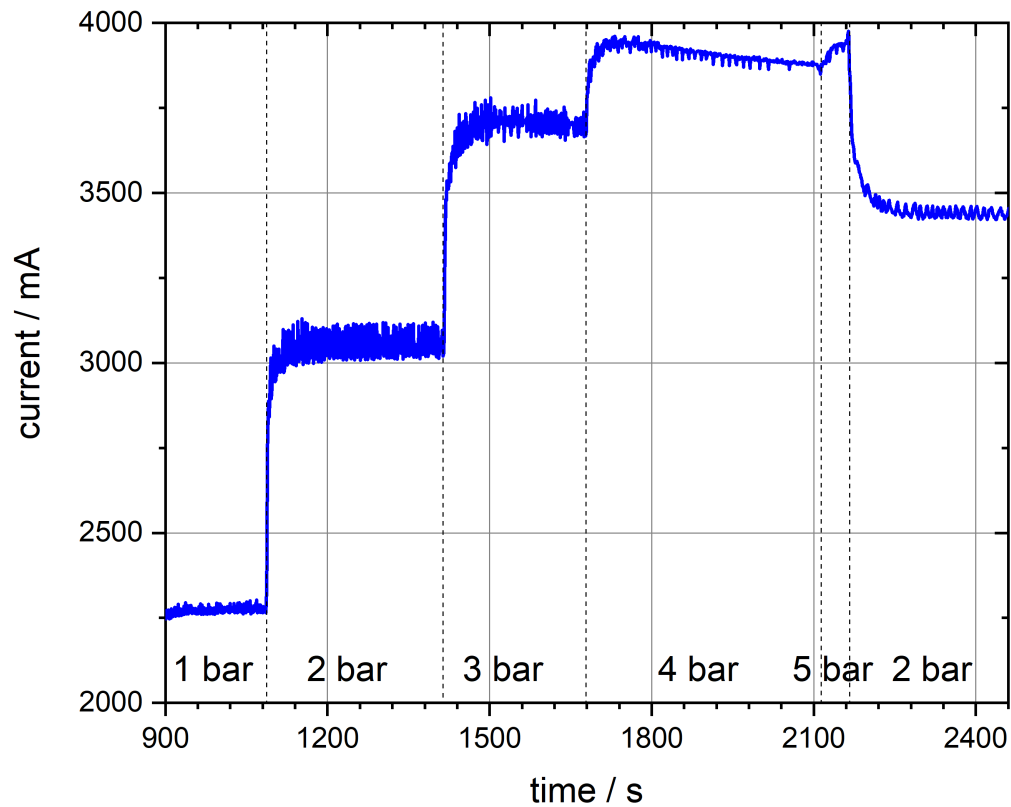
Figure 5.9: Current over time of a Nafion® XL with electrocatalyst mass $\rho_{A,IrOx} = 0.38$ mg/cm^2, and binder mass percentage $f_{w-\%,binder} = 12$ weight $- \%$. The applied voltage is $U = 2$ V. The pressure values are the air pressure on the cylinder $p_{cylinder}$.

high contact pressure. Shortly applying high contact pressures seems to be a useful measure to improve contact overpotential in any case.

For future measurements, the compacting pressure is set to $p_{cylinder} = 3$ bar. Operation at 4 bar shows a decrease in current density over time and the initial increase in current density after increasing the contact pressure from 3 bar is only 0.2 A/cm^2 (compared to about 0.7 A/cm^2 at the increase from 2 to 3 bar.

5.1.2 Optimizing Electrocatalyst

For the amount of electrocatalyst there are two major criteria: First, for high current density applications the voltage needs to remain low, e.g. below $U \approx 2.5$ V at current density of $i = 5$ A/cm². Second, the costs of iridiumoxide limits the amount of applied electrocatalyst.

According to Sambandam and Ramani [25], the optimal binder weight-percentage is $m_{\text{binder}} = 32$ weight $- \%$. This applies primarily to FC mode and Nafion® with equivalent weight $EW = 1100$ g/mol. However, the same binder amount is assumed to be optimal for WE mode and Nafion® XL.

The electrocatalyst itself is more difficult to determine. While in literature, higher amounts of electrocatalyst are often used - for example up to $\rho_{\text{A,IrOx}} = 3.0$ mg/cm² by Kumar and Himabindu [24] -, the reason for this is often not to increase efficiency or cost efficiency, but mostly to realize long-term durability of the electrocatalyst. Lower amounts of electrocatalyst might not show the same efficiencies, but often offer a lot better relative efficiency per mass of electrocatalyst. Figure 5.10 shows four MEAs prepared and tested with different electrocatalyst loadings. The lowest loading $\rho_{\text{A,IrOx}} = 0.26$ mg/cm² is clearly worse than the other three. The difference between the loadings 0.44, 0.66 and 0.94 mg/cm² is low however. Figure 5.11 shows the polarization curves. Whereas the loading of 0.26 mg/cm² shows significantly higher voltages, the lower loadings show similar voltages.

Interesting about this is the fact, that at very low currents (below 100 A/cm²), the voltage is below the thermoneutral voltage E^0 (see figure 5.10). This means, heat is consumed by the reaction because the losses - mostly ohmic and side reactions - do not yield enough heat to keep the reaction running. Instead, the heating of the cell fixture needs to supply additional heat to prevent the cell from being cooled down by the endothermic reaction. The electrocatalyst enables the reaction to happen at a rate high enough to cool the cell quicker than the ohmic losses heat up the cell.

The loadings should be considered carefully. As described in section 4, for these four MEAs a new spraying process was used. It required a new mask, which had drilling holes around the actual central area to be sprayed. A part of the electrocatalyst weighed to determined the loading per area can be found at these holes and subtracts from the actual homogeneous central sprayed area. Figure 5.12 shows one MEA with this addi-
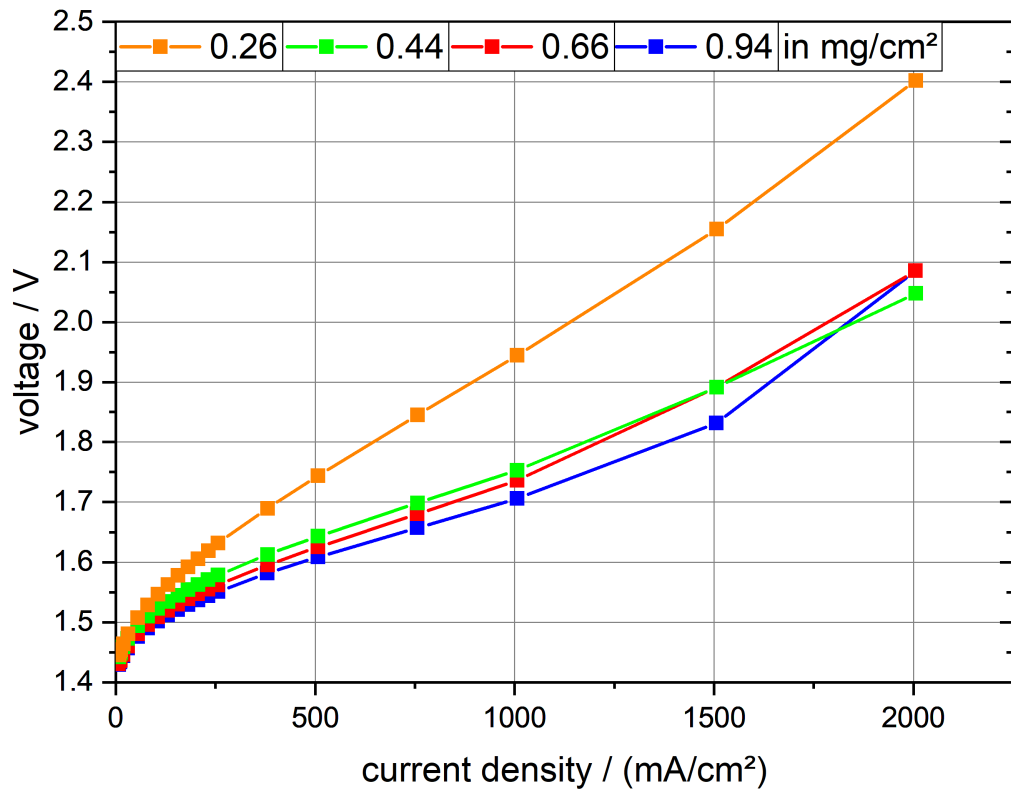
Figure 5.10: Polarization curves of 4 MEAs with Nafion® XL and the same binder amount $f_{\mathrm{w-\%,binder}} = 30 \ \mathrm{weight} - \%$ but different iridiumoxide amounts as electrocatalysts. The graphs are named after their specific electrocatalyst loading in mg/cm². The lines are not measured and are included for visibility.

tional sprayed area at the masks holes not accounted for in the initial calculations of the loading per area.

This mass has therefor to be subtracted from the actual reaction area. While the denomination remains the same, an estimation of the actual loading per area of the center is given by:

$$\frac{A_{\mathrm{tot}}}{A_{\mathrm{MEA}}} = \frac{\rho_{\mathrm{A,IrOx,tot}}}{\rho_{\mathrm{A,IrOx,MEA}}} \Leftrightarrow \rho_{\mathrm{A,IrOx,MEA}} = \frac{A_{\mathrm{MEA}}}{A_{\mathrm{tot}}} * \rho_{\mathrm{A,IrOx,tot}} \ .$$
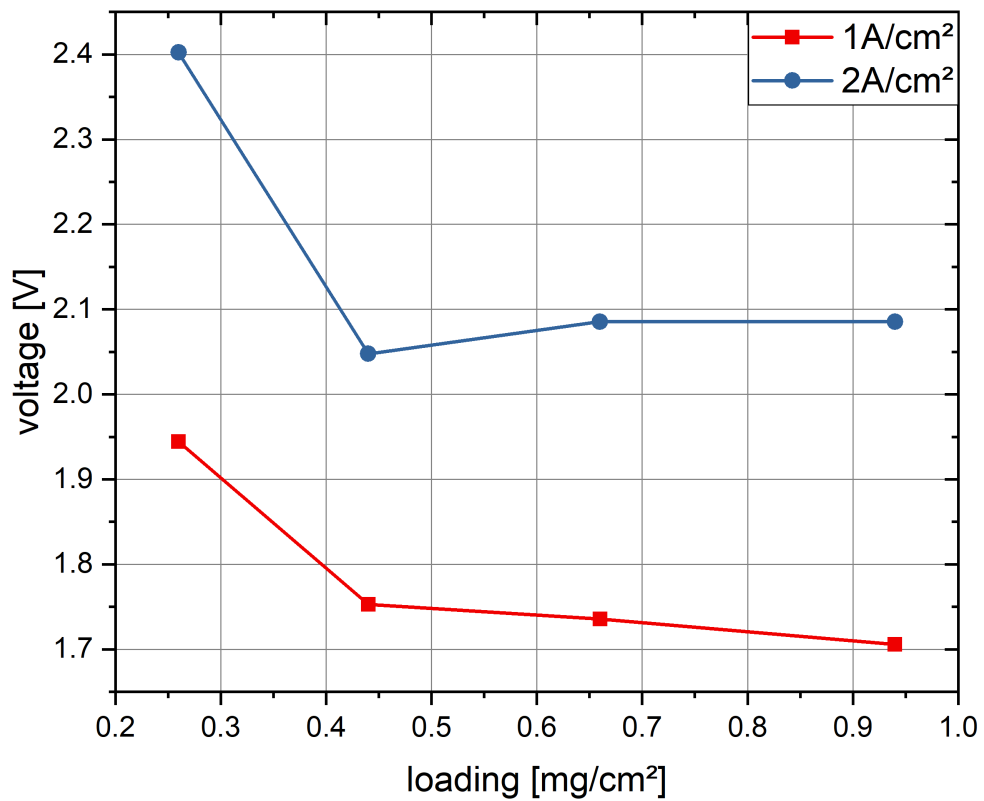
Figure 5.11: Voltage across the MEAs with Nafion® XL with different loadings. Shown are the values for both $i_1 = 1$ A/cm² and $i_2 = 2$ A/cm². The lines are not measured and are included for visibility.

Here, A_{tot} is the total sprayed area, $A_{\text{MEA}} = 6.25$ cm² the central homogeneous area of the MEA, $\rho_{\text{A,IrOx,tot}}$ the total loading per area including the holes surrounding the MEA area and $\rho_{\text{A,IrOx,MEA}}$ the loading reduced to the MEA area, which is being looked for. The total sprayed area A_{tot} is the sum of the MEA area A_{MEA} and the effective area of the non-homogeneous sprayed holes. Looking at figure 5.12, it can also be included that these holes are only sprayed with a lower percentage, for example an own estimation of $f = 50$ %. The calculation is therefor:

$$A_{\text{tot}} = A_{\text{MEA}} + A_{\text{holes}} * f \,, \tag{5.1}$$
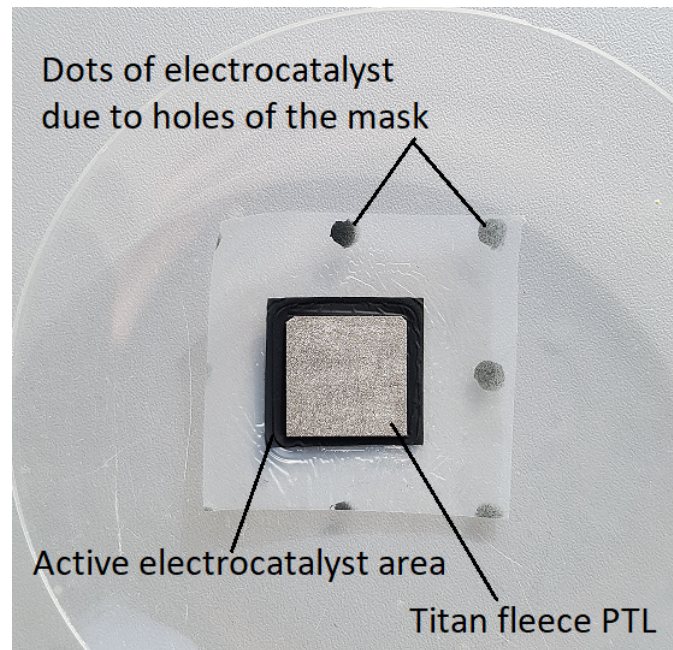
Figure 5.12: MEA with Nafion® XL with electrocatalyst loading $\rho_{A,IrOx} = 0.66 \text{ mg/cm}^2$ and binder $f_{w-\%,binder} = 30 \text{ weight} - \%$. The dots of electrocatalyst around the black square of active reaction area with the titan fleece PTL can be seen. The dots are significantly more transparent than the central active area, which indicates lower loading.

with the assumption that there are in total about three full holes with a radius of $r_{holes} \approx 2.5 \text{ mm}$:

$$A_{tot} = A_{MEA} + A_{holes} * f = A_{MEA} + 3 * (\pi * r_{holes}^2) * f . \tag{5.2}$$

In this case, the maximum loading can be estimated to be:

$$\rho_{A,IrOx,MEA} = \frac{A_{MEA}}{A_{MEA} + 3 * (\pi * r_{holes}^2) * f} * \rho_{A,IrOx,tot} \tag{5.3}$$

$$= \frac{6.25 \text{ cm}^2}{6.25 \text{ cm}^2 + 3 * (\pi * (2.5 \text{ mm})^2) * 0.5} * 0.94 \text{ mg/cm}^2$$

$$\approx 0.88 \text{ g/cm}^2 .$$

This value is about 6 % lower and needs to be considered for accurate electrocatalyst loadings. Since the difference is low (about 6 %), the original values are used for the

following calculations. The results are still comparable with others in this work, and comparing with other researches is difficult because of the area of 4 cm^2.

Another important aspect to look at is the current per loading of the electrocatalyst. It shifts the focus from the pure efficiency towards power per loaded electrocatalyst and allows conclusions about cost effectiveness. Figure 5.13 shows this for the four tested MEAs. The current per loading j_{loading} calculates as follows:

$$j_{\text{loading}} = \frac{i}{\rho_{\text{A,IrOx}}} \,, \tag{5.4}$$

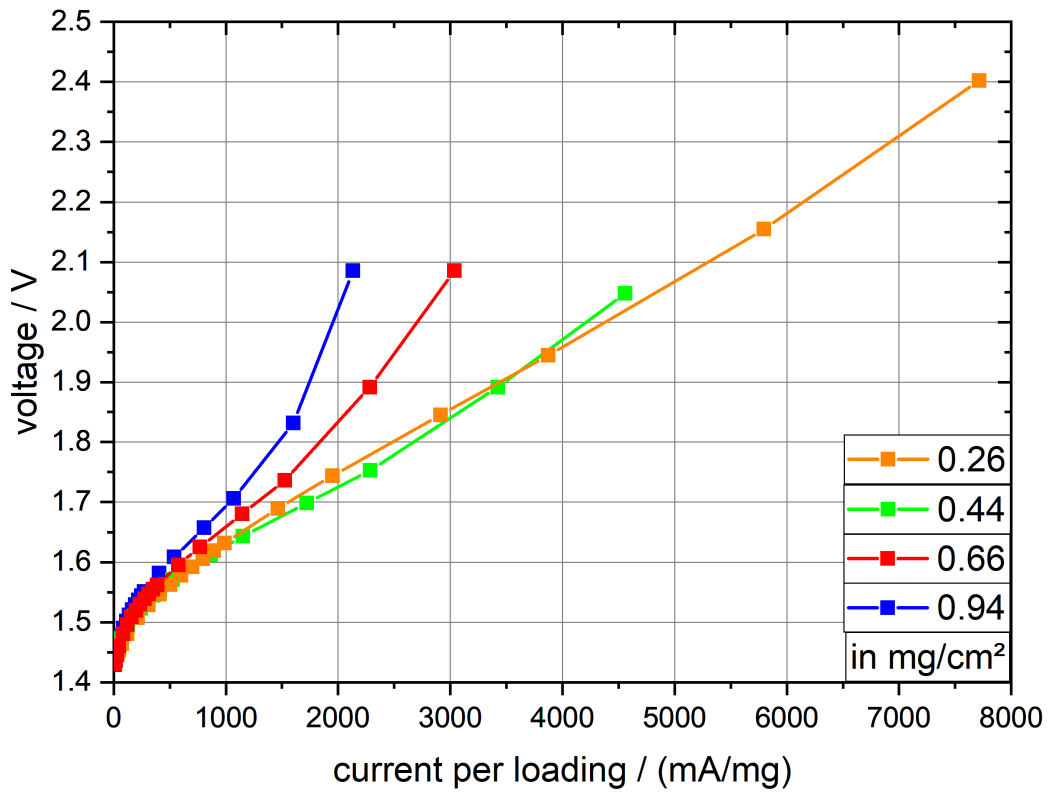with i being the current density and $\rho_{\text{A,IrOx}}$ the loading per area of the membrane.

Figure 5.13: Voltage over current per loading of the four tested MEAs with Nafion® XL with different loadings. The graphs are named after their specific loading in mg/cm^2. The lines are not measured and are included for visibility.

Low loading therefor is strictly better, shifting the slope to lower voltages at the same current densities. Higher loading of above 0.44 mg/cm^2, while often having increased efficiency, adds less efficiency per loading at some point. The lowest efficiency curve of the loading 0.26 mg/cm^2 is better considering the value per electrocatalyst mass than for a higher loading of 0.94 mg/cm^2. However, the next higher loading $\rho_{A,IrOx} = 0.44$ mg/cm^2 is basically at the same range as the loading of 0.26 mg/cm^2 and has much higher efficiencies shown in the polarization curve in figure 5.10. While not being the most efficient, the value per loaded catalyst for a loading of $\rho_{A,IrOx} = 0.44$ mg/cm^2 is a lot higher than of the other higher loaded membranes with the loadings of 0.66 mg/cm^2 and 0.94 mg/cm^2 of iridiumoxide.

5.2 Outcome of the Analysis of Water Transport Effects

The analysis of water transport through the membrane is the second major objective in this work. It becomes even more important regarding the fact that after testing Nafion® 211 a new membrane is being used for WE, the Nafion® XL. Its behavior regarding humidification and water transport needs to be better understood.

5.2.1 Electo-osmotic Drag at High Current Density

The electro-osmotic drag is analyzed first. The experiments are conducted for both current densities $i_1 = 1$ A/cm^2 and $i_2 = 5$ A/cm^2. For the lower current density i_1, the peristaltic pump is set to $p_{peri} = 20\%$ and the reference volume flow $\dot{m}_{nocurrent}$ is measured. Then the potentiostat is activated and the additional current $i_1 = 1$ A/cm^2 flowing reduces the water amount gathered in the container.

However, the higher current density i_2 showed unstable behavior when operating at $p_{peri} = 20\%$. Even though this corresponds to a mass flow of $\dot{m}_a \approx 2.9$ g/min (see calibration table attached) and therefor a stoichiometry $\xi \approx 25$ according to equation (2.12), this amount does not humidify the membrane over its whole surface. The same procedure is repeated for the high current density with a pump's power of $p_{peri} = 30\% \Rightarrow \dot{m}_a \approx 4.3$ g/min $\Rightarrow \xi \approx 39$ and by letting the potentiostat define the voltage, not the current. The set voltage can be adjusted to match an average of $i_2 = 5$ A/cm^2 over the whole duration.

Figure 5.14 shows the experiment with the fixed voltage to achieve average current density of $i_2 = 5$ A/cm^2 over the whole duration. According to previous measurements, the voltage is set to $U = 2.3$ V. The current varies. At the beginning, the current density is below the expected value, but climbs above the expected value within half an hour. Since the mass differences of the water outflow in the container are not taken constantly but only between start and end, the average value of the water mass difference over the whole experiment is the main criterium. This is $i_{2,\mathrm{mean}} = 5.04$ A/cm^2, the standard deviation is rather high at $\sigma_i = 288.4$ mA/cm^2, because of the changing current density over time.

Even though the expected stoichiometry is rather high with $\xi \approx 39$, the operation is still not stable.

The water flow lost in the gas flow $\dot{m}_{\mathrm{a,out,g}}$ calculates by equation (4.21). The temperature is measured over the whole duration of the experiment. For i_1, this is in average $T_{\mathrm{mean}} = 24.2°$C. The mass flow lost in the gaseous phase with the hydrogen gas is therefor $\dot{m}_{\mathrm{a,out,g,i1}} \approx 0.36$ mg/min. This is negligible compared to the amounts consumed and transported and therefor simply multiplied by the gas flow difference for the value at the higher current density i_2 to $\dot{m}_{\mathrm{a,out,g,i2}} \approx 5 * \dot{m}_{\mathrm{a,out,g,i1}} = 1.84$ mg/min.

Table 5.1 shows the results for both current densities i_1 and i_2. The reference mass flow $\dot{m}_{\mathrm{nocurrent}}$ is added as well as the consumed water mass flow $\dot{m}_{\mathrm{cons}}$ (see equation (3.5)), the water mass flow leaving with the produced oxygen gas $\dot{m}_{\mathrm{a,out,g}}$ (see equation (4.21)) and the water mass flow due to electro-osmotic drag $\dot{m}_{\mathrm{eo}}$ (see equation (4.10)). The electro-osmotic drag coefficient n_{eo} is calculated using equation (4.17).

First, these values for the electro-osmotic drag are lower than predicted by Medina and Santarelli. [10] Prior to this experiment, they expected an electro-osmotic drag coefficient of about $n_{\mathrm{eo}} \approx 1.98$ calculated by equation (2.29) at the experiment parameters at i_1. This is higher than the values measured here, but in the same order of magnitude. This can be connected to the current test conditions lying outside of their test case though - Medina and Santarelli used elevated pressures and lower temperatures for their experiments, the parameters here are outside of their tested limits. Also, a completely different membrane is used here. While they used a Nafion® 115, a Nafion® XL is used here. The thickness can be accounted for in the calculations and is expected to have a minor influence on the electro-osmotic drag itself, but the sandwich reinforcement struc-
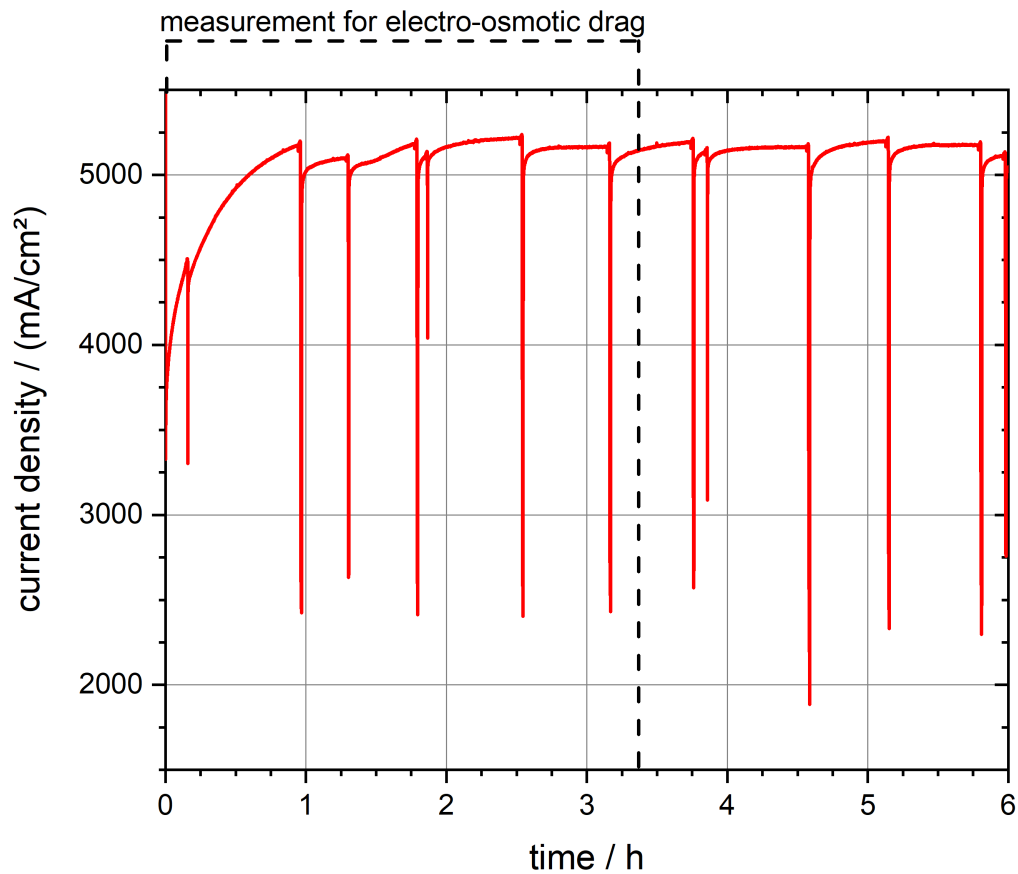
Figure 5.14: Current density over time of the MEA with Nafion® XL with electrocatalyst loading $\rho_{A,IrOx} = 0.94$ mg/cm^2 and binder $f_{w-\%,binder} = 30$ weight $-\%$. The mass flow is $\dot{m}_a \approx 4.3$ g/min, the voltage $U = 2.3$ V.

ture of the Nafion® XL can change parameters significantly by reducing or improving water transport flows.

Qualitatively speaking, the amount of water exiting the cathode is indeed low. The water outflow of the dehumidifier on the cathode side is not measured, but a qualitative estimation can be done. The tubes exiting the cell fixture are transparent and there are significantly less water bubbles exiting through the cathode than through the anode - even when operating at significantly lower stoichiometries than shown in the experiment conducted here. This supports the measured values of a low net water mass

variable	unit	no current	1 A/cm^2	no current	$\approx$ 5 A/cm^2
p_{peri}	%	20	20	30	30
t_1	hh:mm	16:25	08:33	17:23	10:29
t_2	hh:mm	08:52^a	16:25	08:24^a	13:48
Δt	min	987	472	901	199
m_1	g	201.2	201.6	694.8	483.6
m_2	g	2804.0	1418.3	4236.9	1209.4
Δm	g	2602.8	1216.7	3542.1	725.8
$\dot{m}_{\mathrm{nocurrent}}$	g/min	2.64	2.58	3.93	3.65
$\dot{m}_{\mathrm{cons}}$	g/min	0	0.02	0	0.11
$\dot{m}_{\mathrm{a,out,g}}$	mg/min	0	0.36	0	1.84
$\dot{m}_{\mathrm{eo}}$	g/min	0	0.04	0	0.17
n_{eo}	-	0	1.63	0	1.51

Table 5.1: Table showing the measurements to estimate the electro-osmotic drag at current densities $i_1 = 1$ A/cm^2 and $i_2 = 5$ A/cm^2. No current density indicates reference mass flows at two different pump settings (20 % and 30 % respectively) for the corresponding current densities. The (+24:00) indicate a time value on the next day. ^{a} indicates a time on the next day. The membrane used is Nafion® XL.

flow which corresponds approximately with the electro-osmotic drag water mass flow $\dot{m}_{\mathrm{net}} \approx \dot{m}_{\mathrm{eo}} \approx 0.04$ g/min at i_1.

The electro-osmotic drag coefficient does get reduced at higher current densities as shown in figure 5.15. The difference is low, however, only a decrease of $\Delta n_{\mathrm{eo}} \approx 0.12$ from 1 to 5 A/cm^2 and indicates an almost constant relationship. The assumption is that at some point, the increased proton density moving through the membrane has no or a low effect on the number of water molecules transported. More protons may even hinder each other in pulling water molecules with them, because they leave less spaces to be occupied with water in the membrane. As Medina and Santarelli [10] show, increasing the current density from low values to medium values (0.25 A/cm^2 $\leq i \leq 1$ A/cm^2) shows a great decrease in the electro-osmotic drag. The experiment here shows smaller decrease at higher current densities (1 A/cm^2 $\leq i \leq 5$ A/cm^2). This matches the expectation, since a linear decrease would at some point yield negative electro-osmotic drag coefficients, which is not possible by definition. A non-linear behavior is much more
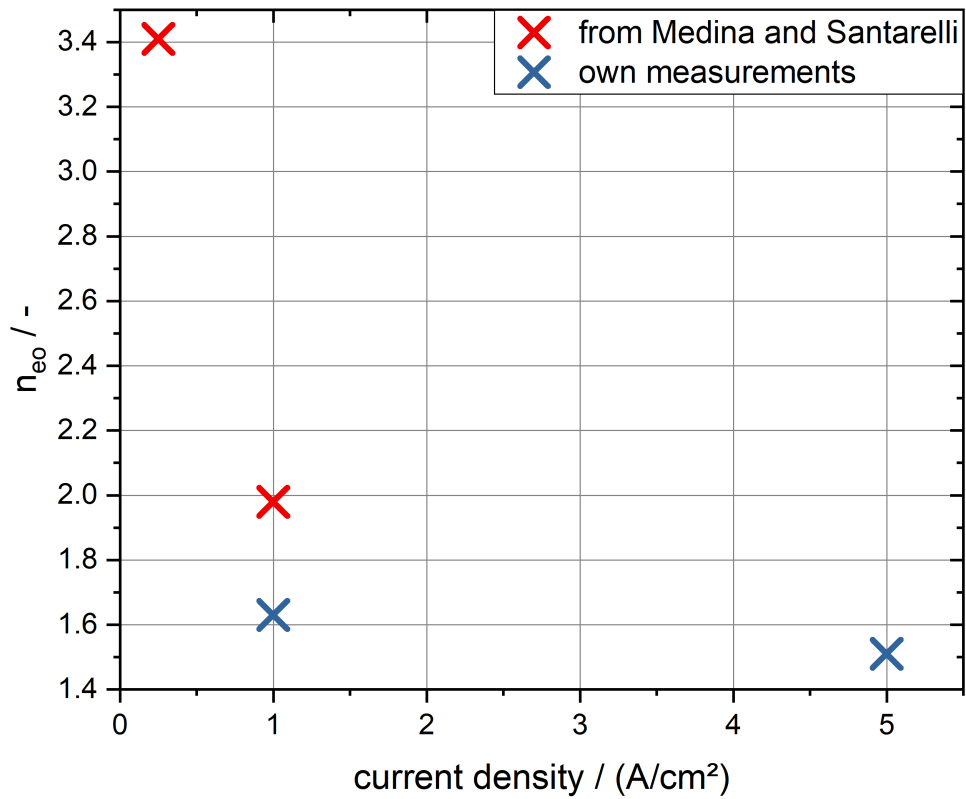
Figure 5.15: Comparing the electro-osmotic drag coefficients from Medina and Santarelli [10] and the own measurements in this work.

suited and supported by these measurements, even though the numerical values differ greatly due to test setup and membrane used.

5.2.2 Outcome of the Current Density Depending on Anode Water Flow Analysis

The current density usually only depends on the applied voltage and the overpotentials. At reduced water flow through the anode, water starvation might occur: gas bubbles developing on the electrocatalyst can block the access of water to the membrane which

can not only stop the reaction at these places, but also dry out the membrane. This can lead to reduced efficiency of the operation and degradation and even failure of the membrane.

The first experiment examines the behavior at higher current density $i_1 = 2$ A/cm^2. As described, applying a current does not work in unstable conditions due to security thresholds of the potentiostat (voltages above $U \approx 5$ V are not allowed). Therefor, based on previous analyses, a voltage is applied which corresponds to a current density. The voltage is adjusted to keep the average current density at the desired value. For the current density $i_1 = 2$ A/cm^2, this voltage ranges around $U_1 = 2$ V which is the initially applied voltage.

Figure 5.16 shows the first analysis of the dependency of the current density on the anode water flow. First decreasing the stoichiometry to $\xi = 2$ and then gradually increasing it. Until $\xi = 3$, the operation is clearly unstable, with current density fluctuating up to $\Delta i = 1.5$ A/cm^2. At $\xi = 4$, the current density shows stable and unstable intervals. These intervals happen even until $\xi = 8$, most likely drops due to single gas bubbles gathering, blocking the TPB and being flushed out. At $\xi = 8$, the stable operation lasts for more than hours but still has a few gas bubbles disturbing the operation.

Based on this, the critical range is around stoichiometry $\xi = 8$. Also, there seems to be a degrading effect happening, the current density decreases over time at constant current. This is most likely due to issues with the electrocatalyst at both electrodes (especially agglomeration of electrocatalyst particles, reducing the active area of both iridiumoxide at the anode and platinum at the cathode) and possibly the titanium fleece PTL, though titanium should be chemically relatively stable except for oxide layers influencing the contact resistance. Non-activated electrocatalyst and humidification issues can also play a role as described before.

Due to this, the experiment is repeated as shown in figure 5.17. The cell is operated for a longer duration at a high stoichiometry, i.e. abundance of water, and the cell voltage already needs to be adjusted to maintain the average current density. Even after more than two hours $t > 2.5$ h, the current now is still increasing. For another one and a half hours $t > 1.5$ h, the operation is stable at a stoichiometry which showed minor instability before, $\xi = 8$. When reducing the stoichiometry to $\xi = 6$, the operation becomes unstable. Not only does the voltage decrease slightly and small irregularities show due

Figure 5.16: Current density over time of the MEA with Nafion® XL with electrocatalyst loading $\rho_{\text{A,IrOx}} = 0.94$ mg/cm² and binder $f_{\text{w}-\%,\text{binder}} = 30$ weight $- \%$. The voltage applied is $U = 2$ V. The anode water mass flow is indicated by the stoichiometry ξ shown at the top. The relevant analysis here lasts until hour $t = 8$ h, then the voltage is changed.

to small gas bubbles, but after about one and a half hours $t \approx 1.5$ h more, the operation becomes significantly more unstable. There even happens a frequent fluctuation of the current at almost the same time interval of about $T = 10$ min after six hours $t = 6$ h. Water seems to be fed to the anode in almost evenly weighting drops.

At the end of the experiment, the membrane breaks. This is most likely due to issues with humidification - a wet membrane swells, a drying membrane shrinks. This effect is a major degradation effect for the mechanical stability of membranes. Due to extended
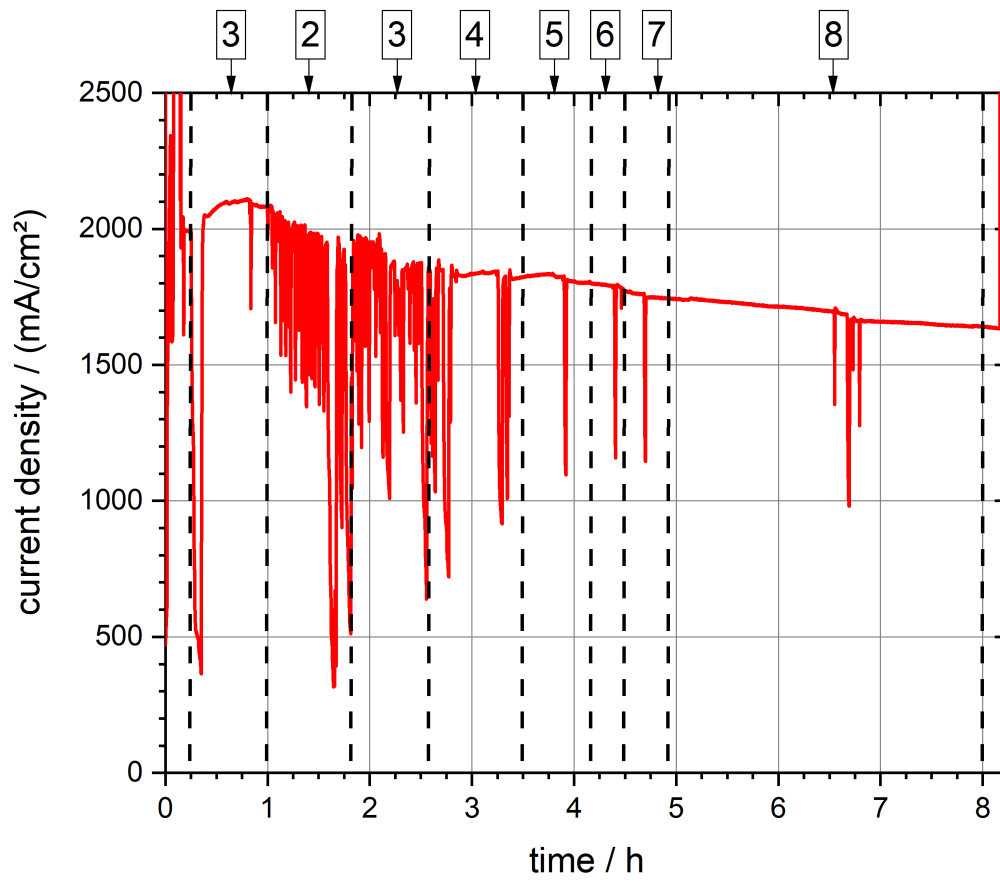
Figure 5.17: Current density over time of the MEA with Nafion® XL with electrocatalyst loading $\rho_{A,IrOx} = 0.94$ mg/cm^2 and binder $f_{w-\%,binder} = 30$ weight $- \%$. The voltage applied is displayed below the graph and adjusted to achieve an average current of $i_1 \approx 2$ A/cm^2. The anode water mass flow is indicated by the stoichiometry ξ shown at the top.

time in changing humidification levels on the anode, even the reinforced Nafion® XL breaks.

This leads to two conclusions: First, operation at stoichiometry $\xi = 8$ seems risky depending on the overall humidification level of membrane and surrounding cell holding. Safe operation is possible at $\xi = 10$, even though a safety factor can be added to reduce

the risk of damaging the membrane. Experiments with longer duration should be conducted to verify the stability at $\xi = 10$ even after long operation.

Second, the degradation and humidification is a difficult topic. In the first experiment (see figure 5.16), low humidification probably promotes degradation which results in a significant decrease in efficiency over time. The second experiment (see figure 5.17) shows an increase of current density after settling within higher humidification levels. The start-up phase and its humidification/stoichiometry seem to have a significant impact on the following stability at lower stoichiometries. A certain level of inertia is assumed in the water management: Changes in anode water flow take time to influence the reaction rate.

Because the membrane is broken in the last experiment, a new one is used. One of the previously tested MEAs is brought into the cell fixture, with electrocatalyst loading of $\rho_{\mathrm{A,IrOx}} = 0.44 \mathrm{~mg/cm}^2$ and binder $m_{\mathrm{binder}} = 30 \mathrm{~weight} - \%$. First, the MEA is tested at a current density of $i = 2 \mathrm{~A/cm}^2$ and shows comparable behavior to the previous MEA except for a higher voltage needed (here: $U \approx 2.23 \mathrm{~V}$ instead of $U \approx 1.90 \mathrm{~V}$ in figure 5.17). The current density is shown in figure 5.18.
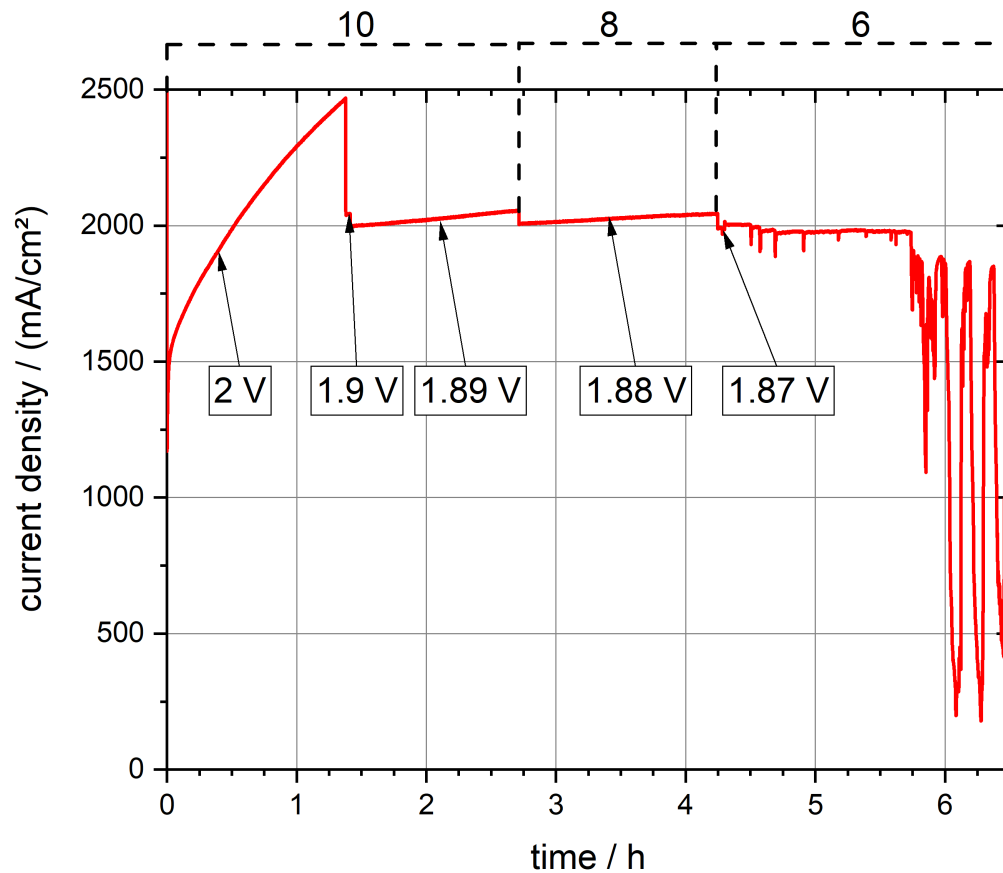
Figure 5.18: Current density over time of the MEA with electrocatalyst loading $\rho_{A,IrOx} = 0.44$ mg/cm^2 and binder $f_{w-\%,binder} = 30$ weight $-$ %. The voltage applied is $U = 2.23$ V. The anode water mass flow $\dot{m}_a$ is the consumed water mass flow $\dot{m}_{cons}$ times the stoichiometry ξ shown at the top.

Then, one long lasting experiment is conducted with a lower currend density of $i = 1$ A/cm^2 as shown in figure 5.19: Starting with a low stoichiometry of $\xi = 8$, increasing it to $\xi = 10$ when instability is clear and after a longer settling time of about 2 h decreasing it to $\xi = 8$ again. Expected is rather quick instability during start-up at low stoichiometry $\xi = 8$, an extended settling time but stable operation at higher stoichiometry $\xi = 10$ and then a long settling time at the lower stoichiometry $\xi = 8$. At some point, operation here is expected to become unstable again.

The voltage is now shown in the same graph, so the adjusting steps to achieve almost constant current density can be clearly seen. The efficiency of the MEA is significantly
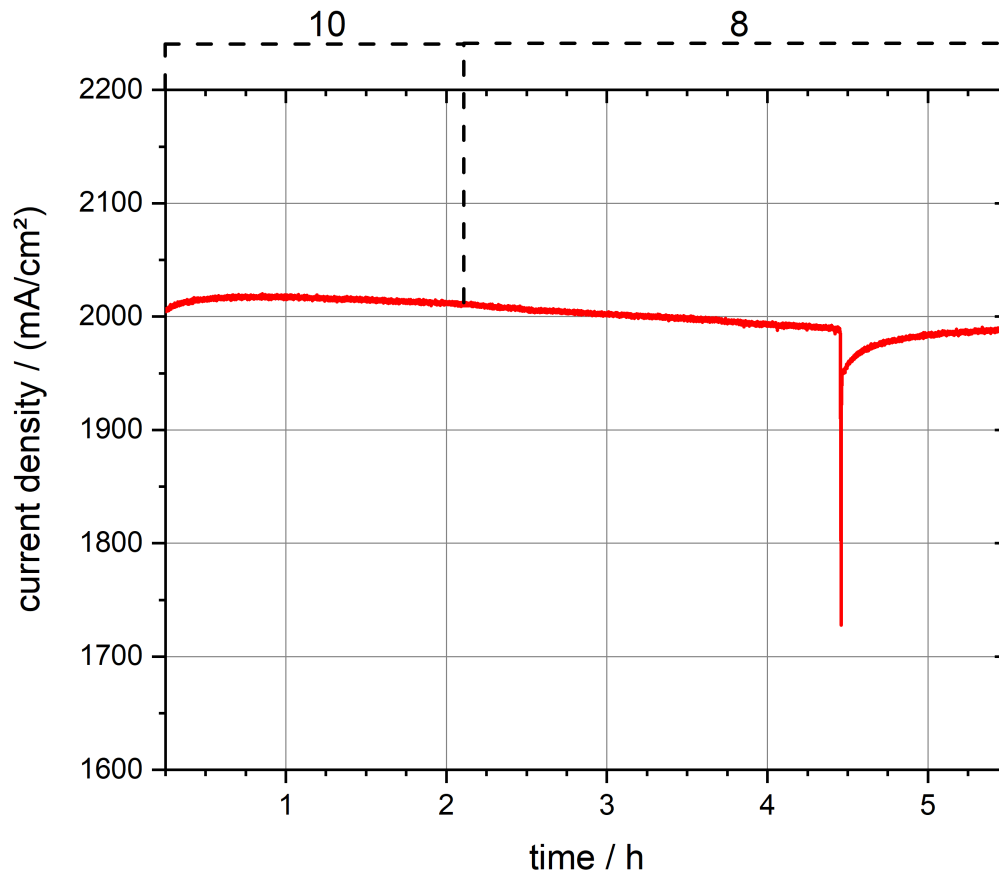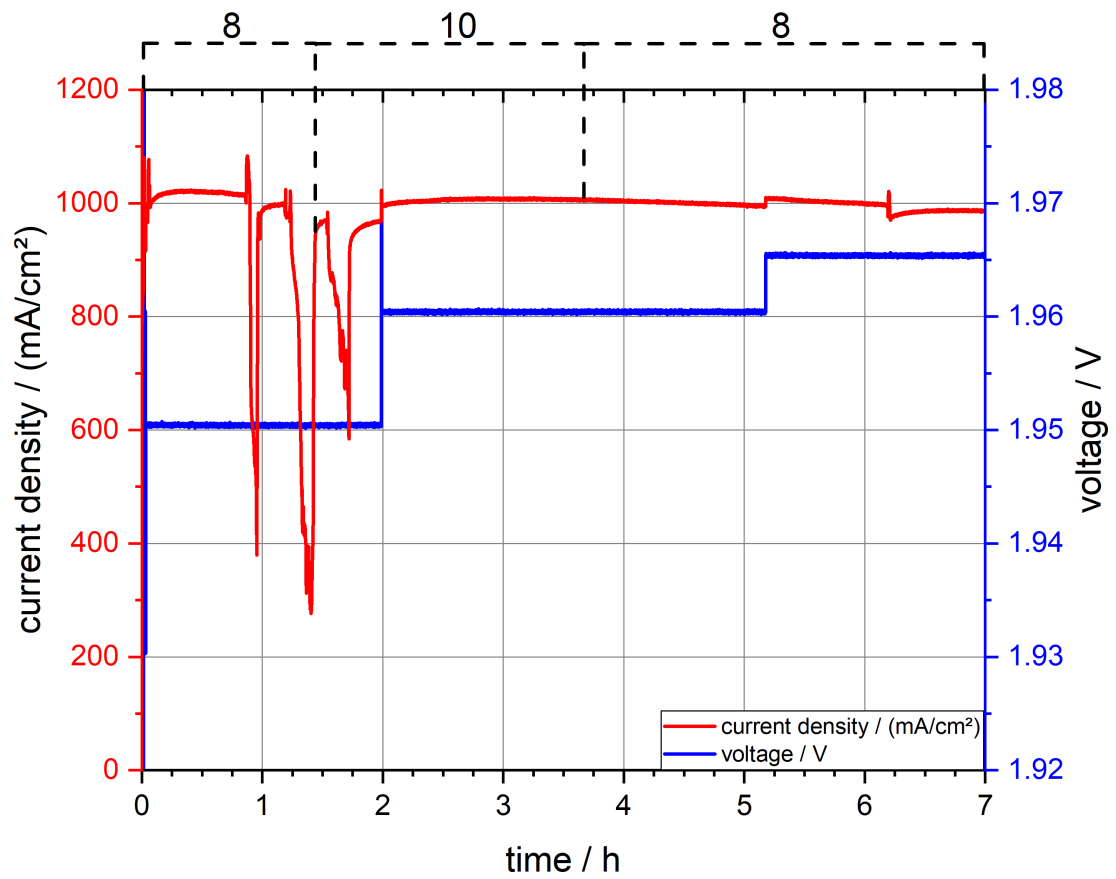
Figure 5.19: Current density over time of the MEA with Nafion® XL with electrocatalyst loading $\rho_{A,IrOx} = 0.44$ mg/cm² and binder $f_{w-\%,binder} = 30$ weight $- \%$. The voltage applied is displayed as well and adjusted to achieve an average current of $i_2 \approx 1$ A/cm².The anode water mass flow is indicated by the stoichiometry ξ shown at the top.

lower, the same voltages yields about half the current density with the previous MEA (here: $U \approx 1.95$ V yields $i \approx 1$ A/cm²). This might be because a long activation time for the electrocatalyst is needed before the operation is running at optimal conditions. Also, because the MEA now used was tested, then stored and only used again for this test, it might have suffered from oxidation, pollution or other degrading effects. The focus of this test is not the efficiency of the operation though, but to show the stability at lower current densities and the inertia of the system.

The main outcome, however, is the inertia of the system when reacting to anode water flow changes. Initial start-up shows instability rather quickly. Stoichiometry $\xi = 8$ seems to yield too little water to the TPB and gas bubbles repeatedly block the access. When increasing the stoichiometry to $\xi = 10$, the operation takes about $t = 15$ min to achieve stable operation. And when reducing the stoichiometry to $\xi = 8$ again, it takes about $t \approx 2.5$ h for the first gas bubble to evolve and disturb the operation.

It is not impossible for these small gas bubbles to evolve at the increased stoichiometry either after very long operation. Even at the lower stoichiometry, there is only one small gas bubble evolving within several hours of operation, nowhere near as high instability as at start-up. Also, the whole inertia of the system towards changes in anode water flow is possibly a result of the cell fixture - water gathering next to the active area, in dead space of the holding and humidifying the membrane not at the active area. This could be needed to fill at higher stoichiometry before stability can be observed. And it can feed the membrane area at decreasing stoichiometry before actual water defects are observable.

6 Discussion

Based on the results, the two main topics - enabling high current densities and analyzing the water transport effects - are discussed.

6.1 Discussion of Measures to Enable High Current Densities

The most efficient MEA is the one with a loading of 0.94 mg/cm^2. This MEA is tested at higher current densities to give a full spectrum of the efficiency with figure 6.1 showing the polarization curve. It shows the activation losses in the slope at current densities up to 500 mA/cm^2. Followed by the almost linear ohmic losses and gives an idea of the transport overpotential in the slight non-linear increase at current density $i = 4$ A/cm^2. The operation at high current density $i = 5$ A/cm^2 is stable though, so the transport losses can not play a large part in the total losses.

This polarization curve is improved over the measured curve in section 5.1.2. Up to $i = 1$ A/cm^2, the values are almost equal. But where the first measured polarization curve shows a starting transport overpotential at 2 A/cm^2 (see figure 5.10), this happens at higher currents of 4 A/cm^2 if at all in the new measurement (see figure 6.1). This might be connected to not fully activated electrocatalyst or changes in the structure of the electrocatalyst. Humidification can also play a role here. At high current densities, gas bubbles evolve quickly enough to hinder access of water to the membrane leading to drying of the membrane. The improvement of the efficiency of the measurement at high current densities compared to the measurement right after the first stable operation is most likely due to a longer settling time and therefor better activation of the electrocatalyst. It is connected to forming oxide and hydroxy groups for optimal electrocatalyst structure. [42]

The efficiency η_i at a set current density generally is an indicator for the overall performance of the MEA including activation, ohmic and transport overpotential as well as the whole resistance of the cell holding. It can be calculated by:

$$\eta_i = \frac{E^0}{U_i} \, .$$

(6.1)
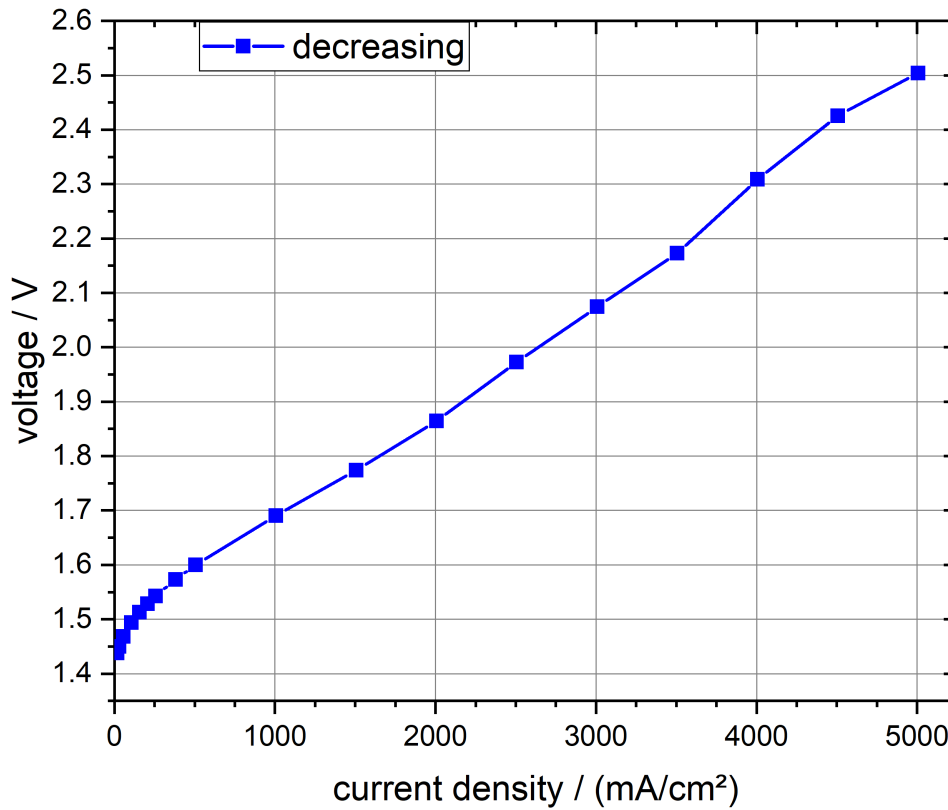
Figure 6.1: Polarization curve of the MEA with Nafion® XL with electrocatalyst loading $\rho_{\mathrm{A,IrOx}} = 0.94$ mg/cm^2 and binder $m_{\mathrm{binder}} = 30$ weight $- \%$. The measurements are taken with decreasing current density. The lines are not measured and are included for visibility.

$E^0 = 1.48$ V is the thermoneutral voltage and U_i the voltage at a current density. Table 6.1 shows the results for the highest loading MEA. With decreasing current density, the efficiency increases. When stating efficiencies, it is therefor needed to mention the current density as well. Stating the voltage has the same meaning as the efficiency. Comparing the voltage at a defined current density can qualitatively evaluate the efficiency, higher voltages indicating lower efficiencies.

Kumar and Himabindu [24] gathered several voltages at a current density of $i = 1$ A/cm^2. For iridiumoxide as anode catalyst, they state voltages from 1.58 V $\leq U \leq 1.7$ V. The

current density	voltage	efficiency
mA/cm^2	V	-
5006.3	2.50	0.59
4006.2	2.31	0.64
3006.6	2.07	0.72
2005.8	1.86	0.80
1006.0	1.69	0.88
506.8	1.60	0.93
105.7	1.49	0.99

Table 6.1: Table showing the efficiencies of the MEA with Nafion® XL with electrocatalyst loading $\rho_{\mathrm{A,IrOx}} = 0.94$ mg/cm^2 and binder $m_{\mathrm{binder}} = 30$ weight $- \%$ at various current densities. The efficiency is calculated with equation (6.1).

results from the experiment conducted here is $U = 1.69$ V. This is in the same range as previous results in the literature. While the value is expected to be improved by the thin membrane, higher electrocatalyst loadings can play a role in improving the efficiency. This does not necessarily improve the current per loading as shown in figure 5.13. Gas crossover can also play a major role in reducing the MEA's efficiency, indicated by the Faradaic efficiency. This can not be measured with the current test stand however. Investigation of the gas crossover needs an upgrade of the test stand or a whole new test setup.

6.2 Discussion of Analysis of Transport Effects

The two main objectives of the analysis of the transport effects were successfully achieved. First, the electro-osmotic drag coefficient does not seem to decrease linearly with the current density. Instead, at increased current densities the decrease is low, indicating an exponentially decreasing relationship as seen in figure 5.15. Since the test setup including the membrane is significantly different from previous measurements, a wider spectrum of measurements at more current density values needs to be conducted for more detailed numerical results.

Second, the optimal stoichiometry for stable operation is $\xi = 10$. The ten-fold of the consumed water mass needs to flow though the anode, otherwise evolving gas bubbles can block the access to the TPB and the operation becomes partially unstable. This can, however, heavily depend on the setup as well. A small MEA as used here ($A = 4$ cm^2) may only need low water flows and corresponding low water velocities. These low water

velocities can reduce the potential of pushing gas bubbles out of the cell. This experiment shows the results for small area MEAs.

Figure 5.14 shows, that at higher current densities, the necessary stoichiometry can be higher than at lower current densities. For $i_1 = 2$ A/cm^2 and $i_2 = 1$ A/cm^2, the resulting optimal stoichiometry seems to be equal. This should be examined further at high current densities up to 5 A/cm^2.

It also shows the inertia in the system which is important for future analyses - the effect of changing anode water flows takes time to show influence on the current density. Not only does it show the needed test duration of up to 3 h until instability effects show (see figure 5.19), but it also hints towards optimization tasks during start-up phase. Starting with a high stoichiometry of $\xi = 10$ might be needed and the anode water flow can get reduced to $\xi = 8$ afterwards for a certain duration. Developing proper start-up protocols for low stoichiometry operation can reduce the operational costs due to lower DI water consumption/water flow needed.

7 Conclusion

The objectives described in section 1.2 are achieved. The results show that high current density operation is possible with the test stand and the MEA setup with the Nafion® XL membrane, the iridiumdioxide loading of $\rho_{A,IrOx} = 0.94$ mg/cm^2 and the compacting air pressure of about $p_{cylinder} \approx 3$ bar. The conclusions are:

1. While the Nafion® 211 does not suit WE operation at increased compacting pressure of about $p_{cylinder} \approx 3$ bar (to minimize contact resistance), the Nafion® XL has the necessary physical stability. This allows minimizing the ohmic resistance.

2. The electrocatalyst at the anode has high activity and even small amounts of $\rho_{A,IrOx} = 0.44$ mg/cm^2 yield experimental results in efficiency comparable with literature values. Extending the loading of the membrane does not improve the efficiency in the same range. Increasing the electrocatalyst loading above $\rho_{A,IrOx} = 0.44$ mg/cm^2 shows low improvements in efficiency. When looking at efficiency per loading of electrocatalyst, increasing the loading can even decrease this value. Increasing the electrocatalyst loading from $\rho_{A,IrOx} = 0.44$ mg/cm^2 shows a higher current per loading at the same voltage than an electrocatalyst loading of $\rho_{A,IrOx} = 0.94$ mg/cm^2.

3. The electro-osmotic drag coefficient decreases very little from a current density of $i \approx 1$ A/cm^2 on. While the decrease is high at low current densities according to Medina and Santarelli [10], the further decrease is much slower as seen in figure 5.15. It seems to be an exponential decrease, not a linear one.

4. From stoichiometry $\xi = 10$ upwards, the operation is stable with the setup used in this work. Current densities tested are $i_1 = 2$ A/cm^2 and $i_2 = 1$ A/cm^2.

However, several questions remain unanswered or result from these findings:

1. The gas crossover of the Nafion® XL membrane needs to be analyzed before using it in further WE operation. The gas crossover can reduce the efficiency significantly and even pose security issues when mixing hydrogen into the oxygen outflow.

2. The electro-osmotic drag should be further analyzed from very low to very high current densities. More current densities from 0.25 A/cm^2 to 5 A/cm^2 need to be tested with the same setup. Then a proper model can be derived.

3. Start-up protocols can play a major role for stable operation. Analyses of the start-up period should be developed and long-term tests be conducted to analyze stability of the operation at different anode water flows in this period. E.g. starting with a high anode water flow and reducing it after a while could prove to result in stable operation.

Looking at the stability of the system might also not be the main issue. As shown in figure 5.14, the operation at high current densities seems to promote evolving gas bubbles, but it does not have a high influence on the overall operation. The disturbances are very short, but the settling after each disturbance takes up to half an hour. This does reduce the average current density, but it might not be too problematic for the membrane. The membrane mainly suffers from extended water defects, promoting physical stress to the membrane material. This happens as seen in figure 5.17, where the membrane breaks at the end. Possible reasons are shrinkage of dehumidified membrane parts, gas bubbles increasing pressure on small surface areas or thermal problems where gas bubbles prevent water from cooling. This is a complex issue and needs to be analyzed further.

Another important issue about the stability is the control mechanism. Applying a set current density is helpful for a specific yield of hydrogen and oxygen gas. Even short water defects, however, can increase the voltage significantly. When the control setup does not allow high voltages (which is the case with the potentiostat used here), the operation stops. When applying certain voltages, however, the current decreases during water defects. While this yields fluctuating product gas yields, the operation usually continues afterwards without shutting down. This way, safe long-term experiments can be conducted.

For the Re-Flex project, bi-functional electrocatalysts should be tested next. These can influence the water management and require further experiments. Also, the gas crossover should be examined to investigate the suitability of Nafion® XL especially for WE operation.

Bibliography

[1] "Fuel cell-gas turbine hybrid system design part I: Steady state performance", McLarty et al., *Journal of Power Sources*, **2014**, *257*, 412.

[2] "Emerging Energy Storage Solutions for Transportation - A Review", Alahakoon & Leksell, 3rd International Conference on electrical systems for aircraft, railway, ship propulsion and road vehicles, **2015**.

[3] "International Aspects of a Power-to-X Roadmap - A report prepared for the World Energy Council Germany", Perner & Bothe, Weltenergierat -Deutschland e.V. https://www.weltenergierat.de/ptxstudie, **2018**.

[4] "Energiewirtschaftliche und ökologische Bewertung eines Windgas-Angebotes", Sterner et al., Assessment. Fraunhofer-Institut für Windenergie und Energiesystemtechnik (IWES), **2011**.

[5] "PKL Electrochemical Cell and the Peukert's Law", Khan et al., *International Journal Of Advance Research And Innovative Ideas In Education*, **2018**, *4*, 4219.

[6] "Complex Metal Hydrides for Hydrogen, Thermal and Electrochemical Energy Storage", Møller et al., *Energies*, **2017**, *10*, 1645.

[7] "Comparison of Fuel Cell Technologies", U.S. Department of Energy's Office of Energy Efficiency and Renewable Energy, USA, https://www.energy.gov/eere/fuelcells/comparison-fuel-cell-technologies, **2019**.

[8] "Comparative study of different fuel cell technologies", Mekhilef et al., *Renewable and Sustainable Energy Reviews*, **2012**, *16*, 981.

[9] "A review on unitized regenerative fuel cell technologies, part-A: Unitized regenerative proton exchange membrane fuel cells", Wang et al., *Renewable and Sustainable Energy Reviews*, **2016**, *65*, 961.

[10] "Analysis of water transport in a high pressure PEM electrolyzer", Medina & Santarelli, *International Journal of Hydrogen Energy*, **2010**, *35*, 5173.

[11] "An overview of polymer electrolyte membrane electrolyzer for hydrogen production: Modeling and mass transport", Rahim et al., *Journal of Power Sources*, **2016**, *309*, 56.

[12] "Performance Analysis of Polymer-Electrolyte Water Electrolysis Cell at a Small-Unit Test Cell and Performance Prediction of Large Stacked Cell", Onda et al., *Journal of The Electrochemical Society*, **2002**, *149*, A1069.

[13] "One-Dimensional Dynamic Modeling of PEM Electrolysis for Solar Hydrogen Production", Ommi et al, 2st International Conference and Exhibition on Solar Energy (ICESE), **2015**.

[14] "Behaviors of a proton exchange membrane electrolyzer under water starvation", Sun et al., *RSD Adv.*, **2015**, *5*, 14506.

[15] "Dynamic modeling and simulation of a proton exchange membrane electrolyzer for hydrogen production", Awasthi et al., *Fuel and Energy Abstracts*, **2011**, *36*, 14779.

[16] "PEM electrolysis hydrogen production system design for improved testing and optimization", Dale et al., The National Hydrogen Association - Annual Hydrogen Conference, **2007**.

[17] "A comprehensive review on PEM water electrolysis", Carmo et al., *International Journal of Hydrogen Energy*, **2013**, *38*, 4901.

[18] "Hydrogen Production: Fundamentals and Case Study Summaries", Harrison et al., 18th World Hydrogen Energy Conference, **2010**.

[19] "Continuous-flowelectroreductionofcarbondioxide", Endrodi et al., *Progress inEnergyandCombustionScience*, **2017**, *62*, 133.

[20] "Numerical Modeling the Effect of Operating Variables on Faraday Efficiency in PEM Electrolyzer", Tijani & Rahim, 3rd International Conference on System-integrated Intelligence: New Challenges for Product and Production Engineering, **2016**.

[21] "A Review on the Fabrication of Electrospun Polymer Electrolyte Membrane for Direct Methanol Fuel Cell", Jaafar et al., *Journal of Nanomaterials*, **2015**, *2015*, 16.

[22] "Influence of Equivalent Weight of Ionomer on Proton ConductionBehavior in Fuel Cell Catalyst Layers", Shen et al., *Journal of The Electrochemical Society*, **2019**, *166*, F724.

[23] "Application of X-ray Photoelectron Spectroscopy to Studies of Electrodes in Fuel Cells and Electrolyzers", Artyushkova et al., *Journal of Electron Spectroscopy and Related Phenomena*, **2017**, *231*, 127.

[24] "Hydrogen production by PEM water electrolysis - A review", Kumar & Himabindu, *Materials Science for Energy Technologies*, **2019**, *2*, 442.

[25] "Influence of binder properties on kinetic and transport processes in polymer electrolyte fuel cell electrodes", Sambandam & Ramani, *Physical chemistry chemical physics: PCCP*, **2010**, *12*, 6140.

[26] "State of Understanding of Nafion", Mauritz & Moore, *Chemical reviews*, **2004**, *104*, 4535.

[27] "Physical and chemical modification routes leading to improved mechanical properties of perfluorosulfonic acid membranes for PEM fuel cells", Subianto et al., *Journal of Power Sources*, **2013**, *233*, 216.

[28] "Structure/property relationship of Nafion XL composite membranes", Shi et al., *Journal of membrane Science*, **2016**, *516*, 123.

[29] "Effect of flow regime of circulating water on a proton exchange membrane electrolyzer", Ito et al., *International Journal of Hydrogen Energy*, **2010**, *35*, 9550.

[30] "Numerical prediction of mass-exchange between cathode and anode channels in a PEM fuel cell", Dutta et al., *International Journal of Heat and Mass Transfer*, **2001**, *44*, 2029.

[31] "Analysis of a Two-Phase Non-Isothermal Model for a PEFC", Birgersson et al., *Journal of The Electrochemical Society*, **2005**, *152*, A1021.

[32] "The effect of channel-to-channel gas crossover on the pressure and temperature distribution in PEM fuel cell flow plates", Oosthuizen et al., *Applied Thermal Engineering*, **2005**, *25*, 1083.

[33] "PEM FC with improved water management", Kratyberg & Ein-Eli, *Journal of Power Sources*, **2006**, *160*, 194.

[34] "A macroscopic PEM fuel cell model including water phenomena for vehicle simulation", Boulon et al., *Renewable Energy*, **2012**, *46*, 81.

[35] "Quantifying water transport in anion exchange membrane fuel cells", Eriksson et al., *International Journal of Hydrogen Energy*, **2019**, *44*, 4930.

[36] "Hydrogen and oxygen generation with polymer electrolyte membrane (PEM)-based electrolytic technology", Badwal et al., *Ionics*, **2006**, *12*, 7.

[37] "A novel non-carbon gas diffusion layer for PEM water electrolysis anodes", Borisov et al., *Izvestiya po Khimiya Bulgarska Akademiya na Naukite*, **2013**, *45-A*, 186.

[38] "PEM Water Electrolysis-Present Status of Research and Development", Smolinka, World Hydrogen Energy Conference, **2010**.

[39] "Critical Review - Identifying Critical Gaps for Polymer Electrolyte Water Electrolysis Development", Babic et al., *Journal of The Electrochemical Society*, **2017**, *164*, F387.

[40] "Spatially Resolved Quantification of Ionomer Degradation in Fuel Cells by Confocal Raman Microscopy", Böhm et al., *Journal of The Electrochemical Society*, **2019**, *166*, F3044.

[41] "Humidity Conversion Formulas", Vaisala Oyj, https://www.hatchability.com/Vaisala.pdf, **2013**.

[42] "The influence of iridium chemical oxidation state on the performanceand durability of oxygen evolution catalysts in PEM electrolysis", Siracusano et al., *Journal of Power Sources*, **2017**, *366*, 105.
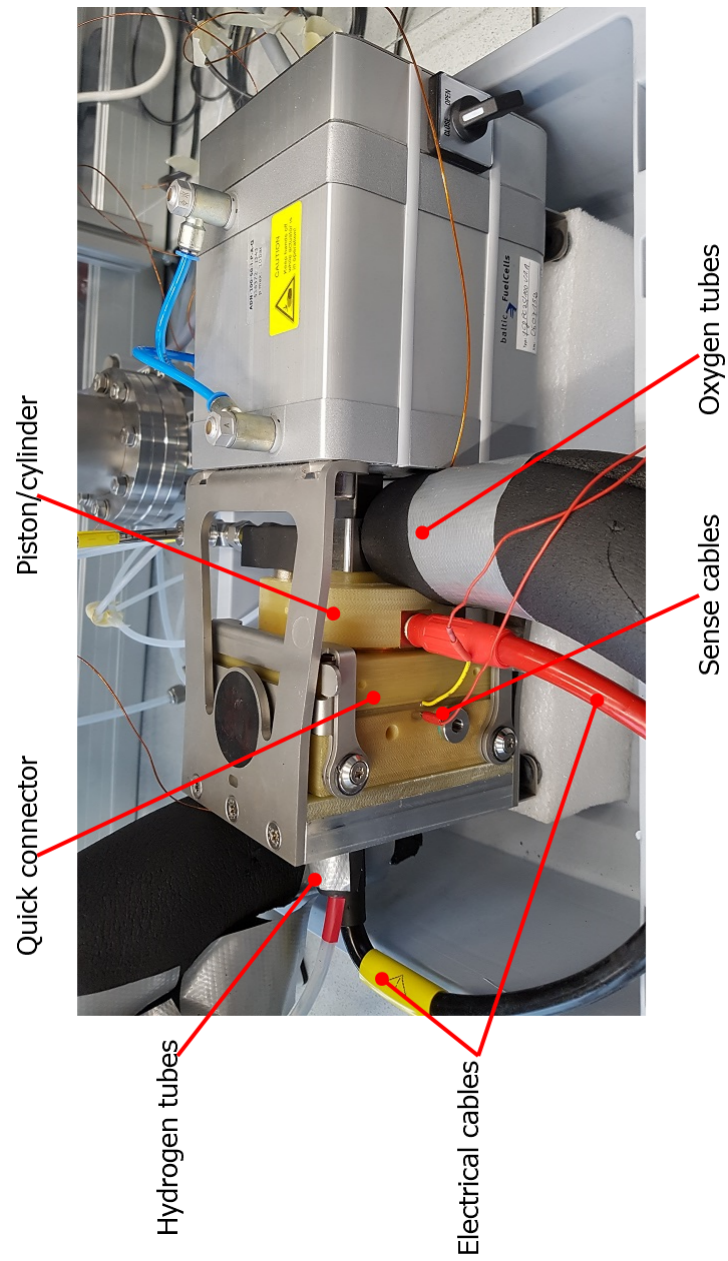
Appendices

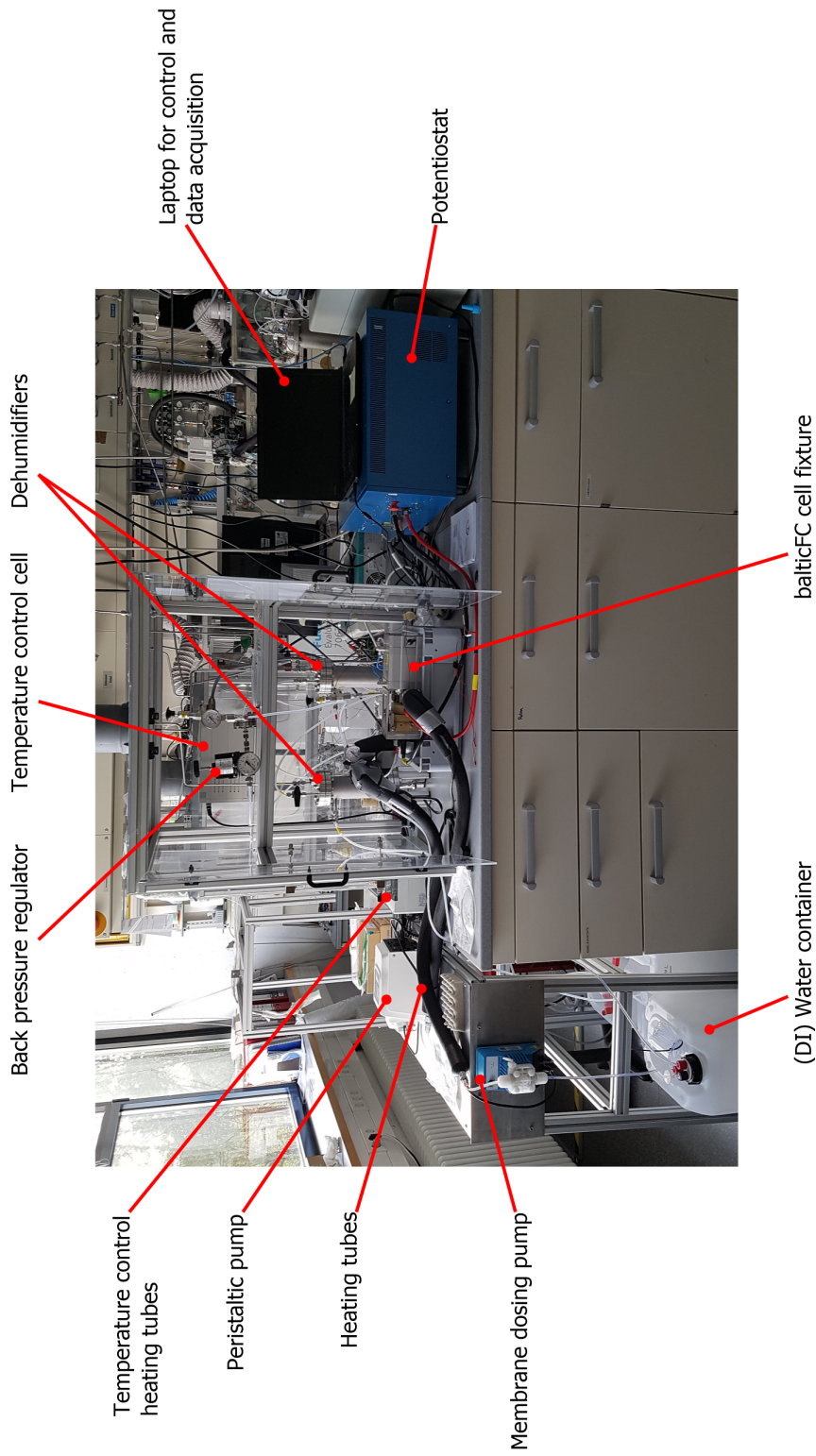Figure 7.1: Picture and description of the quick connecting system.

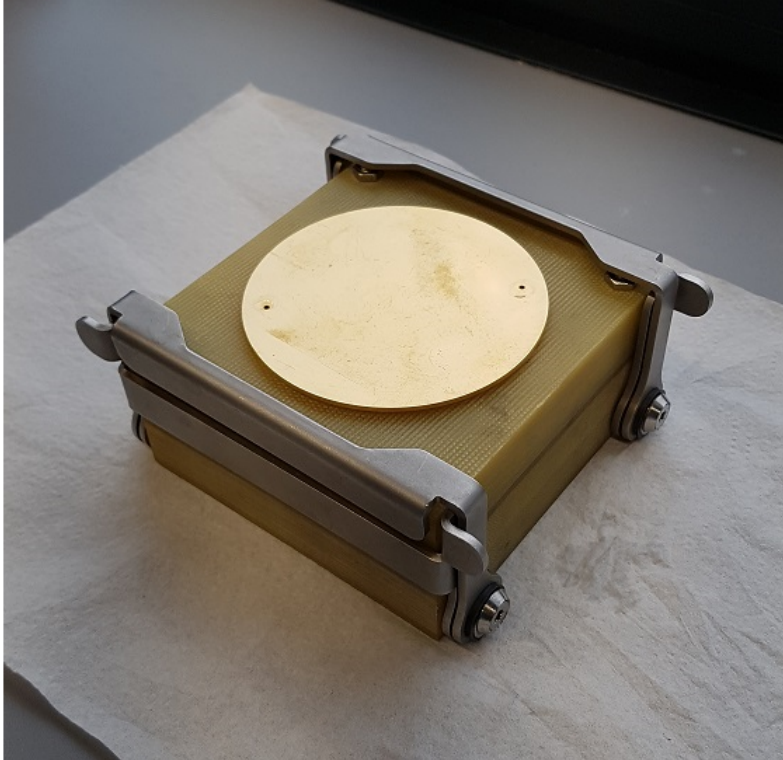Figure 7.2: Picture and description of the test stand used in this thesis.

Figure 7.3: Picture of the assembled quick connector. The gold covered area is where the piston/cylinder applies the contact pressure.
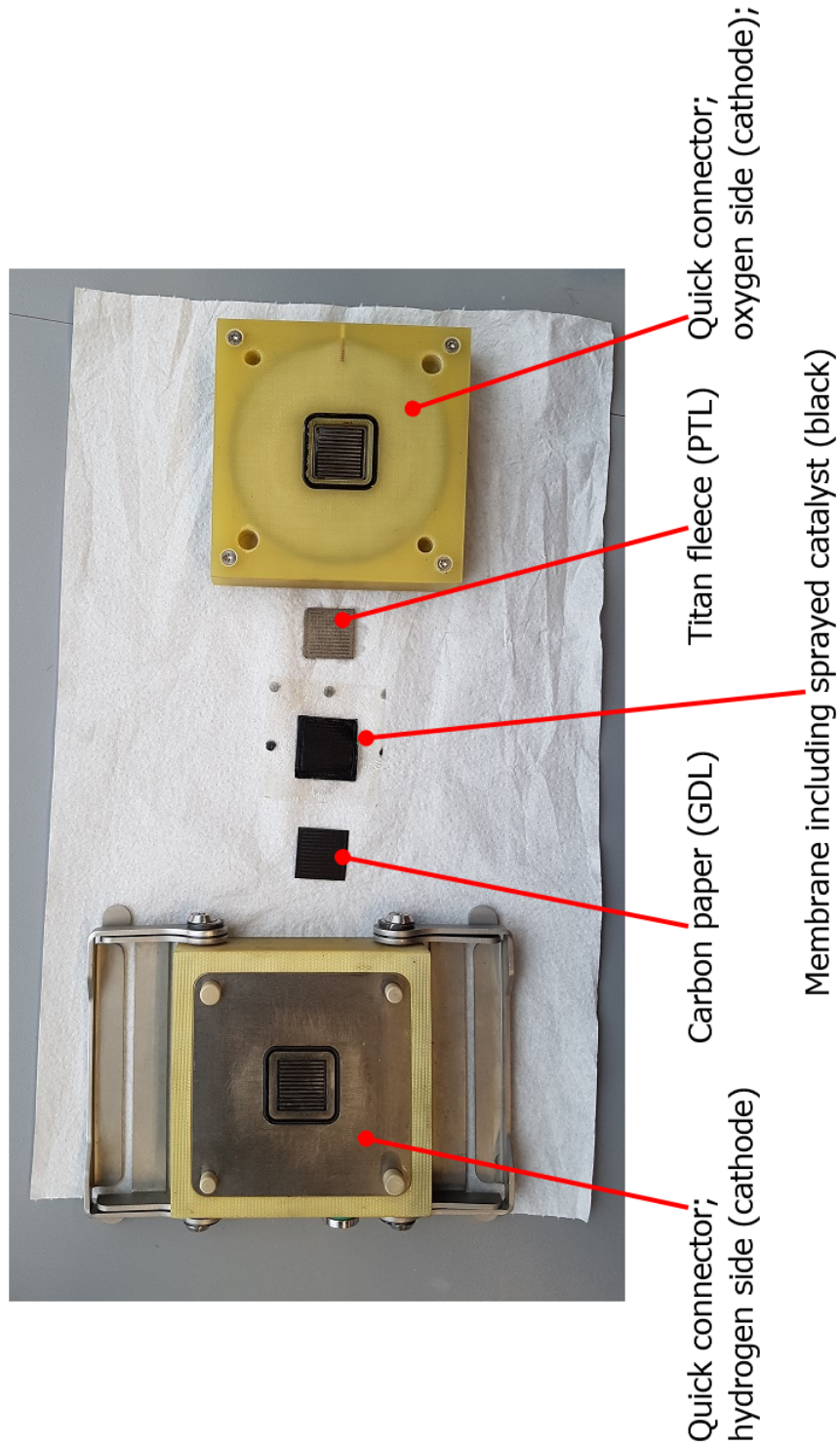
Figure 7.4: Picture and description of the disassembled quick connector including a disassembled MEA.

Nafion™ XL
Ion Exchange Materials

## Perfluorosulfonic Acid (PFSA) Membranes for Fuel Cells

Product Information

Description

Nafion™ PFSA membranes are widely used for proton exchange membrane (PEM) fuel cells and water electrolyzers. The membrane performs as a separator and solid electrolyte in a variety of electrochemical cells that require the membrane to selectively transport cations across the cell junction.

Nafion™ XL membrane is an extended lifetime reinforced membrane based on chemically stabilized perfluorosulfonic acid/polytetrafluoroethylene (PTFE) copolymer in the acid (H^+) form. The reinforcement improves the membrane's handling and physical properties. When the reinforcement is combined with the chemically stabilized polymer, the membrane exhibits both substantially lower fluoride ion release and longer operating durability under fuel cell conditions.

The membrane is positioned between a backing film and a cover sheet. This composite is wound on a plastic core, with the backing film on the core side, as shown in Figure 1. A 6 in ID plastic roll core is standard.

Figure 1. Roll Unwind Orientation (Cover Sheet Facing Out)
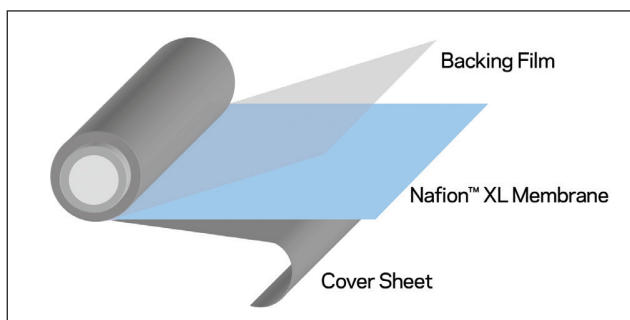
The backing film facilitates transporting the membrane into automated MEA fabrication processes, while the cover sheet protects the membrane from exposure to the environment during intermediate handling and processing. In addition, the cover sheet (in combination with the backing film) eliminates rapid changes in the membrane's moisture content and stabilizes the dimensions of the membrane when removed from the roll.

Order and Packaging Information

The standard product dimensions for membrane rolls include:

Width: Standard width is 12 in (30 mm); other widths are available from 190 368 mm in 3.175 mm increments on special order.

Length: 100 m standard roll lengths, and intermediate lengths of 20 and 50 m are available on special order.

There is a 100 m^2 minimum order requirement for nonstandard roll widths and a per roll packaging surcharge for standard widths in nonstandard lengths less than 100 m. Please contact Chemours Customer Service for details and availability.

Rolls are splice free. Multiple rolls may be shipped to meet orders for nonstandard lengths.

The water content and conditioning of the membrane will affect its dimensions, and the change may not be symmetrical in the length, width, and thickness directions. Once the cover sheet and backing film are removed, the membrane will respond to the environmental conditions of the workplace. If the membrane remains on the backing film, the membrane's response to relative humidity conditions, for example, may cause the combination

of membrane/backing film to curl. In addition, certain manufacturing steps performed by the customer also may affect the membrane's dimensions and flatness.

Separating Nafion™ XL Membrane from the Cover Sheet and Backing Film

- Attach tapes to front and back sides of the membrane "package" at one corner, as shown in Figure 2. To prevent the tapes from sticking to each other, do not "overlap" the adhesive surfaces at the extreme edges.

- Pull the tapes apart to separate the cover sheet from the membrane/backing film. The membrane typically adheres to the backing film during this step. The coversheet is 1 mil polyester film.

- Attach tapes to the membrane side and the backing film side at one corner, as shown in the diagram. To prevent the tapes from sticking to each other, do not "overlap" the adhesive surfaces at the extreme edges.

- Pull the tapes apart to separate the membrane from the backing film, which is a 3 mil polyester film.

Figure 2. Separating Layers
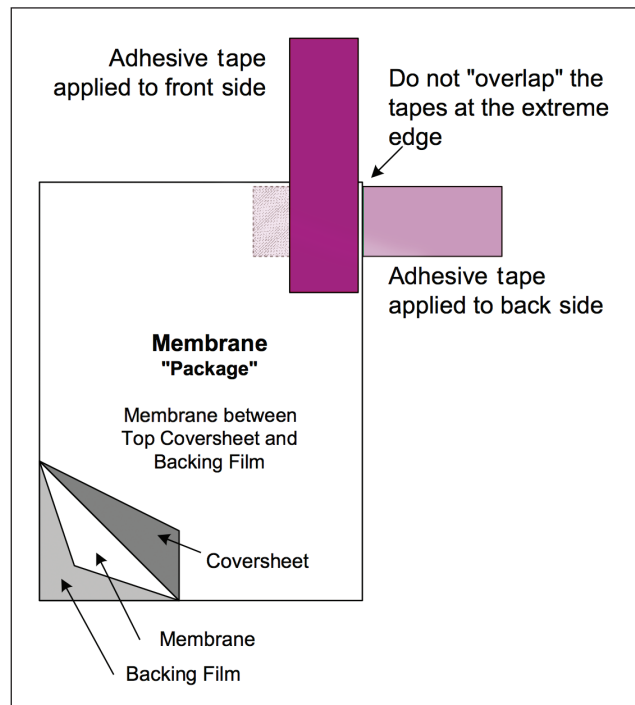
Product Labeling

A self adhesive product label, similar to Figure 3, is located on the inside of the roll core and the outside over wrap of each roll. The label indicates the product roll's width and length in both metric and English units.

- GMC (D code) is a product setup code specific to the thickness, roll width and length, and other packaging features.

- BN is a two part code, with the first part identifying the production lot and the second part indicating the master roll number (wide stock roll before slitting).

- Manufactured Date is the wide stock roll's slit date (mm/yyyy).

- Tracking Code/Bar Code is generated for each product roll.

Figure 3. Finished Product Roll Label
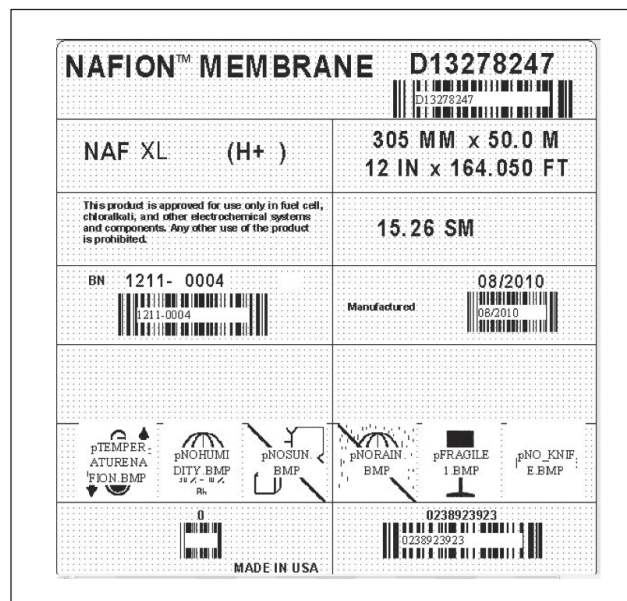
Recommended Roll Storage Conditions

Unopened roll packages of Nafion™ PFSA membrane should be stored in the original shipping box, out of direct sunlight, and in a climate controlled environment maintained at 10 30 °C (50 86 °F) and 30 to 70% relative humidity. Before opening the package, pre condition the membrane roll to the processing area temperature for 24 hr.

Once opened and exposed to the environment, the membrane will equilibrate to the ambient relative humidity and change in dimensions accordingly. Membrane order dimensions are specified and measured at 23 °C (73 °F) and 50% relative humidity.

Handling Practices

Ventilation should be provided for safe handling and processing of Nafion™ PFSA membrane. The amount of local exhaust necessary for processing Nafion™ PFSA membrane at elevated temperatures will depend on the combined factors of membrane quantity, temperature, and exposure time.

Scrap Disposal

Preferred disposal options are (1) recycling and (2) landfill. Incinerate only if incinerator is capable of scrubbing out hydrogen fluoride and other acidic combustion products. Treatment, storage, transportation, and disposal must be in accordance with applicable federal, state/provincial, and local regulations.

Static Discharges

The composite structure and individual layers can pick up a strong charge of static electricity, because of the good dielectric properties of the membrane, backing film, and cover sheet. Unless this charge is dissipated as it forms, by using ionizing radiation devices or special conducting metal tinsel, it can build to thousands of volts and discharge to people or metal equipment. In dust or solvent laden air, a flash fire or an explosion could follow. Extreme caution is needed to prevent static accumulation when using flammable solvents while coating membrane surfaces. Solvent coating equipment should incorporate the means for detecting and extinguishing fire.

Safe Handling and Use of Nafion™ PFSA Membranes

The following information should be reviewed before handling and processing Nafion™ PFSA membranes:

- "Safe Handling and Use of Perfluorosulfonic Acid Products" bulletin (DFC301.0708).

- "Guide to Safe Handling of Fluoropolymer Resins", Fourth Edition, November 2005, Published by the Fluoropolymers Division of the Society of the Plastics Industry, Inc.

Properties of Nafion™ PFSA Membrane

Thickness and Basis Weight Properties[1]		
Membrane Type	Typical Thickness, μm	Basis Weight, g/m^2
XL	27.5	55

Physical Properties			
	Typical Values[2]		Test Method
	MD	TD	
Measured at 50% RH, 23 °C (73 °F)			
Tensile Strength, max., MPa	45	40	ASTM D882
Non Standard Modulus, MPa	613	400	ASTM D882
Elongation to Break, %	200	185	ASTM D882

Other Properties		
	Typical Values	Test Method
Conductivity[3], mS/cm		Chemours
In Plane	>72.0	
Through Plane	>50.5	
Hydrogen Crossover[4], mL/min cm^2	<0.015	Chemours

Hydrolytic Properties		
	Typical Values	Test Method
Water Content, % water[5]	5.0 ± 3.0%	ASTM D570
Water Uptake, % water[6]	50.0 ± 5.0%	ASTM D570
Linear Expansion, % increase		
From 50% RH, 23 °C (73 °F) to water soaked, 23 °C (73 °F)	1% (MD), 5% (TD)	Chemours
From 50% RH, 23 °C (73 °F) to water soaked, 100 °C (212 °F)	3% (MD), 11% (TD)	Chemours

[1]Measurements taken with membrane conditioned to 23 °C (73 °F), 50% RH
[2]Where specified, MD machine direction, TD transverse direction Condition state of membrane given
[3]Conductivity measurements at 23 °C (73 °F), 100% RH
[4]Hydrogen crossover measured at 65 °C (149 °F), 100% RH This is not a routine test
[5]Water content of membrane conditioned to 23 °C (73 °F) and 50% RH (dry weight basis)
[6]Water uptake from dry membrane to conditioned in water at 100 °C (212 °F) for 1 hr (dry weight basis)

FuelCellStore

www.fuelcellstore.com
sales@fuelcellstore.com
(979) 703-1925

Nafion™ NR211 and NR212

Ion Exchange Materials

Solution Cast Membranes

Product Information

Nafion™ NR211 and NR212 membranes are based on chemically stabilized perfluorosulfonic acid (PFSA)/ polytetrafluoroethylene (PTFE) copolymer in the acid (H⁺) form and exhibit substantially lower fluoride ion release compared to the non stabilized polymer a sign of improved chemical durability. Nafion™ PFSA membranes are proton exchange membranes (PEM) that are used for various applications, including but not limited to fuel cells, water electrolyzers, and flow batteries. The membrane performs as a separator and solid electrolyte in a variety of electrochemical cells that require the membrane to selectively transport cations across the cell junction. The polymer is chemically resistant and durable.

The membrane is positioned between a backing film and coversheet. This composite is wound on a 6 in ID plastic core, with the backing film facing out, as shown in Figure 1. A 6 in ID plastic roll core is standard; however, a 3 in ID plastic roll core is used for roll lengths that are less than 25 m long.

Figure 1. Roll Unwind Orientation (Coversheet Facing Out)
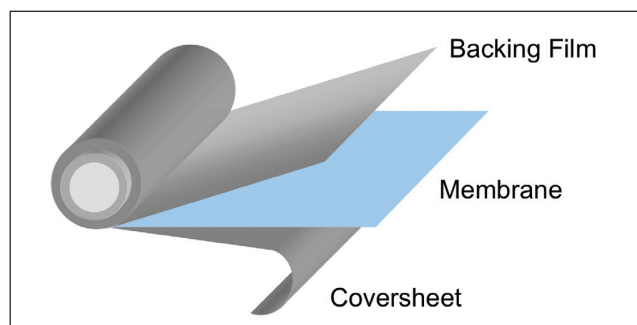
The 3.0 mil backing film facilitates transporting the membrane into automated fabrication processes, while the 0.92 mil coversheet protects the membrane from exposure to the environment during intermediate handling and processing. In addition, the coversheet (in combination with the backing film) eliminates rapid changes in the membrane's moisture content and stabilizes the dimensions of the membrane as it is removed from the roll.

Order and Packaging Information

Nafion™ PFSA membranes are available in two thickness values: NR211 (1 mil) and NR212 (2 mil).

Product dimensions for membrane rolls include:

Width:
- Standard roll widths are 305 mm and 610 mm
- Special order intermediate widths available in 3.175 mm increments from 200 mm (min.) up to 610 mm (max.)

Length:
- Standard roll length is 100 m
- Special order intermediate lengths of 10 m and 50 m

There is a 100 m² minimum order requirement for *non standard* roll widths and a per roll packaging surcharge for standard widths in non standard lengths less than 100 m. A roll core leader is available at a nominal charge per roll. Please contact Nafion™ Customer Service for details and availability.

Rolls are splice free when ordered in standard 100 m lengths. Non standard roll lengths may contain splices under the following conditions: a 5 m minimum distance between splices and a maximum of 3 splices per roll that is less than 100 m in length.

The water content and conditioning of the membrane will affect its dimensions, and the change may not be symmetrical in the length, width, and thickness directions. Once the coversheet is removed, the membrane will respond to the environmental conditions of the workplace. If the membrane remains on the backing film, the membrane's response to relative humidity (RH) conditions, for example, may cause the combination of membrane/backing film to curl. In addition, certain manufacturing steps performed by the customer also may affect the membrane's dimensions and flatness.

If specified in the purchase order, a roll core leader is attached to the membrane as shown in Figure 2. The roll

core leader material is the same as the backing film and the length specified in the purchase order.

Figure 2. Splice Design for Attaching Roll Core Leader to Backing Fillm
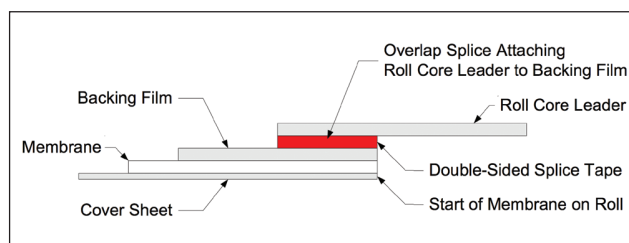
Table 1. Properties of Nafion™ PFSA Membrane

Thickness and Basis Weight Properties[1]		
Membrane Type	Typical Thickness (µm)	Basis Weight (g/m²)
Nafion™ NR211	25.4	50
Nafion™ NR212	50.8	100

Physical Properties[1]					
	Typical Values				
	Nafion™ NR211		Nafion™ NR212		
Property[2]	MD	TD	MD	TD	Test Method
Tensile Strength, Max., MPa	23	28	32	32	ASTM D882
Non Standard Modulus, MPa	288	281	266	251	ASTM D882
Elongation to Break, %	252	311	343	352	ASTM D882

Other Properties			
Specific Gravity	1.97	1.97	See footnote[1]
Available Acid Capacity, meq/g	0.92 min.	0.92 min.	See footnote[3]
Total Acid Capacity, meq/g	0.95 1.01	0.95 1.01	See footnote[4]
Hydrogen Crossover, mL/min cm²	<0.020	<0.010	See footnote[5]

Hydrolytic Properties		
Water Content, % water[6]	5.0 ± 3.0%	ASTM D570
Water Uptake, % water[7]	50.0 ± 5.0%	ASTM D570
Linear Expansion, % increase[8] from 50% RH, 23 °C (73 °F) to water soaked, 23 °C (73 °F)	10	ASTM D756
to water soaked, 100 °C (212 °F)	15	ASTM D756

[1]Measurements taken with membrane conditioned to 23 °C (73 °F), 50% RH

[2]Where specified, MD machine direction, TD transverse direction Condition state of membrane given

[3]A base titration procedure measures the equivalents of sulfonic acid in the polymer and used the measurements to calculate the available acid capacity of the membrane (acid form)

[4]A base titration procedure measures the equivalents of sulfonic acid in the polymer and used the measurements to calculate the total acid capacity or equivalent weight of the membrane (acid form)

[5]Hydrogen crossover measured at 22 °C (72 °F), 100% RH, and 50 psi delta pressure This is not a routine test

[6]Water content of membrane conditioned to 23 °C (73 °F) and 50% RH (dry weight basis)

[7]Water uptake from dry membrane to conditioned in water at 100 °C (212 °F) for 1 hr (dry weight basis)

[8]Average of MD and TD MD expansion is similar to TD expansion for NR membranes

Product Labeling

A self adhesive product label, with information content similar to **Figure 3**, is located on the inside of the roll core and the outside over wrap of each roll. The label indicates the product roll's width and length in both English and metric units.

Figure 3. Finished Product Roll Label

> GMC: D13278258
> Product: Nafion™ NR212 (H+)
> Width: 12 IN x Length: 328 FT
> Width: 305 MM x Length: 100.0 M
> BN: X091 0103
> Manufacture Date: 01/2009
> 0433232101
> ‖‖ ‖ ‖‖ ‖ ‖‖‖ ‖ ‖‖‖ ‖ ‖‖‖‖ ‖‖ ‖ ‖ ‖‖

- GMC is a product setup code specific to the thickness, roll width, length, and other packaging features.

- BN is a two part code, with the first part identifying the production lot and the second part indicating the master roll number (wide stock roll before slitting).

- Manufacture Date is the wide stock roll's slit date (mm/yyyy).

- A tracking code/bar code is generated for each product roll.

Recommended Roll Storage Conditions

Unopened roll packages of Nafion™ PFSA membrane should be stored in the original shipping box, out of direct sunlight, in a climate controlled environment maintained at 10 30 °C (50 86 °F) and 30 70% relative humidity. Before opening the package, pre condition the membrane roll to the processing area temperature for 24 hr.

Once opened and exposed to the environment, the membrane will equilibrate to the ambient relative humidity and change in dimensions accordingly. Membrane order dimensions are specified and measured at 23 °C (73 °F) and 50% relative humidity.

Handling Practices

Ventilation should be provided for safe handling and processing of Nafion™ PFSA membrane. The amount of local exhaust necessary for processing Nafion™ PFSA membrane at elevated temperatures will depend on the combined factors of membrane quantity, temperature, and exposure time.

Scrap Disposal

Preferred disposal options are (1) recycling and (2) landfill. Incinerate only if incinerator is capable of scrubbing out hydrogen fluoride and other acidic combustion products. Treatment, storage, transportation, and disposal must be in accordance with applicable federal, state/provincial, and local regulations.

Static Discharges

The composite structure and individual layers can pick up a strong charge of static electricity, because of the good dielectric properties of the membrane, backing film, and coversheet. Unless this charge is dissipated as it forms, by using ionizing radiation devices or special conducting metal tinsel, it can build to thousands of volts and discharge to people or metal equipment. In dust or solvent laden air, a flash fire or explosion could follow. Extreme caution is needed to prevent static accumulation when using flammable solvents while coating membrane surfaces. Solvent coating equipment should incorporate the means for detecting and extinguishing fire.

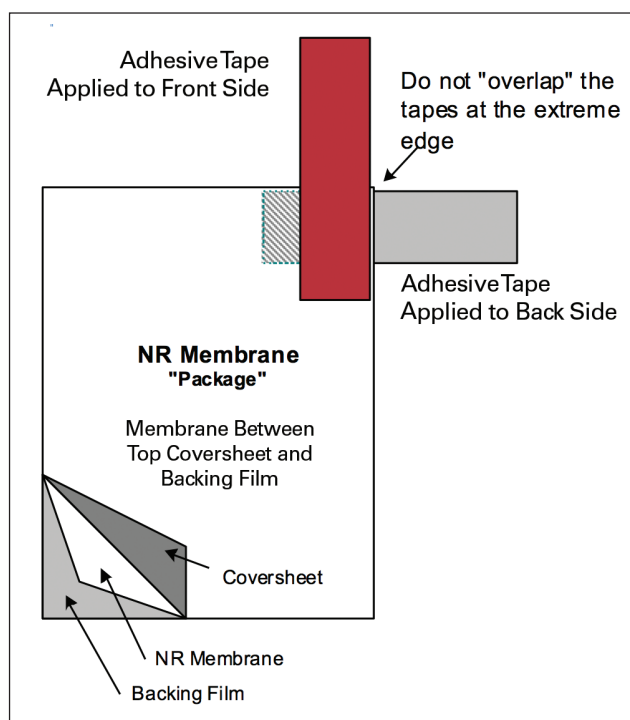## Safe Handling and Use of Nafion™ PFSA Membranes

The following information should be reviewed before handling and processing Nafion™ PFSA membranes:

- Material Safety Data Sheet for Nafion™ PFSA membranes NR211 and NR212

- Nafion™ "Safety in Handling and Use" technical bulletin, T 01

- "Guide to Safe Handling of Fluoropolymer Resins", Fourth Edition, November 2005, Published by the Fluoropolymers Division of the Society of the Plastics Industry, Inc.

Separating NR Membrane from the Coversheet and Backing Film

- Attach tapes to the front and back sides of the NR membrane "package" at one corner, as shown in Figure 4. To prevent the tapes from sticking to each other, do not "overlap" the adhesive surfaces at the extreme edges.

- Pull the tapes apart to separate the coversheet from the membrane/backing film. The membrane typically adheres to the backing film during this step. The coversheet is 0.92 mil polyester film.

- Attach tapes to the membrane side and backing film side at one corner, as shown in **Figure 4**. To prevent the tapes from sticking to each other, do not "overlap" the adhesive surfaces at the extreme edges.

- Pull the tapes apart to separate the membrane from the backing film. The backing film is 3.0 mil polyester film.

Figure 4.

FuelCellStore

www.fuelcellstore.com
sales@fuelcellstore.com
(979) 703-1925

Figure 7.5: R&I scheme of the finished test stand.

Re-Flex test stand: humidifier water cycle

B: humidifiers for fuel cell mode
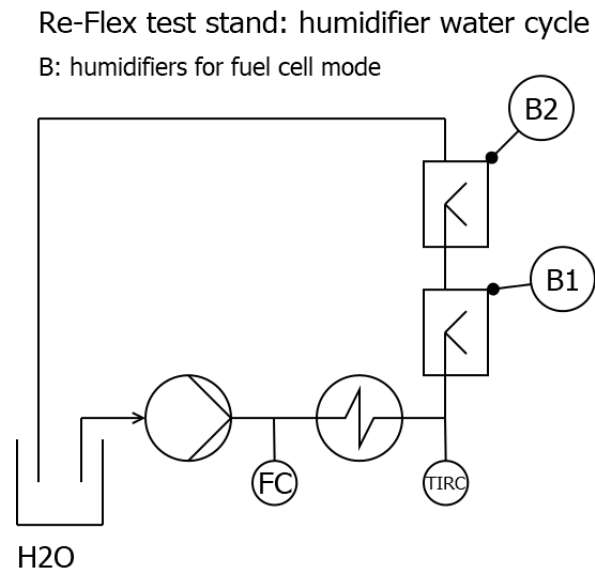

Figure 7.6: R&I scheme of the finished test stand. Shown is the humidification cycle.

Calibration peristaltic pump: long suction tube, jammed into pump frame, finished test stand

%	Δt	m1	m2	m3	m4	m5	
[-]	[s]	[g]	[g]	[g]	[g]	[g]	
100	3600	469,20	1335,70	2215,10	243,80	1119,4	schwallartig
50	3600	251,20	535,70	851,10	1304,30		schwallartig
50	1800	332,10	560,70	780,30	962,90		schwallartig
50	7200	1224,00	2090,40				schwallartig
20	3600	230,60	379,80	543,40	713,70		schwallartig

%	ṁ1 / g/s	ṁ2 / g/s	ṁ3 / g/s	ṁavg / g/min
100	0,240694444	0,244277778	0,243222222	14,56388889
50	0,079027778	0,087611111	0,125888889	7,553333333
50	0,127	0,122	0,101444444	7,008888889
50			0,120333333	7,12952381
20	0,041444444	0,045444444	0,047305556	2,683888889
0	0	0	0	0

y = 0,1447x
R² = 0,9995
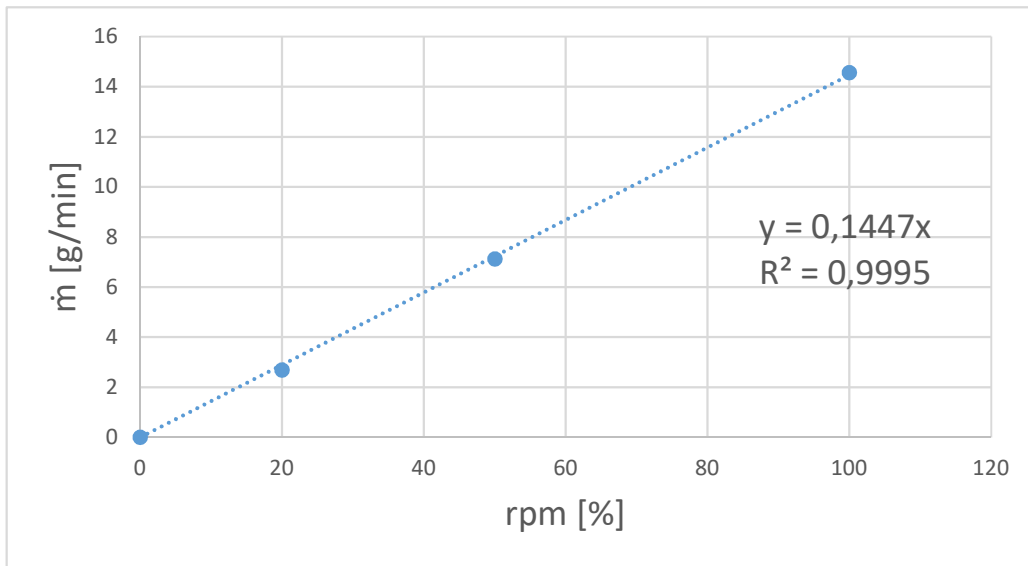
ṁ desired	rpm
[g/min]	[%]
5	34,55

Calibration dosing pump; finished test stand, atmospheric (0 bar(g))

%	Δt	m1	m2	m3	m4	m5	
[-]	[s]	[g]	[g]	[g]	[g]	[g]	
20	3600	235,80	1605,40	2973,70	204,90	1515,6	konstant
15	3600	203,50	784,30	1397,00	2010,70		schwallartig
10	3600	182,60	451,90	837,80	1207,90		schwallartig
30	600				2010,70	2299,8	konstant

%	Δt	ṁ_1	ṁ_2	ṁ_3	ṁ_avg		
[-]	[s]	[g/s]	[g/s]	[g/s]	[g/s]	[g/min]	[l/h]
20	3600	0,3804	0,3801	0,3641	0,3749	22,4922	1,3495
15	3600	0,1613	0,1702	0,1705	0,1673	10,0400	0,6024
10	3600	0,0748	0,1072	0,1028	0,0949	5,6961	0,3418
30	600	0,0000	0,0000	0,4818	0,4818	28,9100	1,7346
7	0	0	0	0	0	0	0

dosing pump, ṁ_avg @ 0bar(g)

y = 1,6371x - 11,725
R² = 0,9593
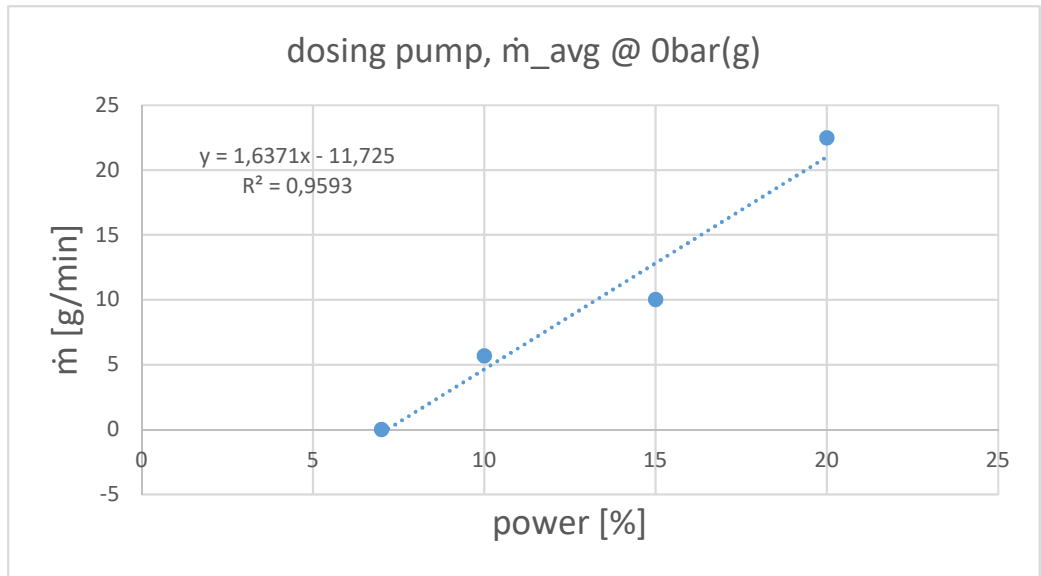
ṁ desired	power
[g/min]	[%]
10	13,2704172

Calibration dosing pump; finished test stand, 6 bar(g)

%	Δt	m1	m2	m3	m4	m5	
[-]	[s]	[g]	[g]	[g]	[g]	[g]	
30	3600	220,00	1474,80	2730,80	191,30	1342,6	konstant
20	7200	250,00	1505,50	225,00	884,00	1212,3	
10	7200	162,00	684,20	833,50	1054,10		

%	Δt	ṁ_1	ṁ_2	ṁ_3	ṁ_avg		
[-]	[s]	[g/s]	[g/s]	[g/s]	[g/s]	[g/min]	[l/h]
7	0	0	0	0	0	0	0
10	7200	0,0725	0,0207	0,0613	0,0561	3,3674	0,2020
20	7200	0,1744	0,1831	0,1824	0,1780	10,6800	0,6408
30	3600	0,3486	0,3489	0,3198	0,3445	20,6726	1,2404

dosing pump, ṁ_avg @ 6bar(g)

y = 0,875x - 5,9755
R² = 0,995
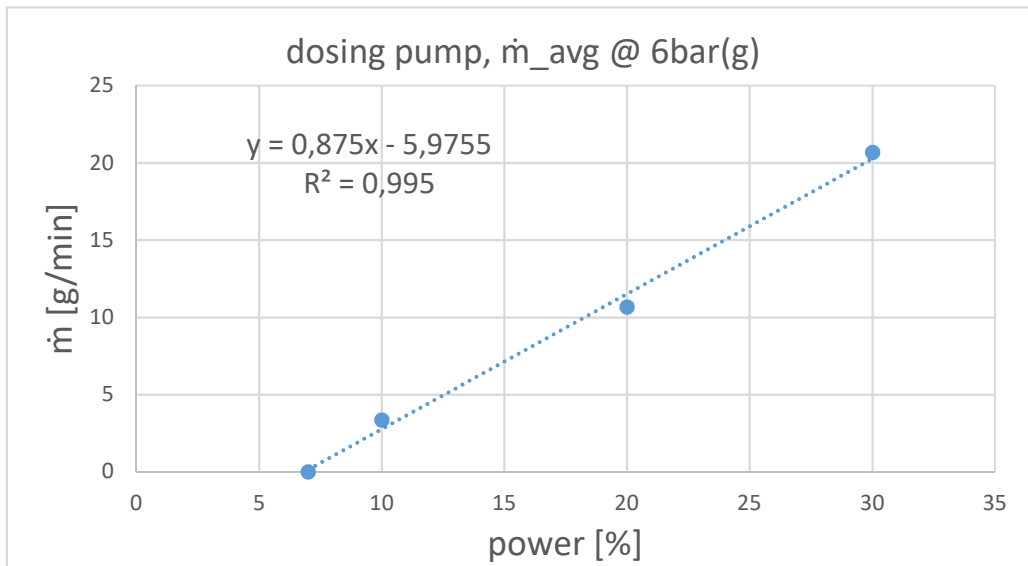
	exp		lin
ṁ desired	power		power
[g/min]	[%]		[%]
0,398	1,81190139		7,284

baltic FuelCells GmbH

Calculation of contact pressure incl. Back pressure

active area [mm^2]:   400

diameter of cylinder in qCF [mm]:   100

diameter of piston in the cell fixture [mm]   70

cyinder area [mm^2]:   7854

piston area [mm^2]:   3848

back pressure [bar]:   0,0

Bar (in qCF cylinder)	Bar (on piston)	kPa	N/mm²	N
0,50	9,82	982	0,98	393
0,50	9,74	974	0,97	390
0,50	9,74	974	0,97	390
0,49	9,70	970	0,97	388
3,09	60,63	6063	6,06	2425